2019

Three-Dimensional Human Neural Stem Cell Culture for High-Throughput Assessment of Developmental Neurotoxicity

Pranav Joshi

THREE-DIMENSIONAL HUMAN NEURAL STEM CELL CULTURE FOR HIGH-THROUGHPUT ASSESSMENT OF DEVELOPMENTAL NEUROTOXICITY

PRANAV JOSHI

Bachelor of Science in Electronics Engineering

Tribhuvan University

March 2010

Submitted in partial fulfillment of requirements for the degree

DOCTOR OF PHILOSOPHY IN APPLIED BIOMEDICAL ENGINEERING

Specializing in Cellular and Molecular Medicine

at the

CLEVELAND STATE UNIVERSITY

May 2019

We hereby approve this dissertation

for

Pranav Joshi

Candidate for the Doctor of Philosophy in Biomedical Engineering degree

for the Department of Chemical and Biomedical Engineering

and

CLEVELAND STATE UNIVERSITY's

College of Graduate Studies by

Moo-Yeal Lee, Ph.D., Dissertation Committee Chairperson

Chemical and Biomedical Engineering, 04/22/2019

Chandra Kothapalli, Ph.D., Dissertation Committee Member

Chemical and Biomedical Engineering, 04/22/2019

Joanne Belovich. Ph.D., Dissertation Committee Member

Chemical and Biomedical Engineering, 04/22/2019

Nolan B. Holland, Ph.D., Dissertation Committee Member

Chemical and Biomedical Engineering, 04/22/2019

Xue-Long Sun, Ph.D., Dissertation Committee Member,

Chemistry, 04/24/2019

Date of Defense: April 17th, 2019

This student has fulfilled all requirements for the Doctor of Philosophy degree.

Chandra Kothapalli, Ph.D., Doctoral Program Director

DEDICATION

This thesis is dedicated to my wife, Matina Shakya, my mother Bashanti Joshi, sister Prabina Joshi Mulmi, brother Prashant Joshi, and my late father Pradip Joshi.

ACKNOWLEDGMENTS

I would first like to offer my sincere gratitude to all my committee members. First and foremost, I would like to thank Dr. Moo-Yeal Lee for taking me as his PhD student and giving me the opportunity to take a lead on this project. He has always been an incredible advisor and mentor both in research and in real life. I would not have come this far without his constant guidance and suggestions in solving the research problems as well as his motivation to bring out the best in me. I would like to thank Dr. Chandra Kothapalli for his valuable feedback in the research and manuscripts. I would also like to thank Dr. Joanne Belovich, Dr. Nolan Holland, and Dr. Xue-Long Sun, all of whom served on my committee, helped me with research questions as they came up, without which these experiments would not be possible.

I would like to thank all the past and present members of our group, especially Soo-Yeon Kang for her tremendous help and support throughout the project, Dr. Kyeong-Nam Yu for her help in Aim 1, and Rushabh Patel for his help in Aim 2 of this dissertation. Akshata Datar, Dr. Alex Roth, and Dr. Jyotsna Joshi who were there to lend me support when I struggled in my early years of PhD, and everyone else who has helped me in one way or the other in the lab. I would like to thank Gautam Mahajan for his inputs on various topics of my research and Dr. Kurt Farrell who provided his guidance and support during the initiation of this project. I would also like to thank Rebecca Laird and Darlene Montgomery and acknowledge other staff throughout the department and college who helped along the way.

This work would not have been possible without the generous financial support from NIH RO1, the Cellular and Molecular Medicine Fellowship, Dissertation Research Awards

(DRA), the College of Graduate Studies travel award, and startup funds to Dr. Lee at CSU. I am grateful for the depth of knowledge that I gained and the skills that I acquired during my time at CSU and look forward to spreading this knowledge to those in need.

THREE-DIMENSIONAL HUMAN NEURAL STEM CELL CULTURE FOR HIGH-THROUGHPUT ASSESSMENT OF DEVELOPMENTAL NEUROTOXICITY

PRANAV JOSHI

ABSTRACT

Only a few hundred of compounds, among tens of thousands of commercially available compounds, have been tested for developmental neurotoxicity (DNT) due to the limitations of current guidelines for DNT which are based entirely on *in vivo* experiments. *In vivo* studies are highly expensive and time-consuming, which often do not correlate to human outcomes. There is a key gap in our ability to predict *in vivo* outcomes accurately and robustly using *in vitro* assays. This is particularly the case for predicting the toxicity of chemicals on the developing human brains. Conventional *in vitro* assays are typically performed in two-dimensional (2D) cell culture systems and use cytotoxicity assays that do not provide the information on mechanisms of toxicity. High-content imaging (HCI) assays performed on three-dimensional (3D) cell cultures can provide better understanding of mechanisms of toxicity needed to predict DNT in humans. However, current 3D cell culture systems lack the throughput required for screening DNT against a large number of chemicals. Thus, there is a need for cost-effective, high-throughput, alternative *in vitro* test methods based on mechanisms of toxicity.

In this study, we first developed a miniaturized, 3D human NSC culture with ReNcell VM on the micropillar chip platform and established a high-throughput promoter-reporter assay system using recombinant lentiviruses on human NSC spheroids to assess

cell viability, self-renewal, and differentiation. Next, we identified major ion channels and ABC-transporters expressed in ReNcell VM *via* RNA-seq analysis and established high-throughput ion channel and ABC-transporter assays in 3D-cultured ReNcell VM on the 384-pillar plate. In the third step, we established high-content imaging (HCI) assays in 3D-cultured ReNcell VM with multiple assays which were tested with four model compounds. Finally, we established a high-throughput metabolism-mediated neurotoxicity testing system by combining 3D-cultured ReNcell VM on the 384PillarPlate and HepaRG spheroids in a ULA 384-well plate. Alternative *in vitro* systems for high-throughput neurotoxicity assessment established in this study will enable researchers to screen a library of test compounds with high confidence in terms of predictability of adverse reactions *in vivo* from those compounds.

TABLE OF CONTENTS

LIST OF TABLES

LIST OF FIGURES

CHAPTER I

INTRODUCTION

1.1. Current issues on developmental neurotoxicity

The disabilities associated with the functioning of developing nervous system is known as neurodevelopmental disorders which include disabilities such as attention deficit/hyperactivity disorders (ADHD), autism, cerebral palsy, intellectual disability (mental retardation), and learning disabilities. One out of six children in US are diagnosed with a neurodevelopmental disorder and ADHD alone affects 14% of the children born in US each year. Neurodevelopmental disorders can occur due to combination of genetic, biological, psychosocial and environmental risk factors [1]. Out of all the cases of neurodevelopmental disorders, genetic factors contribute to nearly 30-40% of it whereas rest of the cases are more likely attributed to environmental risk factors [2].

Environmental risk factors such as use of alcohol, tobacco, and opioids during pregnancy, premature birth, and prenatal or childhood exposure to environmental toxicants can all contribute towards the above mentioned disorders [1]. According to US National Research Council, 3% of developmental disabilities are directly related to environmental exposure of toxic chemicals while another 25 % is the result of interaction between other environmental factors and genetic susceptibility of individuals [3].

Developmental neurotoxicity (DNT) can be defined as any adverse effect in the structure or function of the nervous system resulting from chemical exposure during the prenatal or gestational period [4], [5]. The developing nervous system is known to be more vulnerable to chemical exposure as compared to the adult nervous system due to the complexity of human brain development consisting of various processes such as proliferation, differentiation, migration, cell to cell communication that must take place in a highly controlled time frame. The blood-brain barrier (BBB) which protects the adult brain is also not completely developed until about 6 months after birth. Moreover, the susceptibility of developing brain to environmental chemicals is further augmented by their increased exposures, absorption rates, and decreased ability to detoxify as compared to fully developed adult brain [3], [6].

Despite the potential vulnerability of developing brain to the environmental toxicants, there is only a small amount of data available for developmental neurotoxicity. Out of more than 200 chemicals known to be neurotoxic, only 5 of these have been documented to be the cause of developmental neurotoxicity. However, it is highly likely that many of these chemicals are capable of causing developmental neurotoxicity [2], [7]. This lack of documentation is mainly because there is no *a priori* requirement for chemicals to be tested for DNT effects prior to their registration and use under the present regulation. DNT study is not a mandatory requirement in the USA for pesticides, biocides, pharmaceuticals or industrial chemicals and is carried out only when relevant observations are made in other studies based on structure activity relationships or evidence of neurotoxicity in standard *in vivo* adult, developmental or reproduction studies either after acute exposure, or sub-acute and sub-chronic or chronic exposure [6]–[9].

Identification of chemicals for their potential to cause DNT is primarily based on the guidelines from organization for economic co-operation and development (OECD), OECD TG 426 (an update to the US EPA DNT guideline (OPPTS 8706300, EPA 712-C-98-239)) and OECD TG 443 guidelines. These guidelines require neurobehavioral determination of cognitive, sensory and motor functions accompanied by morphometric and histopathological evaluation of the brain and are entirely based on animal studies performed mainly in rat. Since, the *in vivo* studies are extremely resource intensive in terms of the number of animals used, time and overall cost [10], these guidelines have been used only for a limited number of chemicals (approximately 120) [11], [12]. In addition, *in vivo* studies are unsuitable for screening large numbers of chemicals, due to the use of large number of animals and long duration of tests [7].

Identification of chemical's toxic effect on developing brain is an important first step towards prevention of neurodevelopmental disorders thereby restricting the use and limiting the exposure of those chemicals [3]. Therefore, an alternative approach to identify DNT chemicals and further guide chemical prioritization for testing in a rapid and cost-effective manner needs to be developed [6].

1.2. Conventional methods of developmental neurotoxicity assessment: In vivo vs. In vitro models

Current guidelines for DNT based on *in vivo* studies are ethically questionable, time-consuming, and highly expensive. Testing one compound requires about 700 rodents, lasts up to 12 months and costs up to one million USD [10], [11], [13]. However, even with the time-consuming and expensive *in vivo* studies, the predictability of human neurotoxicity is still questionable due to the lack of pharmaco-/toxicodynamics relation of the developing brain of rodents with humans [14], [15] and concern over species-specific

differences in the extrapolation of human neurotoxicity [7], [16], [17]. Studies have shown that toxicity testing in rodents are predictive of human toxicity in less than only half of the cases [18] and mouse brains differ in the temporal aspects of neurogenesis from human brains [19], which is important for developmental neurotoxicity (DNT) [9].

Reliable, fast and efficient screening and assessment tools are needed to improve the identification, and evaluation of chemicals with the potential to induce DNT in shorter time, cost-efficient manner, and with human-specific toxicity pathways [7], [20]. This requires a major shift from the current OECD guidelines with animal experiments towards new *in vitro* approaches to identify the mechanism of toxicity [9], [21], [22]. Replacing the OECD guidelines requires an *in vitro* test battery of DNT responses to provide data predicting the adverse effect of chemicals on human health [23], [24]. Prevention of neurodevelopmental disorders has been severely restricted due to the lack of *in vitro* testing of environmental pollutants and toxic chemicals. Moreover, mimicking the complexity of the central nervous system (CNS) and modeling of functional disturbances manifested by neurotoxicity *in vitro* pose a serious challenge for *in vitro* assessment of neurotoxicity [12]. Therefore, efforts have been made to overcome these hurdles to some extent by developing *in vitro* neurotoxicity testing system in platforms such as 96-well plates [25], cellular microarrays [26], and microfluidic devices [27].

1.2.1. Well Plate Assays

Several *in vitro* models for neurotoxicity testing have been developed in 96-well plates due to the ease of use and flexibility to test different culture conditions. Neurotoxic effect of various toxicants including heavy metals [28], insecticides [29], nanoparticles [30], and therapeutic drugs [25] and their differences among human and mouse models

have been widely investigated using the 96-well plate platform [30], [31]. For example, Chang *et al.* reported that human NSCs treated with MeHg underwent caspase-dependent apoptosis, autophagy, and inhibition of differentiation [32]. Similarly, Zychowicz *et al.* demonstrated the effect of MeHg on viability, proliferation, and differentiation of NSCs, cultured on various bio-functionalized surfaces coated with fibronectin, vitronectin, and poly-L-lysine (PLL) in 96t-well plate. All three endpoints were shown to be significantly inhibited in cells attached to PLL, whereas cells attached to fibronectin and vitronectin were shown to be less sensitive to MeHg toxicity at certain doses [28]. Likewise, the effects of insecticides and nanoparticles on human NSCs have also been well studied using this platform. For example, Lee *et al.* evaluated the mechanisms involved in neurotoxic effects of chlorpyrifos (CPF) on human neural progenitor cells (hNPCs) for the first time. The authors demonstrated the effect of oxidative stress in CPF-induced cell death *via* activation of NF-kB mediated p53 pathway [29]. Liu *et al.* investigated the neurotoxic effects of silver nanoparticles (Ag-NPs) in human and rat embryonic NSCs by evaluating endpoints such as viability, proliferation, apoptosis, and oxidative stress. Similar neurotoxic effect of Ag-NPs in both human and rat NSCs in dose and exposure-time dependent manner were observed [30].

1.2.2. Microfluidic Assays

A microfluidic device contains an array of microchannels for cell culture with multiple inlets and outlets providing access to desired reagents (**Figure 1.1**). Microfluidic devices enable miniaturized biochemical assays (also known as "*lab on a chip"*) with the advantage of culturing cells under various flow conditions in a single chip. This platform has been implemented for various applications such as *in vitro* drug toxicity testing [33],

anticancer drug screening [34], and intracellular signaling studies [35], [36]. It has also been commonly used to study the self-renewal [37], differentiation [38]–[40], and migration [41], [42]. For example, Lee *et al.* [38] demonstrated the utility of microfluidics technology for the study of neurite outgrowth and axonal guidance of neural cells derived from human embryonic stem cells (hESCs). H9 hESCs were differentiated into neuronal lineages and the migration of axons into the microchannels were studied *via* pre-neural cell marker fluorescent staining such as TUJ1 (neuron-specific class III beta-tubulin) [38].

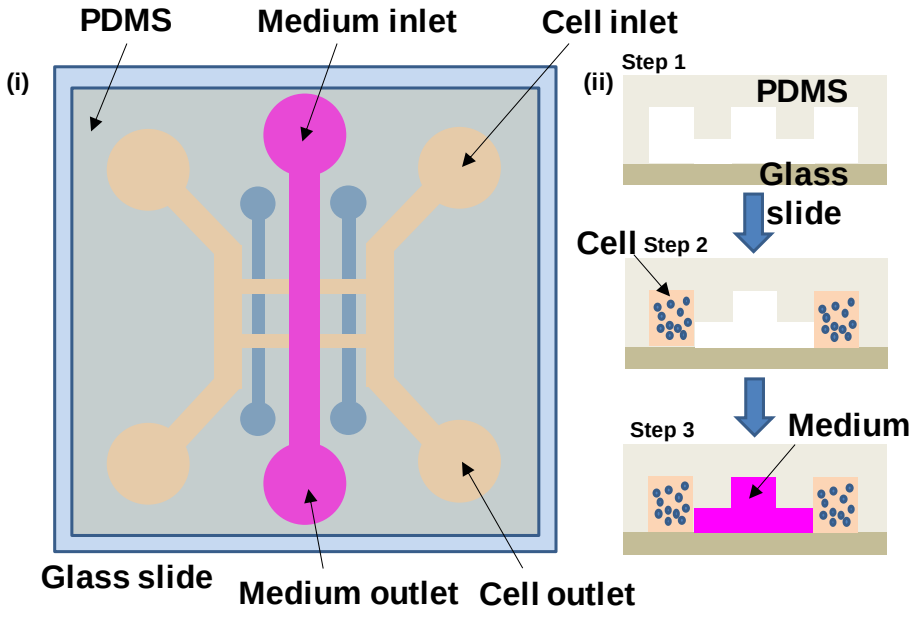

Figure 1.1. Microfluidic device. (i) Top view of a bilayer microfluidic chip fabricated with PDMS on top of a glass slide. Several inlet and outlet channels provide parallel access to cell suspension, growth medium and other reagents. (ii) Overview of the cell culture process in the microfluidic device: (Step 1) Bi-layer chip is fabricated with PDMS containing several channels on top of a glass slide. (Step 2) A mixture of cells and hydrogel precursor is fed from the cell inlet channel. (Step 3) A growth medium is supplied from the medium inlet channel for cell culture. (*Farrel, K., Joshi, P., Roth, A., Kothapalli, C.R., Lee, M.Y., High-throughput screening of toxic chemicals on neural stem cells, Human Stem Cell Toxicology, Royal Society of Chemistry, 31-63 (2016))*

Similarly, an advanced microfluidic platform capable of generating stable concentration gradient was used for studying the migration of NSCs within stable linear cytokine stromal cell-derived factor 1α (C-X-C motif chemokine 12, or CXCL12) gradients [41]. Other work, which includes the capability of brain-derived neurotrophic factor (BDNF) to direct chemotaxis of NSCs towards CXCL12 without affecting the migration speed, has been demonstrated. This effect was mediated through the CXCL12/ C-X-C chemokine receptor type 4 (CXCR4) system [41]. In addition, Yang *et al.* reported a microfluidic array platform providing *in vivo*-like 3D niche conditions for the study of NSC self-renewal and differentiation. Four combinations of ECM proteins were used to develop the *in vivo*-like 3D niche environment under low oxygen (*i.e.*, hypoxic) culture conditions, and its effects on hNSC self-renewal and differentiation were investigated [37]. The application of microfluidic devices have been demonstrated in wide areas of neuroscience research such as the study of neurite response to growth factor gradient [43], testing of neurotoxic effect of amyloid beta proteins [27], neurotoxicity testing in co-culture of neurons and astrocytes [44]. However, these studies were all based on the use of primary neurons and studies implementing NSCs are limited only to the investigation of stem cell differentiation and migration. Issues such as air bubble trapping and clogging of microchannels from cells also pose limitations for high-throughput application of this platform. For these reasons, limited work specific to developmental neurotoxicity has been applied using this platform.

1.2.3. Cellular Microarrays

Cellular microarray technology is a miniaturized platform consisting of 3D cell spots encapsulated in a hydrogel matrix on glass slides or plastic chips (**Figure 1.2)**. The

microarray platforms have already found their niche in various applications such as *in vitro* testing of drug candidates and their metabolites for metabolism-induced toxicity [45], [46], screening of anticancer drug efficacy [47], and stem cell differentiation and toxicity [48][49]. For example, Fernandes *et al.* demonstrated the utility of 3D cell-based microarray platform for the study of embryonic stem cell differentiation with the combination of retinoic acid and fibroblast growth factor-4 (FGF-4) [48]. However, it is only recently that this platform was applied for neurotoxicity testing with hNSCs [26][49].

(A)

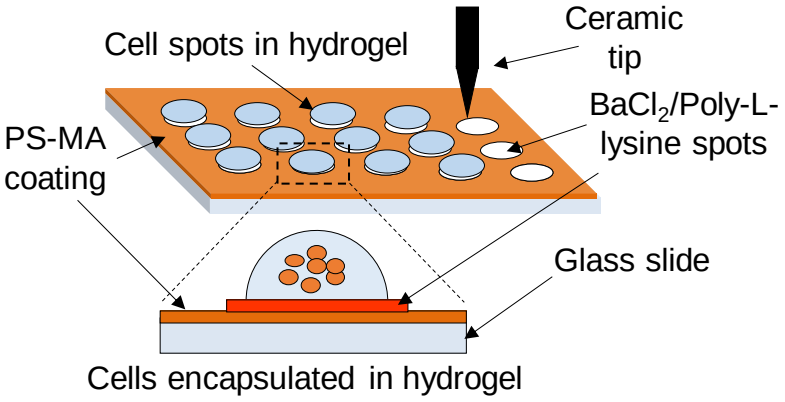

(B)

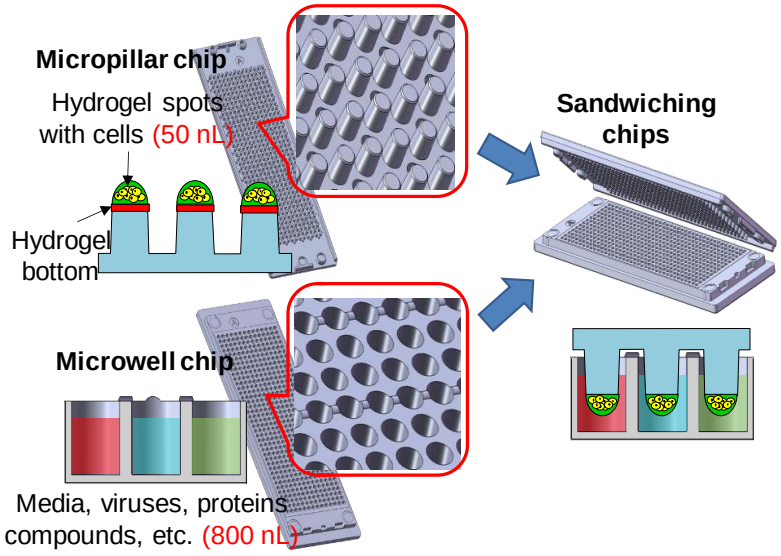

Figure 1.2. (A) Cellular microarrays on a functionalized glass slide. A mixture of cells and hydrogel precursor is printed on a glass slide coated with poly(styrene-co-maleic anh ydride) (PS-MA). Various polymer coating is done on top of the PS-MA coating to attach different hydrogels to the glass slide. Cells are encapsulated in a hydrogel matrix, forming 3D structures after gelation (which occurs via various mechanisms). **(B) Cellular microa rrays on a micropillar/microwell chip platform.** Cells mixed with hydrogel are printed on top of the micropillar chip. After gelation, the micropillar chip containing cells encaps ulated in hydrogel is sandwiched with a complementary microwell chip containing growt h media or other reagents. (*Farrel, K., Joshi, P., Roth, A., Kothapalli, C.R., Lee, M.Y., High-thr oughput screening of toxic chemicals on neural stem cells, Human Stem Cell Toxicology, Royal S ociety of Chemistry, 31-63 (2016))*

Apart from the above mentioned platforms, toxicity testing in NSCs have been performed using various other culture platforms such as cell-culture flasks [50] and petri dishes [51]. The convenience of culturing NSCs and the flexibility to modify the culture conditions m ay drive researchers to use simple cell culture flasks and dishes. For example, Demir and Laywell [50] used culture flasks for testing neurotoxicity of azidothymidine (AZT), an an ti-HIV drug, in which neural colony-forming cell (NCFC) assay was performed along wit h drug treatment. Long-term administration of AZT was found to be associated with pertu rbations in both proliferative capacity and neurogenesis [50]. In another example, Bai *et a l.* investigated the neurotoxic effects of ketamine in hNSCs and neurons on petri dishes an d demonstrated that short term exposure of ketamine increased hNSC proliferation, where as long-term exposure caused apoptosis in neurons without affecting hNSCs [51].

1.3.Representative cell-based assays for neurotoxicity assessment

Evaluation of DNT in an *in vitro* system possess challenge due to the dependency of adverse effect of toxicants on not only the dosage and duration of exposure but also on the developmental stage of the brain at the time of exposure [6], [52]. In addition,

mimicking the complex physiological organization of the nervous system with network of several cell types in an *in vitro* system is a major hurdle in implementing *in vitro* cell-based assay systems for DNT testing [53]. For any *in vitro* model to be highly predictive, it should recapitulate the basic processes involved in CNS development such as proliferation, migration, differentiation, and synaptogenesis. Therefore, endpoints such as cell viability, apoptosis, proliferation, differentiation, migration, and neurite outgrowth are commonly used to evaluate neurotoxicity [25], [28], [30], [54].

Current *in vitro* methods for neurotoxicity testing have been developed utilizing various cellular models such as immortalized cell lines, neural stem cells (NSCs), and primary cells from both rodent and human species. Primary cells are limited in their ability to proliferate and differentiate, and transformed cell lines derived from tumors such as PC12 cell lines (rat pheochromocytoma) and B50 cell lines (rat neuroblastoma) do not represent the native neural cells [55]. In addition, species-specific differences exist between rodents and humans in terms of sensitivity to toxins [25], [30]. Therefore, human NSCs are highly desirable for developing a predictive model system for developmental neurotoxicity assay due to its ability to self-renew and to differentiate into neurons, astrocytes and oligodendrocytes [8], [26], [56]. Various assays have been developed to evaluate neurotoxicity in NSCs which are summarized in **Table 1.**

Table 1. Conventional *in vitro* assays used for neurotoxicity screening in NSCs.

Application	Assays/Endpoints	Reference
Generation and assessment of neurons for drug screening	Differentiation, cell viability, mitochondria, nuclei tracking	[57]
HTS of neurotoxic compound	Cell viability, cellular morphology	[25]
Evaluate the influence of cell-ECM interaction on response to toxic compounds	Viability, proliferation, differentiation	[28]
Investigating MeHg-induced cytotoxicity pathway	Proliferation, western blot analysis for apoptosis, autophagy, differentiation marker	[32]
Investigating the mechanism involved in CPF-induced neurotoxicity in NSC	Viability, cytotoxicity, intracellular ROS and malondialdehyde (MDA) measurement, nuclear morphology, western blot analysis	[29]
Determining the toxic effects of Ag-NPs in NSCs	Viability, cytotoxicity, proliferation, apoptosis, oxidative stress	[30]
HTS of chemical-induced toxicity	Proliferation, apoptosis, viability	[31]
Quantification of neurite growth in high-density cultures for toxicity detection	Viability, algorithm for neurite identification, western blot analysis	[54]
HTS of neurotoxic compounds	Viability, proliferation, western blot analysis of marker proteins, immunofluorescence assay	[26]
Evaluate the neurotoxic effect of AZT drug	NCFC assay, neurosphere assay, proliferation, neurogenesis, SAβGal+ labeling	[50]

Abbreviations: extracellular matrix (ECM), methylmercury (MeHg), chlorpyrifos (CPF), r eactive oxygen species (ROS), silver nanoparticles (Ag-NP), azidothymidine (AZT), neur al colony-forming cell (NCFC), senescence-associated β-galactosidase (SAβGal) (*Farrel, K., Joshi, P., Roth, A., Kothapalli, C.R., Lee, M.Y., High-throughput screening of toxic chemicals on neural stem cells, Human Stem Cell Toxicology, Royal Society of Chemistry, 31-63 (2016))*

1.4. Neural stem cells (NSCs) and 3D culture

Human *in vitro* neuronal cultures derived from NSCs have been intensively studied over the past decade as they are self-renewable, and can be differentiated into several neuronal and glial cell types [6], [56]. NSCs have been identified in several regions of the

human brain in all stages of development [58]. A substantial population of NSCs are present in ventricular and subventricular zones (VZ and SVZ, respectively). Studies in rat embryogenesis CNS models have shown that NSCs compose most of the neural crest and around 50% of the spinal neural tube [59]. NSCs have the capability to self-renew and differentiate into neurons, astrocytes, and oligodendrocytes and therefore play a critical role in the developing embryonic nervous system where the ability for self-renewal is important for normal functions, such as learning, memory, and response to injuries. NSCs expand and maintain an undifferentiated phenotype in the presence of epidermal growth factor (EGF) and/or basic fibroblast growth factor (bFGF), and differentiate into neuronal and glial lineages upon the removal of these growth factors [60]. The proliferation, differentiation, and migration of NSCs are crucial in human brain development; disturbance of which has been linked to neurodevelopmental disorders [8], [61]. Therefore, NSCs can be used to model neurodegeneration and are considered as the most suitable cells for DNT testing [62], [63].

NSCs derived from induced pluripotent stem cells (iPSCs), the NIH approved H9 (WA09) hESC line, or cells derived from human fetal brain tissue immortalized *via* retroviral transduction with the myc oncogene (e.g., ReNcell VM, ReNcell CX) are commercially available from vendors including Life Technologies, Alstem, and EMD Millipore. In addition, NSCs are also directly harvested from either embryonic or adult mammalian brain tissue using established protocols [64]. Due to the efficient harvesting and expansion of these cells, they have been successfully implemented as models for *in vitro* DNT tests [65]. Moreover, NSCs are highly sensitive to neurotoxicants, as compared to other neural cell types [53], [66].

It is now widely accepted that cells cultured in conventional two-dimensional (2D) systems differ from three-dimensionally (3D) cultured cells in terms of their morphology, physiology, protein/gene expression, and metabolism [67]–[71]. Stem cells are known to lose phenotypic properties in 2D monolayer culture due to the lack of intercellular contacts and interactions thereby restricting the formation of *in-vivo* like tissue structures [67], [68], [70], [71]. In addition, important biological cues provided to cells by the ECM in response to external stimuli are also missing in 2D grown cells.

On the other hand, 3D cell culture have been known to maintain normal cell function such as differentiation, migration, and proliferation [72], [73] and have further been shown to recapitulate *in vitro* brain tissue physiology and microenvironmental conditions [6], [74], [75]. In addition, complex tissue structures can be developed in controlled conditions with the combination of 3D cell culture technology and the knowledge on stem cell differentiation. Efforts have been made towards developing 3D cell culture platform capable of maintaining specific *in vivo*-like biochemical and morphological features of human cells [13]. For example, Pasca *et al.* generated a laminated cerebral cortex with spheroid culture of pluripotent stem cells demonstrating electrophysiologically mature neurons from various cortical layers [76]. Likewise, Kim *et al.* developed a model system for characterization of Alzhiemer's disease using 3D culture of neural stem cells [77]. Therefore, a 3D cellular model with NSCs enhances the understanding of the molecular and cellular mechanisms underlying DNT/NT and serves as a powerful tool for assessing the impact of chemical exposure on developing brain [13], [78].

1.5. High-throughput, high-content imaging (HCI) platforms for neurotoxicity assessment

There is an urgent need to develop *in vitro* neurotoxicity testing system which are high-throughput, economically-feasible, and highly-predictive [8]. However, due to the challenge in mimicking the complexity of the CNS, there have been limited development in terms of high-throughput *in vitro* assays for screening toxic chemicals for their effect on developing nervous system. Development of high-throughput screening (HTS) assays utilizing hNSCs will therefore prove to be beneficial in assessing the chemical toxicity on stem cells and their differentiated lineages, providing a predictive model system for evaluating neurotoxicity [26]. Several *in vitro* cell-based assays have been developed with NSCs to study the toxic effect of various neurotoxicants; however, only a few of them have been able to demonstrate HTS capability for neurotoxicity screening. For example, Malik *et al.* developed a 96-well *in vitro* cell-based assay where 2000 compounds including drugs, natural products, and bioactive compounds were tested on human NSCs and rat cortical mixed cells with results highlighting species-specific differences in the toxicity of the compounds [25]. Nearly a hundred of these compounds showed significant toxicity to hNSCs without affecting rat cortical mixed cells. This HTS assay was built on an *in vitro* model developed by Efthymiou *et al.* to culture human NSCs and differentiate into neurons and astrocytes for HTS application in drug discovery [57].

Conventional high-throughput cell-based assays implemented for toxicity screening in NSCs evaluates a single endpoint involved in decreased cellular health or death. This approach often lacks the ability to provide predictive information of the NSC responses *in vivo* against toxic chemicals and drug candidates, which is critical to reduce

the high attrition rate in downstream drug discovery pipelines and determine the toxicity of environmental toxicants [67], [79]. Modeling the functional disturbances manifested by neurotoxicity *in vitro* possess a big hurdle in developing a highly-predictive assay for neurotoxicity assessment [12]. Based on the knowledge that impairment in the development of nervous system is the combined effect of disturbances/impairment in various neuro-developmental processes/endpoints [13], [80], the screening of large number of neurotoxic chemicals require characterization of those chemicals based on their biological activity i.e. the ability to trigger an impairment of specific end points. This can be achieved by investigating the effects of chemicals at the molecular and cellular level implementing high-content imaging (HCI) assays with particular emphasis on studying the mechanisms of neurotoxicity [81]–[85].

HCI assays are high-throughput, automated, cell-based assays that provide information on multiple properties of individual cells simultaneously by utilizing several fluorescent dyes thereby enabling a systematic and accurate evaluation of neurotoxicants [86], [87]. HCI assays are capable of analyzing numerous cellular functions and features such as cell growth, cell viability/cytotoxicity, nuclear morphology, apoptosis/necrosis, mitochondrial membrane potential, oxidative stress, intracellular calcium levels, and glutathione levels at the individual cell level which enables us to understand the mechanism of action of drug candidate and toxic chemicals [88], [89]. Various fluorescent probes/reagents are used to label different parameters for example Hoechst 33342 (ex. 361 nm/em. 497 nm) for nuclear morphology and cell count, calcein AM (ex. 495 nm/em. 515 nm) and propidium iodide (PI) (ex. 535 nm/em. 620 nm) for cell viability, tetramethyl rhodamine methyl ester (TMRM, ex. 545 nm/em. 575 nm) for mitochondrial membrane

potential (MMP), fluo-4 AM (ex. 490 nm/em. 520 nm) for intracellular calcium levels, YO-PRO-1 (ex. 490 nm/em. 510 nm) for apoptosis, monochlorobimane (mBCl, ex. 380 nm/em. 460 nm) for glutathione levels, and H_2DCFDA (ex. 495 nm/em. 527 nm) for oxidative stress damage [88], [90]–[93]. The fluorescent dyes/reagents target specific organelles or function and does not interfere with global physiological conditions of cells.

HCI assays have been implemented on various cellular models such as primary cells [94], immortalized cell lines [88], and stem cells [95] for investigating the toxic effects of various drug compounds, nanoparticles and environmental chemicals in human organs. Although there has been some progress in developing HCI assays to assess neurotoxicity, most of the assays are based on differentiated neuronal cell models [96]–[98] and does not correlate well with potential *in vivo* neurotoxicity mechanisms. Furthermore, conventional 3D cell culture systems are not amenable to high-throughput platform mainly due to difficulty in handling large volume of viscous solutions and acquisition of 3D-cultured cell images. For example, dispensing the mixture of cell suspension and viscous hydrogel and changing growth media over time without affecting the consistency and reproducibility in 96-well plate is a challenging task [70]. Moreover, the cost of reagents and compounds in conventional 3D culture system limits the number of assays that can be performed for HCI [99]. Image acquisition and processing of 3D cells on polymer scaffolds pose significant challenges due to growth of cells in multiple focal plane. This issue is addressed to some extent with confocal microscopy followed by 3D image reconstruction, however, with the compromise in throughput. In addition, some polymer scaffolds are inadequate for imaging due to their opaque nature. Few HCI assays,

therefore, have been implemented on 3D culture system due to the above-mentioned limitations of 3D cell culture systems for HTS.

HTS of large libraries of toxic chemicals for prediction of neurotoxicity requires miniaturization as it offers several advantages such as reduced sample volume, decrease in cost, and an increase in efficiency over contemporary macro-scale cell culture technology such as 3D NSC cultures in 96-well plates [46], [47]. Cellular microarrays based on a micropillar chip and a complementary microwell chip have recently been developed for high-throughput cell based assays such as 3D culture of mammalian cells, enzymatic reactions, viral infection, and compound screening [46], [47]. Cellular microarrays on the chip offers several advantages in HTS of compound libraries assays as they require extremely small amount of cells, natural and synthetic hydrogels or extracellular matrices (ECMs), growth factors, compounds, and reagents for 3D cell cultures [46], [47]. Reduction in assay volume and reagent consumption further facilitates the use of expensive hNSCs, thereby leading to enhanced predictability of *in vivo* responses towards toxicants [100]. Moreover, the image acquisition period is shorter and the process in itself becomes simpler due to the thin depth of focus position of samples, further leading to increased signal-to-noise ratios [101]. Varieties of cell culture conditions and individual drugs/mixtures of drugs in combinations can be tested, making it well suited for early stage HTS of compound libraries. In addition, miniaturized 3D cell culture on the chip can provide a microenvironment that simulates *in vivo* ECM conditions, and thus help maintain biochemical functions and morphological features similar to *in vivo* human tissues [102]. Therefore, high-throughput microarray platforms with HCI can be an attractive tool for studying the NSC response against large library of neurotoxicants.

The goal of our research is to develop 3D bioprinting chip platforms for HTS of compounds including drug candidates and environmental toxicants for mechanistic toxicology and chemical metabolism with organotypic cells. Specifically, to overcome the limitations of existing HTS technologies for neurotoxicity and enhance predictability of compound toxicity *in vivo*, we proposed to construct physiologically-relevant cellular microarrays in 3D using human NSC cultures and elucidate mechanistic toxicity by using HCI techniques, all in a high-throughput fashion.

The specific aims of this project are to:

1) ***Develop three-dimensionally (3D) cultured, neural stem cell (NSC) microarrays for high-throughput assessment of developmental neurotoxicity.***
2) ***Establish high-throughput ion channel and ABC-transporter assays on 3D-cultured NSCs for neurotoxicity assessment.***
3) ***Establish high-content imaging (HCI) assays on 3D NSC microarrays to investigate mechanistic profiles of toxicity by compounds and their metabolites.***

1. **Develop three-dimensionally (3D) cultured, neural stem cell (NSC) microarrays for high-throughput developmental neurotoxicity**

   We aim to establish 3D culture of NSC with extracellular matrices and synthetic hydrogels on the chip platform. High-throughput assessment of key variables critical for growth and induced differentiation of NSCs will be performed on the chip using recombinant lentiviruses with fluorescent NSC biomarkers.

2. **Establish high-throughput ion channel and transporter assays on 3D-cultured NSCs for the neurotoxicity assessment.**

We aim to establish high-throughput ion channel and transporter assays on 3D NSC microarrays to evaluate whether model compounds interact with cell surface receptors such as ion channels and transporters on NSCs.

3. **Establish high-content imaging (HCI) assays on 3D-cultured NSCs for the assessment of mechanistic neurotoxicity by the test compounds and their metabolites.**

   We aim to establish HCI assays on 3D NSC microarrays to evaluate toxic effects of various compounds and their metabolites within NSCs. For this, we will first establish high-content imaging (HCI) assays in 3D-cultured NSC microarrays for the assessment of mechanistic neurotoxicity which will be combined with human liver cell spheroids expressing cytochrome P450 enzyme to demonstrate metabolism-mediated neurotoxicity.

CHAPTER II

OPTIMIZATION OF 3D-CULTURED NEURAL STEM CELL (NSC) MICROARRAYS FOR HIGH-THROUGHPUT DEVELOPMENTAL NEUROTOXICOLOGY

Pranav Joshi[a#], Kyeong-Nam Yu[a#], Soo-Yeon Kang[a], Seok Joon Kwon[b], Paul S. Kwon[b], Jonathan S. Dordick[b], Chandrasekhar R. Kothapalli [a*], Moo-Yeal Lee[a*]

[a]Department of Chemical & Biomedical Engineering, Cleveland State University, Cleveland, Ohio, OH 44115-2214, USA

[b]Department of Chemical and Biological Engineering, Rensselaer Polytechnic Institute, Troy, NY 12180, USA

Accepted (21 July 2018) in Experimental Cell Research

2.1. Introduction

Exposure to toxic compounds during early fetal development has been linked to various neurodevelopmental disorders such as attention deficit disorders, autism, cognitive and behavioral alterations, and mental retardation [3], [13], [103]. Conventional animal models for developmental neurotoxicity (DNT) testing are expensive, time-consuming low-

throughput, subject to genetic and age-related variability, and often poorly correlate with human toxicity [104]. Species-specific differences exist in the microarchitecture of mammalian brains, and rodents, for example, are predictive of human neurotoxicity in only half the cases [9]. In addition, a substantial number of drug candidates have failed in clinical trials even after successful animal studies. Therefore, various alternatives have been pursued, including embryonic stem cells [105]–[107], neural stem/progenitor cells (NSCs) [28], [108], [109], primary neuronal cells [97], [110], [111], and immortalized neuronal cell lines [96], [112], [113] to reduce the use of animal models and provide predictive developmental neurotoxicity. The focus of these alternatives is the development of *in vitro* assay platforms for mechanism-based, target-specific endpoints to evaluate the human health risk of various chemicals and environmental toxicants [8], [16], [61].

NSCs have been identified in several regions of the human brain in all stages of developmental [58], and are capable of self-renewal and differentiation into neurons, astrocytes, and oligodendrocytes. NSC proliferation, differentiation and migration are crucial in human brain development; disturbance of which has been linked to neurodevelopmental disorders [8], [61]. Therefore, development of an *in vitro* assay system for assessing self-renewal and differentiation of NSCs is essential not only to identify compounds that can cause neurodevelopmental disorders, but also to restrict the use of those chemicals [3], [114], [115].

High-throughput assessment of NSC viability in an *in vitro* system, characterization of its self-renewal and differentiation into specific lineages, and real-time monitoring with quantification of the differentiation process are critical to implement *in vitro* cultures of NSCs for applications in tissue engineering, disease modeling, and drug development. NSC

differentiation is typically determined by monitoring changes in cell morphology and assessing neural and glial lineage-specific biomarkers *via* often nonspecific immunofluorescence assays. In addition, measuring the efficiency of NSC differentiation under different culture conditions and as a function of time is tedious, inherently low-throughput, and involves destruction of analyzed samples [116].

An *in vitro* model system for DNT testing should be capable of mimicking *in vivo* human neurodevelopment. Assays carried out in two dimensional (2D) cell cultures are limited in terms of cell-cell and cell-matrix interactions that are crucial for cell-signaling and gap-junction connection formation, as well as for promoting proliferation and differentiation [8]. To address these limitations, we have developed a miniaturized three-dimensional (3D) NSC microarray platform for high-throughput assessment of cell viability. This platform exploits a promoter-reporter assay system that generates stable mCherry- and EGFP-expressing NSCs for high-throughput characterization of self-renewal and differentiation. Using this high-throughput, high-content *in vitro* platform we demonstrated high-throughput assessment of cell viability, self-renewal and lineage-specific differentiation of 3D NSC culture in spontaneous and directed differentiation methods, thereby eliminating the need to use low-throughput immunofluorescence staining to monitor the developmental stages of NSCs.

2.2. Materials and Method

2.2.1. Human NSC cultures

Human NSCs (ReNcell VM; EMD Millipore, Burlington, MA, USA) were passaged in a complete ReNcell medium (ReNcell NSC maintenance medium, EMD Millipore) supplemented with 20 ng/mL epidermal growth factor (EGF, EMD Millipore),

20 ng/mL basic fibroblast growth factor (bFGF, EMD Millipore), and 1% (v/v) penicillin/streptomycin (Thermo Fisher, Waltham, MA, USA), on laminin-coated, tissue culture-treated, T-75 flasks in a humidified 5% CO_2 incubator at 37 °C (Heracell 150i, Thermo Fisher). The complete medium was replaced every two days with a freshly prepared complete medium until the cells reached 90% confluency, after which they were detached with accutase (EMD Millipore), suspended in ReNcell NSC maintenance medium, and centrifuged. The resulting cell pellets were resuspended in the complete medium, cell concentration determined, and 1.5×10^6 cells were seeded on freshly prepared laminin-coated T-75 flasks.

2.2.2. Preparation of 3D-cultured ReNcell microarrays

All chemicals and reagents were from Sigma-Aldrich (St. Louis, MO, USA), unless specified otherwise. For 3D microarray culture of ReNcell VM, micropillar chips (Medical & Bio Device (MBD) Korea, Suwon, Republic of Korea) were coated with 0.01% (w/v) poly(maleic anhydride alt-1-octadecene) (PMA-OD) and dried. A mixture of poly-L-lysine (PLL) and barium chloride ($BaCl_2$) was prepared at a final concentration of 0.0033% (w/v) PLL and 16.66 mM $BaCl_2$ in sterile deionized water and printed on top of the PMA-OD coated micropillar chips at a volume of 60 nL, with an S+ Microarrayer (Advanced Technology Inc. (ATI), Incheon, Republic of Korea) and dried. In parallel, a mixture of PLL and $CaCl_2$ was prepared in an analogous manner at a final concentration of 0.0033% (w/v) PLL and 25 mM $CaCl_2$ in sterile deionized water and printed on top of the PMA-OD coated micropillar chips. The complete medium was printed into microwell chips (MBD Korea) at a volume of 950 nL and stored in a humidified chamber for later use.

ReNcells were encapsulated in either alginate alone or in a mixture of alginate and

growth factor reduced (GFR) Matrigel® (Corning, Corning, NY, USA). For the former, ReNcell suspension was mixed with low-viscosity alginate, prepared from sodium alginate powder reconstituted in sterile deionized water, to achieve a final cell concentration of 6×10^6 cells/mL in 0.75% (w/v) alginate. Similarly, for encapsulation in a mixture of alginate and GFR Matrigel, cell suspension was mixed with alginate and GFR Matrigel to achieve a final cell concentration of 6×10^6 cells/mL in a mixture of 0.75% (w/v) alginate and 1 mg/mL GFR Matrigel and stored on ice until printing. The cell-hydrogel mixtures were then printed on top of dried PLL/$BaCl_2$ or PLL/$CaCl_2$ layers **(Figure 2.1)**, while maintaining the slide deck (loaded with the micropillar chips) at 7 °C. After incubating the chips on the slide deck for 2 mins for gelation, the micropillar chips with cell spots were sandwiched with the microwell chips containing 950 nL of the complete medium. The sandwiched micropillar and microwell chips were then stored in a humidified petri dish and incubated at 37 °C in the 5% CO_2 incubator.

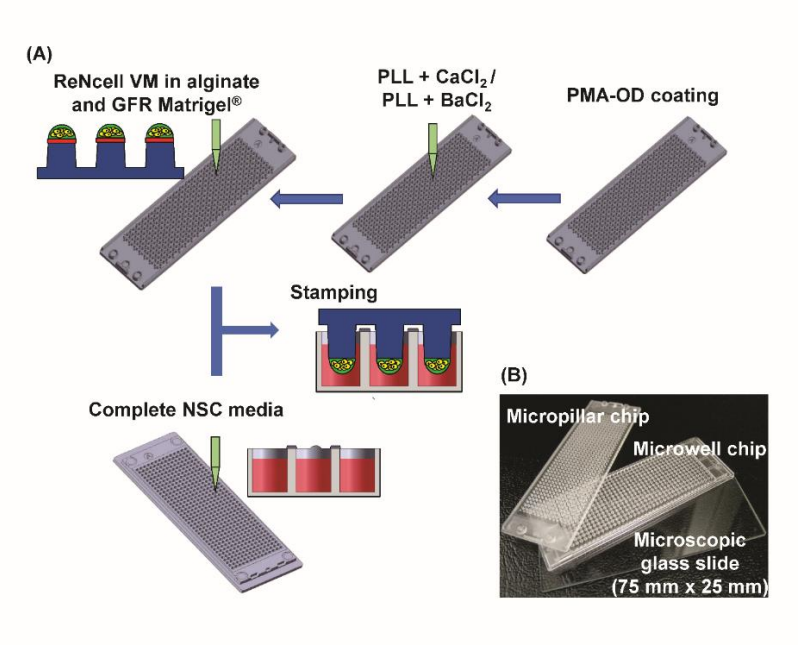

Figure 2.1. Schematic diagram of 3D NSC microarray culture. (A) ReNcell VM in a mixture of alginate and GFR Matrigel was printed on the functionalized micropillar chips, and the complete ReNcell VM medium at a volume of 950 nL was printed into the microwell chips. After hydrogel gelation, the micropillar chip with ReNcell VM spots was sandwiched with the microwell chip containing the complete medium for 3D cell culture. (B) Picture of the injection-molded micropillar and the microwell chips (25 mm x 75 mm) used in this study is shown with respect to microscopic glass slide.

2.2.3. Cell viability assay

Viability and spheroid formation of ReNcell in 3D microarray culture were assessed using Live/Dead® viability/cytotoxicity kit for mammalian cells (ThermoFisher). Briefly, 3D-cultured ReNcells on the micropillar chips were separated from the microwell chips and rinsed twice with a saline solution containing 140 mM NaCl and 20 mM $CaCl_2$. The micropillar chips were then stained with 0.5 μM calcein AM and 1 μM ethidium homodimer-1 at room temperature for an hour, rinsed twice with the saline solution, and dried in the dark for at least 3 hours to ensure complete drying of the micropillar chips. Dried micropillar chips were then scanned with S+ scanner (ATI), an automated epifluorescence microscope developed for rapid image acquisition at 15 frames per second (FPS). Green and red fluorescent cell images were obtained at 4X magnification with the Olympus UPLFLN 4X (numerical aperture (NA) 0.13, f-number 26.5, and depth of field (DOF) ~ 32.3 μm) (Olympus, Tokyo, Japan) and a green filter (XF404 from Omega Optical) and a red filter (TxRed-4040C from Semrock). The images were batch-processed using ImageJ (NIH) to extract fluorescence intensity from the entire cell spots on the micropillar chips. The fluorescence intensities were plotted using SigmaPlot software ver. 12 (Systat Software Inc., San Jose, CA, USA).

2.2.4. Construction of dual reporter lentiviral vectors for the reporter gene assay

To construct lentiviral vectors having a dual reporter system, the promoter regions of the human GFAP gene (ref, PMID: 19457099) and the synapsin I gene (ref, PMID: 19318117) were amplified using phGFAP-fLuc (Addgene 40589) and pLV-hSyn-RFP (Addgene 22909) plasmids, respectively. The MBP (chr18-:72859280-72857953) and SOX2 promoters (chr3+:182911368-182912675) were amplified from the genomic DNA of ReNcell VM. The PCR products of each promoter and EGFP gene were assembled into pLV-mCherry (Addgene 36084) *via* in-fusion assembly of multiple fragments (ref, PMID: 17907578), resulting in constructing pLV-mCherry-hGFAP-EGFP, pLV-mCherry-hSyn-EGFP, pLV-mCherry-hMBP-EGFP, and pLV-mCherry-hSOX2-EGFP, respectively.

2.2.5. Preparation of recombinant lentiviruses

Recombinant lentiviruses were prepared using 2nd generation packaging systems, which require a single packaging plasmid (psPAX2, Addgene 12260), an envelope plasmid (pMD2.G, Addgene 12259), and our transfer vectors including pLV-mCherry-hGFAP-EGFP, pLV-mCherry-hSyn-EGFP, pLV-mCherry-hMBP-EGFP, or pLV-mCherry-hSOX2-EGFP. Briefly, HEK293T cells (ATCC® CRL-3216™, Manassas, VA, USA) were grown in T25 flasks in DMEM supplemented with 10% (v/v) FBS and 1% (v/v) penicillin/streptomycin until 50-60% confluence was achieved. Two viral packaging plasmids (pVSV-G for envelope and psPAX2 for packaging) and one transfer plasmid carrying a gene for each specific biomarker (pLV-mCherry-hSOX2-EGFP for self-renewal, pLV-mCherry-hSyn-EGFP for neurons, pLV-mCherry-hGFAP-EGFP for astrocytes, and pLV-mCherry-hMBP-EGFP for oligodendrocytes) were mixed and added to HEK293T cells and incubated at 37 °C in the 5% CO_2 incubator. After 24 hours, the supernatant was

collected from T25 flasks and fresh DMEM was added to the cells. The supernatant was collected again after 3 days, pooled with the supernatant collected at day 1 and stored at -80 °C until further use. The transfer plasmid contains dual promoters (monomer cherry protein, mCherry and enhanced green fluorescent protein, EGFP), which enables ReNcell transduced with the lentiviruses to express mCherry under the control of CMV promoter, while EGFP is expressed only when the NSC-specific biomarkers are turned on. These recombinant viruses can be used to monitor self-renewal and differentiation of 3D-cultured ReNcell in high throughput on the micropillar/microwell chip platform.

2.2.6. Characterization of ReNcells cultured in 2D

ReNcells were seeded on laminin-coated tissue culture-treated T25 flasks at 7×10^5 cells/flask and incubated at 37 °C in the 5% CO_2 incubator. Once the cells reached 50-60% confluency, lentiviruses containing the reporter for SOX2, GFAP, synapsin1 or MBP were diluted in the complete medium without antibiotics and added to their respective flasks for infection. After overnight incubation, the lentivirus-containing medium was replaced with a freshly prepared complete medium containing antibiotics. Lentivirus-infected cells were grown until they reached 90% confluence, after which the cells were detached and suspended in the complete medium. For 2D culture in 96-well plates, tissue-culture treated flat-bottom 96-well plates were coated with laminin and lentivirus-infected cells were seeded at 5,000 cells/well with 24 replicates per cell type. After two days of culture in the complete medium, differentiation was induced by replacing the complete medium with a differentiation medium (i.e., ReNcell maintenance medium without EGF and bFGF). Differentiation was monitored over 21 days, with medium change every two days.

For 2D culture on the microarray chip platform, the micropillar chips were coated

with 75 µg/mL poly-L-lysine (PLL) for 2 hours at 37 °C, and then with 40 µg/mL laminin for 4 hours at 37 °C. Both lentivirus-infected and non-infected ReNcells in the complete ReNcell medium was printed directly into the microwell chips at 6×10^5 cells/mL and sandwiched with the PLL and laminin-coated micropillar chips. The sandwiched chips with the microwell chip on the top and the micropillar chip at the bottom were incubated overnight at 37 °C in the 5% CO_2 incubator, after which the spent medium was replaced with a fresh medium. The viability of non-infected ReNcell VM after two weeks of culture on the chip platform was assessed from live/dead staining with calcein AM and ethidium homodimer-1. For the assessment of differentiation in lentivirus-infected ReNcells, growth factors (EGF and bFGF) were removed after two days of incubation to induce NSC differentiation. Images were obtained over a period of 10 days to monitor cell differentiation with medium change every two days.

2.2.7. Immunofluorescence assays for comparison of ReNcell differentiation

Non-infected ReNcells were seeded on laminin-coated 96-well plates at 5,000 cells/well and incubated at 37 °C in the 5% CO_2 incubator. The cells were grown for 10 days in the complete medium and in the differentiation medium (without EGF and bFGF), with medium change every two days. The cells were rinsed briefly in 1× sterile PBS and fixed with 4% paraformaldehyde for 10 minutes at 37 °C. After fixation, cells were washed using 1× Tri-buffered saline (TBS) and blocked with 3% bovine serum albumin (BSA) in 1× TBS for 1 hour at 37 °C. The cells were then incubated overnight with their respective primary antibodies for specific biomarkers; SOX2, MBP, GFAP, and synapsin1 (Santa Cruz biotechnology, Dallas, TX, USA), which were diluted at 1:200 in the blocking solution. After overnight incubation with primary antibodies, fluorophore-conjugated secondary

antibodies – Alexa Fluor®488 anti-mouse and AlexaFluor® anti-goat Superclonal™ (Carlsbad, CA, Invitrogen) – were diluted at 1:200 in the blocking solution and added to the cells for 1 hour at room temperature. This was followed by 4′,6-diamidino-2 phenylindole (DAPI; Sigma-Aldrich) staining for 10 minutes at room temperature and image acquisition with an inverted fluorescence microscope (Axio Vert. A1, Zeiss, Germany).

2.2.8. Characterization of ReNcells cultured in 3D

For 3D cell culture, cell suspensions of lentivirus-infected ReNcells were encapsulated in a mixture of 0.75% (w/v) alginate and 1 mg/mL GFR Matrigel and printed on top of PLL/$CaCl_2$ coated micropillar chips. After gelation, the pillar chips were sandwiched with the microwell chips containing 950 nL of the complete medium and incubated at 37 °C in the 5% CO_2 incubator. ReNcells were cultured on the micropillar/microwell chip platform for four days, after which differentiation was induced by replacing the complete medium in the microwell chips with the differentiation medium. The cells were incubated in the differentiation medium for 7 days, with medium change every two days, and ReNcell differentiation was captured using a Zeiss Axio Vert. A1 inverted fluorescence microscope.

2.2.9. Differentiation of lentivirus-infected ReNcells in 2D and 3D cultures with compounds

To induce ReNcell differentiation in 2D and 3D cultures with additives, three differentiation media were prepared in the complete medium by supplementing with 30 ng/mL triiodothyronine (T3) for oligodendrocytes [117]–[121], 1% N2 supplement for

astrocytes [122]–[125], and 0.5 mM 3-iso-butyl-1-methylxanthine (IBMX) for neurons [126]–[128]. For differentiation in 2D culture on the chip, lentivirus-infected ReNcells in the complete medium were printed in the microwell chips at 3×10^6 cells/mL and sandwiched with PLL and laminin-coated micropillar chips. The sandwiched chips were incubated overnight at 37 °C in the 5% CO_2 incubator after which the spent medium was replaced with a fresh medium. After 4 days of incubation, monolayers of ReNcells on the micropillar chip were exposed to the differentiation medium individually for 7 days, with medium change every two days. For differentiation in 3D culture on the chip, lentivirus-infected ReNcells were encapsulated in a mixture of 0.75% (w/v) alginate and 1 mg/mL GFR Matrigel and printed on PLL/$CaCl_2$ coated micropillar chips. After gelation, the micropillar chips were sandwiched with the microwell chips containing the complete medium and incubated at 37 °C in the 5% CO_2 incubator. The cells were incubated for 4 days in the complete medium, with medium change every two days before inducing differentiation. Images of ReNcells in 2D and 3D cultures were obtained at two time-points – 4 days before and 7 days after differentiation with the S+ scanner.

2.2.10. Statistical analysis

All the values were expressed as mean ± SD. For each test condition, n = 126 biological replicates per pillar chip per experiment were studied, and three individual experiments were performed. Statistical analysis was performed with GraphPad Prism 5 (La Jolla, CA) and plotted in SigmaPlot 12 (San Jose, CA). For comparison between various culture conditions, statistical significance ($p < 0.01$) between various culture conditions was measured using a Student's t-test.

2.3. Results

2.3.1. Optimization of 3D ReNcell cultures on the micropillar/microwell chip platform

ReNcell VM was chosen due to its ability to self-renew and differentiate into neurons and glial cells, and for its commercial availability as a human dopaminergic neuroprogenitor cell line. These attributes make ReNcell a useful NSC model, although the v-myc oncogene immortalization by retroviral transduction may impact neural cell differentiation marker expression [129], [130]. Live/dead staining with calcein AM and ethidium homodimer-1 was performed to assess ReNcell viability and spheroid formation on the micropillar chips. The use of alginate hydrogel alone for 3D ReNcell cultures has previously been shown to induce lag-phase of growth [26]. ReNcells encapsulated in 0.75 % (w/v) alginate with 16.66 mM $BaCl_2$ as a crosslinker starting from day 1 of incubation showed a time-dependent decrease in cell viability indicating some degree of cytotoxicity (**Figure 2.2A**). On the other hand, the use of relatively nontoxic $CaCl_2$ when compared to $BaCl_2$ as a crosslinker resulted in significantly improved cell viability and increased 3D spheroid formation of ReNcells in alginate (**Figure 2.2A**). However, there was still an initial lag phase of cell growth in alginate-alone conditions even with $CaCl_2$ **(Figure 2.2B**). This problem was diminished by using a mixture of alginate and GFR Matrigel. Combining GFR Matrigel with alginate significantly increased cell viability, cell growth, and 3D spheroid formation over time on the micropillar chip, compared to the alginate-alone conditions. Since alginate derived from brown seaweed is inert and not degraded by cellular proteases, the mixture of alginate and GFR Matrigel provided strong mechanical support and cell-extracellular matrix (cell-ECM) interactions for long-term culture of ReNcell VM in 3D without any adverse effect on differentiation over two months

(data not shown). Adding 1 mg/mL GFR Matrigel in 0.75% (w/v) alginate greatly enhanced ReNcell VM viability on the micropillar chip over the 9-day cultures and supported formation of ReNcell VM spheroids compared to that within 0.75% (w/v) alginate alone. GFR Matrigel alone was not used as a matrix, as it was difficult to maintain sufficiently low temperatures in the micro-solenoid valves and tubes, and thus prevent unwanted gelation.

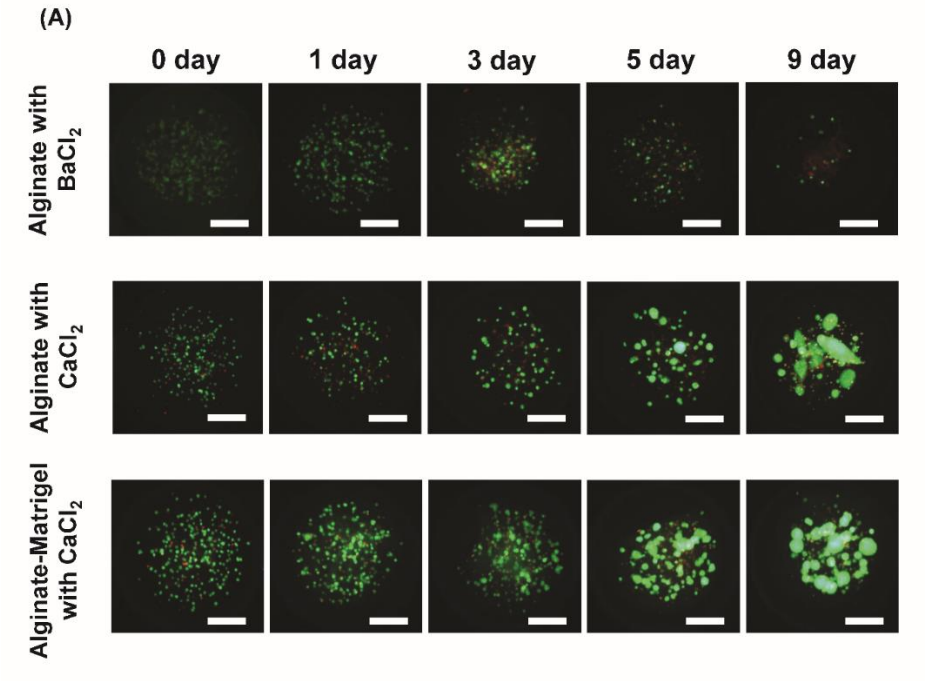

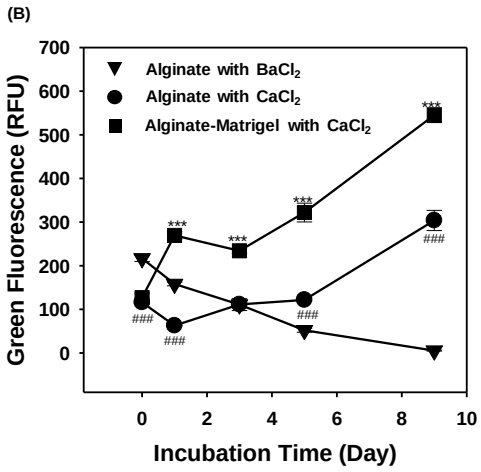

Figure 2.2. Optimization of 3D ReNcell culture conditions on the microarray chip platform. (A) Representative images of ReNcell VM encapsulated in 0.75% (w/v) alginate alone with $BaCl_2$, 0.75% (w/v) alginate alone with $CaCl_2$, and 0.75% (w/v) alginate and 1 mg/mL GFR Matrigel® with $CaCl_2$ on the micropillar chip. Cell viability was determined over a period of 9 days by live/dead staining with calcein AM and ethidium homodimer-1. The scale bar is 150 μm. Green dots from calcein AM staining represent live cells whereas red dots from ethidium homodimer-1 staining represent dead cells. **(B)** Fluorescence intensity extracted from ReNcell VM encapsulated in 0.75% (w/v) alginate alone with $BaCl_2$ (filled triangle), 0.75% (w/v) alginate alone with $CaCl_2$ (filled circle), and 0.75% (w/v) alginate and 1 mg/mL GFR Matrigel with $CaCl_2$ (filled square). Statistically significant fluorescence difference between alginate alone with $CaCl_2$ and alginate-GFR Matrigel with $CaCl_2$ conditions is indicated by *** for $P < 0.001$. The difference between the alginate-alone conditions with $BaCl_2$ and $CaCl_2$ was indicated by $^{###}$ for $P < 0.001$.

2.3.2. Assessment of self-renewal and differentiation via the promoter-reporter assay in 2D and 3D cultures

Recombinant lentiviruses were constructed carrying dual promoters, a mCherry gene for measuring viral gene transduction efficiency and an EGFP gene for determining the expression levels of four NSC-specific biomarkers, including SOX2 for self-renewal, MBP for oligodendrocytes, GFAP for astrocytes, and synapsin1 for neurons (**Figure 2.3**). Various multiplicities of infection (MOIs) were tested to identify the optimum concentrations of each lentivirus by FACS analysis (data not shown). While removing growth factors in the culture medium, real-time monitoring of self-renewal and differentiation of ReNcell VM was performed with the promoter-reporter assay system in 96-well plates over a 21-day period (**Figure 2.4**). Increased expression of MBP, GFAP, and synapsin1 was observed over this period with continued expression of SOX2. Differentiation of non-infected ReNcell VM into neurons, astrocytes, and oligodendrocytes was assessed in parallel, in laminin-coated 96-well plates over 10 days by using immunofluorescence assays (**Figure 2.5**). Expression of all three lineages was observed

over the 10 days period with increased expression of GFAP and synapsin1.

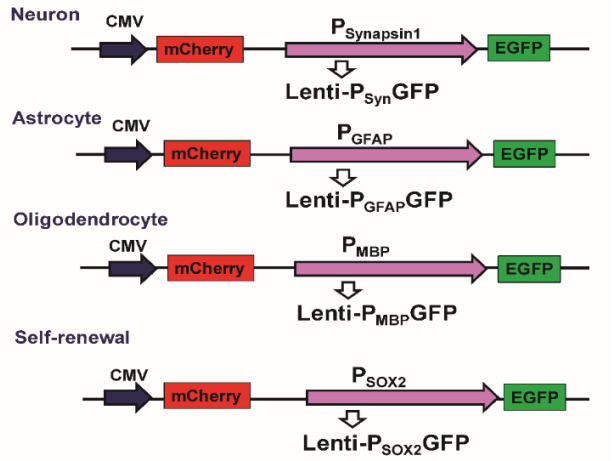

Figure 2.3. Construction of lentiviral vectors carrying promoter-reporter assay system for high-throughput assessment of ReNcell VM differentiation. The CMV promoter-driven mCherry gene is constitutively expressed in ReNcell VM, and EGFP gene are expressed under control of cell-type specific promoters. Four NSC-specific biomarkers, including SOX2, synapsin1, glial fibrillary acidic protein (GFAP), and myelin basic protein (MBP), were used to evaluate self-renewal, neuron differentiation, astrocyte differentiation, and oligodendrocyte differentiation, respectively. (*Lentiviruses constructed by Dr. Dordick's group at RPI*)

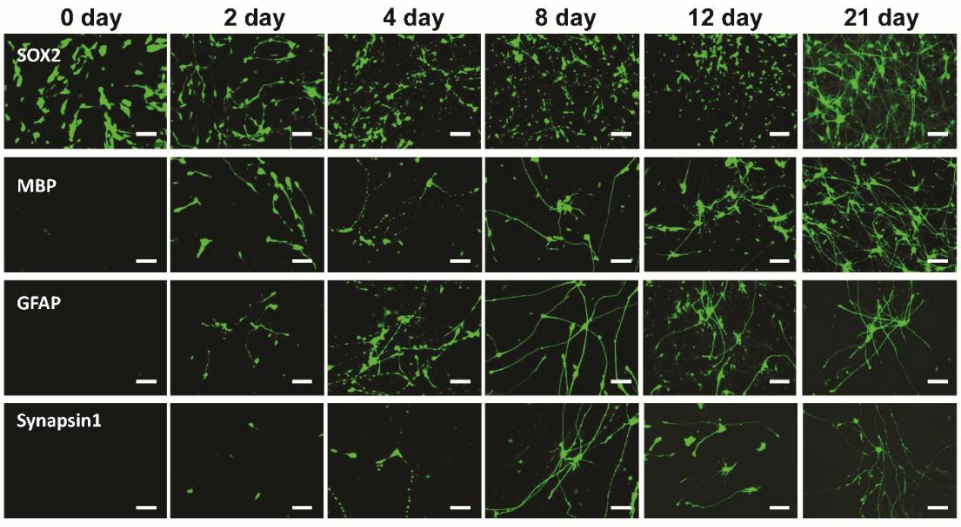

Figure 2.4. Promoter-reporter assay system for monitoring self-renewal and differentaition of lentivirus-infected ReNcell monolayers in 96-well plates. Monolayers of lentivirus-infected ReNcell VM were seeded in 96-well plates, and differentiation was monitored after the removal of growth factors (EGF and bFGF) over a period of 21 days through EGFP expression. The scale bar is 50 μm.

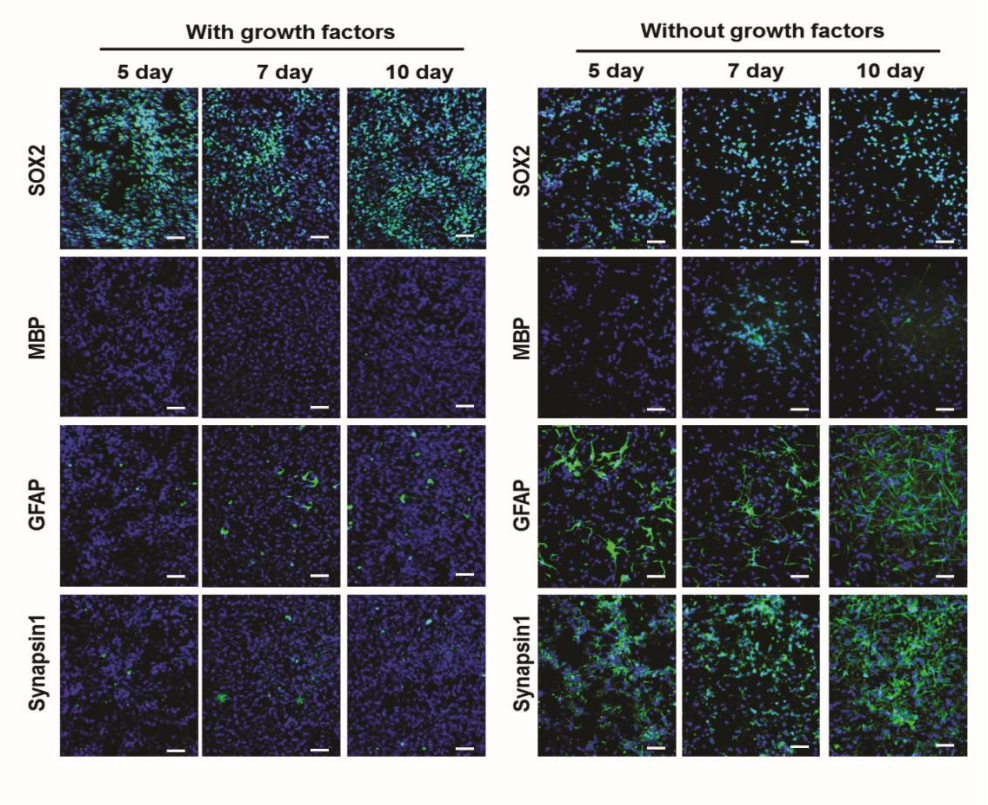

Figure 2.5. **Immunofluorescence assay for monitoring self-renewal and differentaition of non-infected ReNcell monolayers in 96-well plates.** Monolayers of ReNcell VM were seeded in 96-well plates, and the expression levels of lineage-specific markers were monitored after removal of growth factors (EGF and bFGF) over a period of 10 days through immunofluorescence staining with anti-SOX2, anti-MBP, anti-GFAP, and anti-synapsin1 antibodies. The scale bar is 50 μm. Blue dots indicate nucleus stained with DAPI, green fluorescence indicates the expression of the respective biomarkers.

Self-renewal and differentiation characteristics of ReNcell VM were further investigated in both 2D (**Figure 2.6**) and 3D (**Figure 2.7**) cultures on the micropillar/microwell chip platform. mCherry expression indicates live ReNcells infected with lentiviruses whereas EGFP expression indicates differentiation of ReNcells into specific lineages. The cells infected with the SOX2 promoter-reporter lentivirus demonstrated both EGFP and mCherry expression before differentiation, whereas the cells infected with MBP, GFAP, and synapsin1 promoter-reporter lentiviruses showed only

mCherry expression, indicating the self-renewal characteristics of ReNcell VM (**Figures 2.6B and 2.7**). EGFP expression in cells infected with MBP, GFAP, and synapsin1 promoter-reporter lentiviruses was observed only after differentiation. Out of the cell population, 36% were differentiated into oligodendrocytes quantified from the EGFP expression of MBP marker, 10% into astrocytes measured from GFAP marker expression, and 7.5% into neurons measured from synapsin1 marker expression in the 3D culture of ReNcell VM.

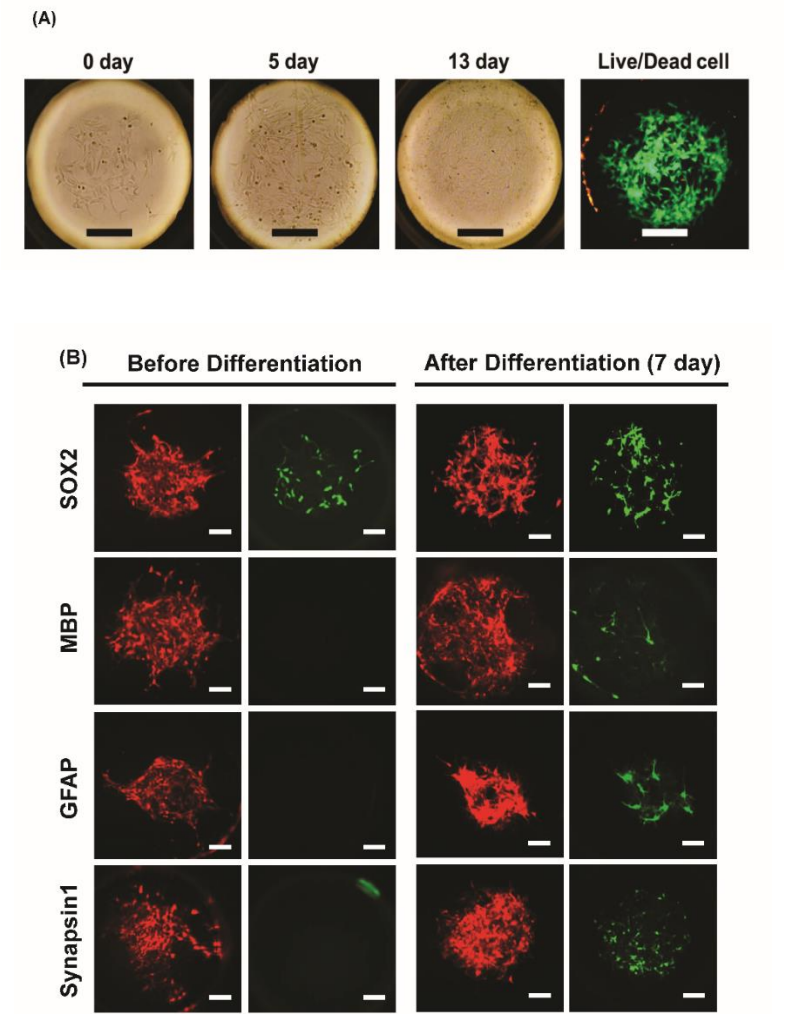

Figure 2.6. ReNcell monolayers cultured in 2D on the micropillar chip before and after infection with lentiviruses. (A) 2D-cultured ReNcells on the micropillar chip were monitored over time using brightfield and fluorescence microscopes. The cells were

stained with calcein AM for determining viability after two weeks of culture on the micropillar chip. The scale bar is 200 µm. **(B)** 2D-cultured ReNcells on the micropillar chip were infected with lentiviruses and monitored over time for self-renewal and differentiation. The red-colored cells indicate ReNcell VM infected with the lentiviruses. The green-colored cells represent ReNcell VM differentiated into respective lineages. The scale bar is 100 µm.

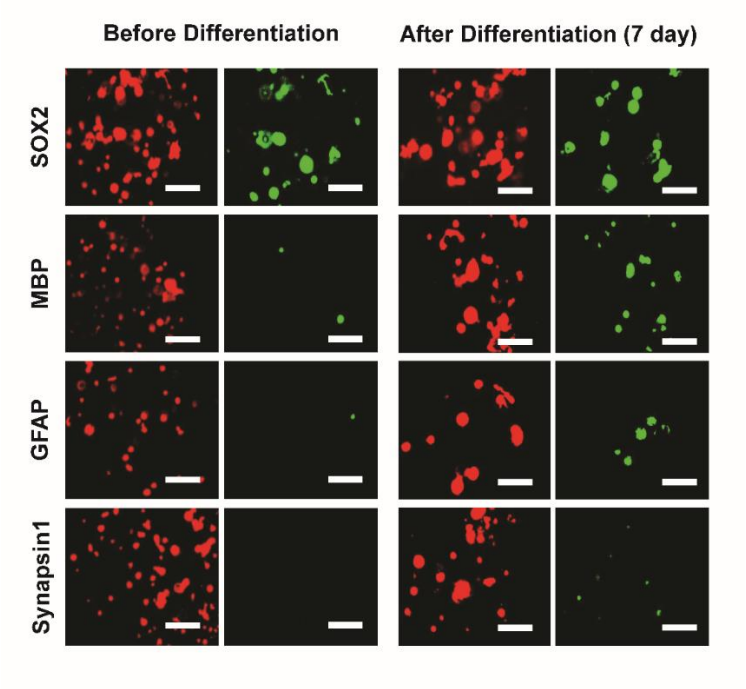

Figure 2.7. ReNcell VM cultured in 3D on the micropillar chip after infection with lentiviruses for self-renewal and differentiation. Lentivirus-infected ReNcell VM encapsulated in a mixture of 0.75% (w/v) alginate and 1 mg/mL GFR Matrigel was printed on the micropillar chip. Differentiation was induced by removing the growth factors (EGF and bFGF) in the growth medium. Images were obtained before and after differentiation (7 days) to determine the self-renewal and differentiation capability of ReNcell VM. The red-colored cells indicate the ReNcell VM infected with the lentiviruses, and the green-colored cells indicate ReNcell VM differentiation into respective lineages. The scale bar is 200 µm.

We further evaluated the robustness and reproducibility of our promoter-reporter assay by calculating the Z′ factor and the coefficient of variation (CV) [131], [132]. The calculated Z′ factors for both self-renewal and differentiation assays were between 0.5 (SOX2) and 0.8 (MBP), indicating that the promoter-reporter assay is highly robust; a Z′ factor between 0.5 and 1 is considered highly robust. Similarly, CV values were < 20%,

showing the reproducibility of the promoter-reporter assay. The CV value for the self-renewal assay was 17%, whereas it was 13% for MBP.

2.3.3. Compound-induced differentiation of 3D-cultured ReNcell microarrays with the promoter-reporter assay

After establishing the promoter-reporter assay for monitoring self-renewal and differentiation of ReNcell VM in the absence of growth factors, we assessed the differentiation of ReNcell VM in 2D and 3D cultures with compounds well known to direct NSCs into specific lineages. As a proof of concept, three compounds including T3, N2 supplement, and IBMX were used at a concentration that was known to direct NSCs into oligodendrocytes, astrocytes, and neurons, respectively. The complete ReNcell medium containing growth factors was supplemented with each of these compounds to prepare three different growth medium forumulations, which were added to ReNcell VM cultures after four days of pre-incubation with complete ReNcell medium. As a result, T3 induced differentiation of ReNcells into oligodendrocytes, as evidenced by EGFP expression in MBP lentivirus-infected cells (**Figure 2.8**). Similarly, the growth medium supplemented with N2 supplement and IBMX induced differentiation of ReNcells into astrocytes and neurons, respectively, which was evidenced by GFAP and synapsin1 expression, respectively, in lentivirus-infected cells. As the outcomes were monitored only over a period of 7 days after inducing diffferentiation, the level of EGFP expression was not particularly high in individual cultures. Nonetheless, the assessment of self-renewal and differentiation of ReNcell VM in both 2D and 3D cultures was observed without using cell fixation and immunofluorescence staining, thus representing a major advantage of the promoter-reporter assay system.

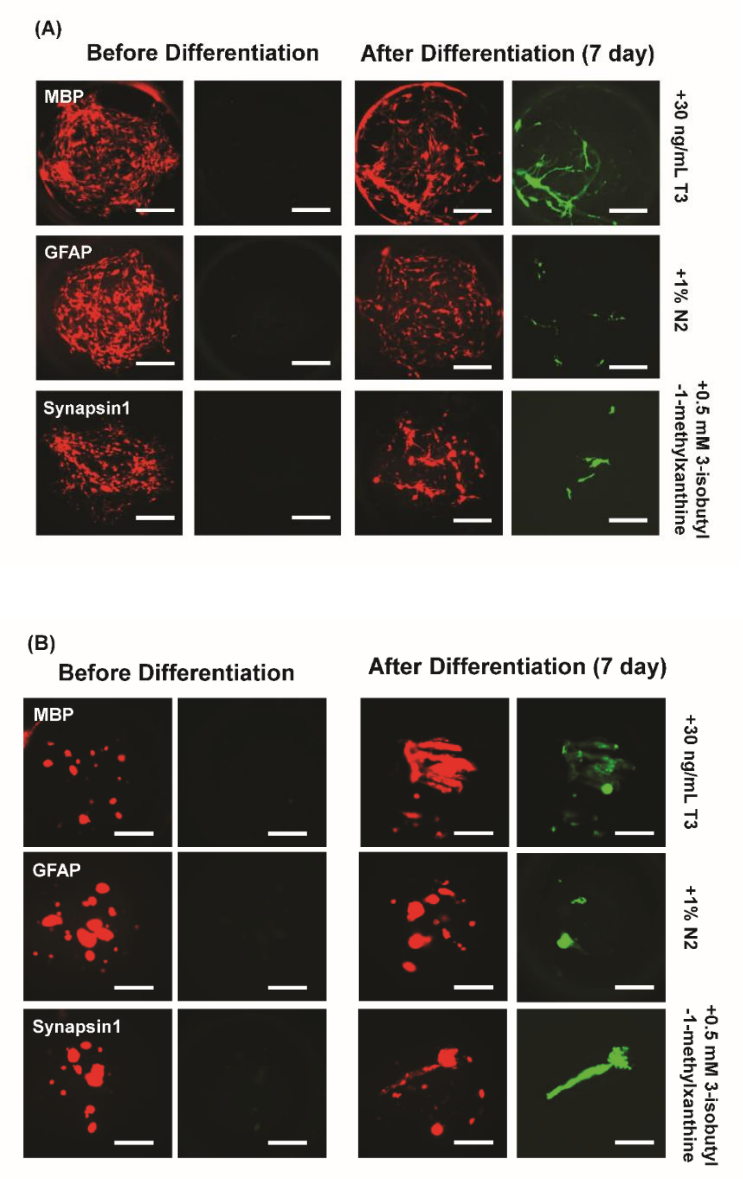

Figure 2.8. ReNcell VM cultured in 2D and 3D on the micropillar chip after infection with lentiviruses and exposed to compounds for inducing differentiation. Lentivirus-infected ReNcell VM were cultured in (**A**) 2D and (**B**) 3D using the complete medium containing the growth factors supplemented with 30 ng/mL T3, 1% (w/v) N2, and 0.5 mM IBMX for differentiation into oligodendrocytes, astrocytes, and neurons, respectively. The scale bar is 50 μm. (*Figure 2.8 generated by Dr. Kyeong-Nam Yu*)

2.4. Discussion

The goal of this study was to develop an NSC-based *in vitro* 3D culture system that enables high-throughput analysis of viability, growth, self-renewal, and differentiation of

human NSCs in real-time, without the need for extensive post-culture sample processing. 3D on-chip NSC microarrays may serve as useful tools to model and analyze neurodegenerative disorders *in vitro*. The features of microarray bioprinting such as automated cell dispensing, miniaturized 3D cell culture, and high-throughput acquisition and analysis of cell images make the micropillar/microwell chip platform of interest in predictive modeling of DNT and high-throughput screening of compounds. ReNcell VM was deemed a useful, albeit imperfect, cellular model, as the cells are capable of self-renewal and differentiation into neurons and glial cells. This platform could be extended to other NSC types such as ReNcell CX®, ENStem-A™, Gibco™ H9-derived NSCs, and NSCs derived from human induced pluripotent stem cells (hiPSCs). Moreover, ReNcell VM is a commercially available human neural progenitor cell line obtained from the midbrain region of a 10-week human fetus and immortalized by retroviral transduction with v-myc oncogene [77], [133]–[135].

Alginate was selected as a cell-encapsulation hydrogel as it is biologically inert [136]. Cell-cell and cell-matrix interactions have been shown to alter cell morphology, signaling mechanisms, and cell function [130], [137], [138]. GFR Matrigel was supplemented with alginate to promote cell-ECM interactions. For cell-cell interactions, which are important for NSC survival and proliferation, relatively high density of ReNcells (6×10^6 cells/mL) were printed on the micropillar chip, resulting in 360 cells/micropillar within 60 nL of cell spots. The viability of ReNcell VM in alginate hydrogel was first assessed with $BaCl_2$ and $CaCl_2$ as crosslinkers. Time-dependent decrease in ReNcell VM viability in alginate gel crosslinked with $BaCl_2$ was observed due to well-documented cytotoxicity of $BaCl_2$ against NSCs [26], [139]. Similar results were observed from human

embryonic stem cells (hESCs) in alginate microcapsules crosslinked with 20 mM $BaCl_2$, where the viability decreased from 90% to 5% after 5 days of encapsulation [140]. Unlike $BaCl_2$, ReNcells encapsulated in alginate with $CaCl_2$ maintained their viability after 5 days of culture and spheroid formation. This lag-phase of ReNcell growth in alginate with $CaCl_2$ has been previously reported [26], and we resolved this issue by supplementing GFR Matrigel in alginate. In addition to cytotoxicity, the selection of divalent cations could influence the permeability of nutrients as well as soluble factors such as growth factors and compounds [139], [140].

The importance of cell-ECM interactions in maintaining self-renewal and in guiding stem cell differentiation has been reported by several groups [141]–[144]. For example, the intrinsic scaffold characteristics such as topology, elasticity, stiffness, porosity, and pore size are known to play a key role in directing the differentiation of stem cells into specific lineages [141], [143], [144]. Laminin is known to influence NSC proliferation and differentiation [137], [142], and laminin-rich Matrigel could be highly-effective in increasing NSC viability, proliferation, and differentiation [142]. Stem cells typically remain in contact with basement membrane proteins during early developmental stages *in vivo*. Matrigel, a basement membrane matrix rich in ECM components such as laminin, entactin, collagen, and heparin sulfate proteoglycans [145], [146], is widely used in 3D culturing of stem cells and neurons to provide cell-ECM interactions [147]. Therefore, addition of GFR Matrigel in alginate significantly enhanced cell viability and spheroid formation of ReNcell VM in 3D culture on the micropillar/microwell chip platform. Due to technical difficulties, such as the maintenance of low temperature in micro-solenoid valves and tubes and reproducible cell printing, we supplemented 1 mg/mL

GFR Matrigel in 075% alginate, which did not cause temperature-induced premature gelation nor increased viscosity, while enhancing cell viability significantly.

NSCs are characterized by their ability of self-renewal and differentiation into neural lineages. Lentiviral vectors are very effective for delivering transgenes into cultured neural progenitor cells due to high tropism levels of neural tissues [148]. Therefore, transgenic ReNcells were created with recombinant lentiviruses for high-throughput analysis of self-renewal and differentiation in 2D and 3D cultures. Expression of NSC-specific markers demonstrated that removal of growth factors (EGF and bFGF) in ReNcell cultures initiate the differentiation into glial and neuronal lineages. ReNcell VM expressed EGFP for SOX2 before differentiation, which is the self-renewal marker of NSCs, whereas there was no expression of EGFP for other differentiation markers, indicating the stemness characteristics of ReNcell VM in the miniaturized 3D culture on the chip, which is in accordance with previous studies [26], [130], [133]. NSCs maintain their pluripotency in the presence of EGF and bFGF signaling (supplemented in the growth medium) [149], and their removal encourages NSCs to differentiate into various lineages. In our study, removal of growth factors induced EGFP expression for MBP, GFAP and synapsin1, indicating the early stage differentiation of ReNcell VM into glial and neuronal lineages. MBP expression was the highest with 36% differentiation compared to GFAP and synapsin1 at 10% and 7.5%, respectively, indicating increased differentiation into oligodendrocytes. Similar results have been reported in microscale 3D NSC cultures in GFR Matrigel, where Olig2 expression for oligodendrocytes was significantly higher after differentiation compared to 3D cultures in collagen gel [40]. The ability of miniaturized 3D cell cultures to accumulate soluble factors released from NSCs could be one reason for the increased expression of

neural specific markers in NSC cultures after differentiation in Matrigel scaffolds [40].

Interestingly, we noted continued expression of SOX2 even after the induction of differentiation. Similar to our observations, other groups have reported that SOX2 was expressed in both 2D and 3D ReNcell VM cultures even after differentiation [130], or SOX2 expression increased in v-myc immortalized cells [129], or SOX2 expression down-regulated after NSC terminal differentiation as shown by expression of the βIII tubulin marker [150]. These results suggest that pluripotency marker SOX2 continues to be expressed until NSCs are terminally differentiated into specific lineages. Considering the short period of induced differentiation (7-10 days) in our study, continued expression of SOX2 could be justifiable.

Finally, we investigated the ability of ReNcell microarrays in 2D and 3D cultures to perform compound-induced differentiation into oligodendrocytes, astrocytes, and neurons. As a proof-of-concept, we selected one compound per lineage based on extensive literature search, i.e., T3 for oligodendrocytes [119], [121], N2 for astrocytes [124], [125], and IBMX for neurons [127], [128], which were chosen based on their role in cell survival and differentiation to specific lineages, both *in vitro* and *in vivo*. For example, Jones *et al.* demonstrated the effect of T3 on proliferation, survival, and differentiation of precursor cells to oligodendrocytes *in vitro* [117]. Similarly, human neural progenitor cells differentiated to oligodendrocytes after one week of treatment with 30 nM T3 [118]. Moreover, the role of T3 on differentiation, survival and proliferation of oligodendrocytes has been validated in various *in vivo* studies with rat models [119], [121]. N2 supplement has been widely used in NSC differentiation [122]–[124]. Shin and Vemuri used N2 to optimally formulate the medium for differentiating human NSCs into astrocytes [122]. In

a recent study, hiPSCs and hESCs were shown to differentiate into functionally mature astrocytes in DMEM/F12 medium supplemented with N2 and B27 [124]. In addition, hiPSC-derived neural progenitor cells in 3D cultures readily differentiated into astrocytes after exposure to N2 in the growth medium [125]. In other studies, 0.5 mM IBMX was shown to induce neuronal differentiation of human mesenchymal stem cells compared to other compounds such as dibutyryl-cAMP and retinoic acid [126], and a significant increase in the differentiation of rat mesenchymal stem cells into neurons was noted with 0.3 mM IBMX compared to other inducers such as 2-mercaptoethanol and tretinoin [127]. Collectively, T3, N2, and IBMX have been widely used for directed differentiation of NSCs into oligodendrocytes, astrocytes, and neurons, which was demonstrated successfully using lentivirus-infected ReNcells on the micropillar/microwell chip platform.

2.5. Conclusions

In this chapter, we successfully established miniaturized 3D ReNcell VM culture in alginate-Matrigel matrices on the micropillar/microwell chip platform and demonstrated high-throughput assessment of lineage-specific differentiation with lentivirus-infected ReNcells by using the growth medium without growth factors as well as the complete growth medium with differentiation inducers. The recombinant lentiviruses with dual promoters – mCherry for constitutive expression to measure viral transduction efficiency and EGFP for NSC-specific biomarkers – were highly effective in quantitatively assessing ReNcell differentiation into neurons, astrocytes, and oligodendrocytes. The promoter-reporter assay system developed herein with recombinant lentiviruses to monitor NSC developmental stages is straightforward to use to calculate the efficiency of cell differentiation and self-renewal by simply comparing green and red fluorescence

intensities from ReNcell cultures on the chip, compared to time-consuming immunofluorescence assays, which are known to give variable specificities and variable responses. In conclusion, our system may be used to predict rapidly and accurately the effects of a variety of compounds on NSC differentiation, survival, and proliferation, with high reproducibility. 3D ReNcell microarrays also may be combined with high-content imaging assays to detect critical changes in NSC morphology, cell function, molecular actions on cell surface receptors, and mechanisms of toxicity, thereby ultimately enhancing the predictability of DNT *in vivo.*

CHAPTER III

ESTABLISHMENT OF ION CHANNEL AND ABC-TRANSPORTER ASSAYS (MEMBRANE PROTEINS) IN 3D-CULTURED NSC MICROARRAYS FOR HIGH-THROUGHPUT NEUROTOXICITY ASSESSMENT

3.1. Introduction

Membrane proteins such as ion channels and transporters are involved in cell-cell signaling, transporting ions and molecules across the membrane, mediating the immune system, and energy transduction [151]. Ion channels are a class of membrane proteins that play a vital role in the development and function of human brains [152]–[155]. They regulate several physiological processes in human brains including proliferation [156], migration [157], and differentiation [152], and are involved in disease pathogenesis as well [158], [159]. Nearly 13% of pharmaceutical drugs target ion channels as their primary therapeutic targets due to their involvement in a wide range of physiological processes and disease pathogenesis [160]–[165]. In addition, several ion channels with relevance to specific diseases have been identified for drug discovery [163]. Therefore, identifying potent and selective ion channel modulators will undoubtedly contribute towards reducing the effect of neurodevelopmental disorders and neurological diseases.

Despite the knowledge of ion channels as a major target for drug discovery, the progress in this field has been limited due to the lack of availability of HTS platforms for the assessment of ion channel activities. Most of ion channel studies still rely on labor intensive patch-clamp electrophysiology assays. Although a new generation of automated patch clamp systems have been developed to record multiple cells simultaneously, their throughput is still limited for applications in HTS of pharmaceutical drugs and industrial chemicals [164] [166]. Despite the sophisticated technologies, automated patch-clamp technology possesses challenges in terms of reproducibility. The patch-clamp assays further require a large number of cells, which is infeasible when it comes to screening potential drug candidates in primary cells from patients. In addition, these patch-clamp methods are expensive, requiring big capital investment and highly skilled personnel [163], [164].

Likewise, influx and efflux transporters represent a major class of membrane proteins that are located on the cell membrane through which they transport nutrients and waste products, and assist in sensing environmental conditions [151][3, 4]. Among them, ATP-binding cassette (ABC) transporters characterized by homologous ATP binding transport various drugs and drug conjugates out of the cells *via* energy-dependent mechanisms and play an important role in drug disposition in humans [167], [168]. Three major drug-transporting ABC-transporters including MDR1, MRP1, and BCRP demonstrate broad substrate specificities for a wide range of compounds such as endogenous compounds, drugs, and metabolites [167]–[169]. Owing to the important role of ABC transporters in absorption and disposition of drugs, pharmaceutical companies have been investigating the interactions between drug candidates and ABC-transporters to

determine the substrate/inhibitor relationship [170]. Several *in vitro* studies have shown the effect of inhibitors and activators on the modulation of these efflux transporters. *In vitro* transporter assays based on cellular models have been recognized as a low-cost and high-throughput alternative for *in vivo* animal studies [171]. One of the most common high-throughput cellular assays used for the assessment of transporter activity is the accumulation assay where the accumulation/uptake of fluorescent dyes is measured in the presence or absence of known transporter modulators. Increased fluorescence intensity due to increased accumulation of fluorescent substrates is observed in the presence of transporter inhibitors whereas decreased accumulation is observed in the presence of activators or inducers [171], [172].

Cell-based assays utilizing bright fluorescent dyes have become a valuable tool to rapidly screen and investigate the effect of potential modulators for ion channels as well as transporters [163], [164], [173]. Several studies have been performed to identify ion channel modulators and transporter inhibitors in various cell lines [173]. However, most of these *in vitro* cell-based studies are performed using cell lines overexpressing ion channels and transporters to amplify signal intensity, which often do not represent indigenous neural stem cells (NSCs) that are important for the assessment of developmental neurotoxicity. In addition, current ion channel and transporter assays have been performed on 2D monolayers, which may limit predictivity of the assays [56]. Thus, 3D cell culture platforms are necessary to investigate potential developmental neurotoxicity of drug candidates and environmental toxicants using high-throughput assays for ion channels and transporters. The overarching goal of this study is to establish high-throughput ion channel and transporter assays on a 384-pillar plate with 3D-cultured ReNcell VM, an immortalized

human neural stem cell line, which can be used for screening ion channel modulators and transporter inhibitors. RNA sequencing data analysis of ReNcell VM is performed to identify ion channels and transporters uniquely expressed in ReNcell VM. In addition, fluorescence-based ion channel and transporter assays have been established in 3D-cultured ReNcell VM and validated with model compounds.

3.2. Materials and Methods

3.2.1. Analysis of RNA-sequencing (RNA-Seq) data

For RNA-Seq data analysis of ReNcell VM, raw sequencing files were obtained from the Sequence Read Archive (SRA) with accession number GSE89623 and converted into FASTQ files. Quality control (QC) of the RNA-Seq reads was performed using FastQC. The mean quality score for each base pair was verified to be above 28, indicating good quality base calls in the library. Reads in the FASTQ files were then processed and aligned to the UCSC homo sapiens reference genome (build hg38) using Spliced Transcripts Alignment to a Reference (STAR) Version 2.5.2b-0. The aligned BAM files were used to find abundance of gene expression using Salmon. Abundance data was normalized using edgeR to find count per million transcripts (CPM) for each gene variant, and the genes of interest were extracted. Since RNA-Seq can provide alternatively spliced variant of each gene, the splice variant with the highest abundance was selected. The expression data was visualized using web-based data visualization tool called Clustergrammer (**Figure 3.1**).

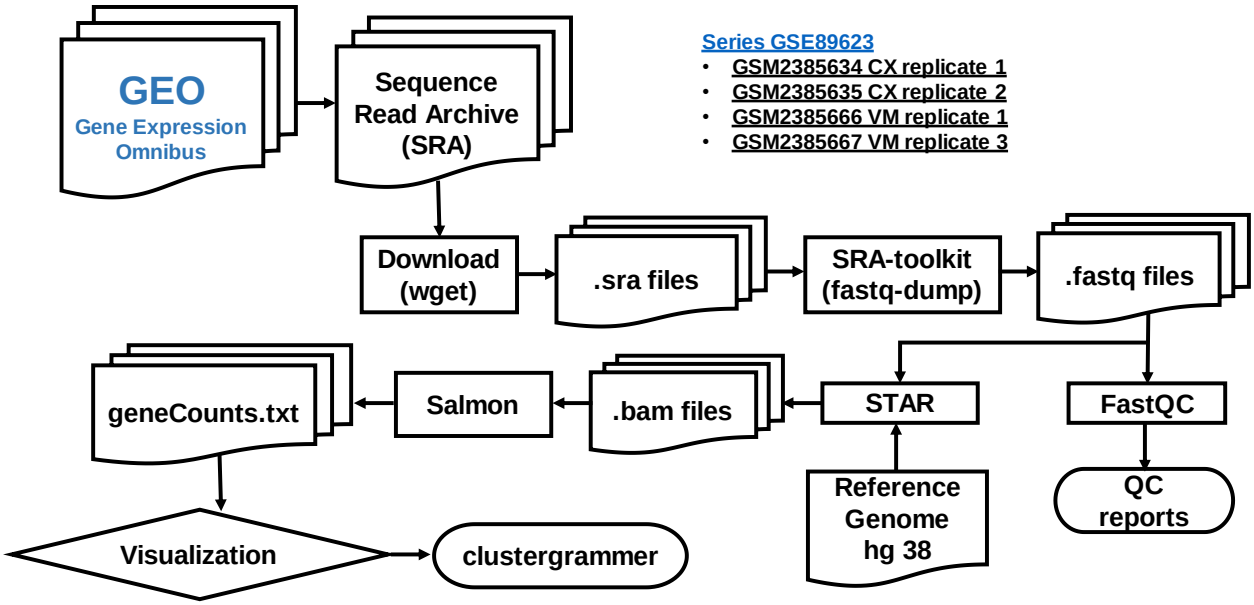

Figure 3.1. Workflow of the different steps carried out in RNA-Seq data analysis pipeline. Raw data was obtained from SRA with accession number GSE89623 and converted into FASTQ files. Quality control (QC) for the RNA-Seq reads was assessed using FastQC. The reads in the FASTQ files were aligned to the human genome with Spliced Transcripts Alignment to a Reference (STAR). Salmon was applied to assign reads to genes, and visualization of gene clusters was implemented with web-based data visualization tool called Clustergrammer (*Data analysis performed by Rushabh Patel*).

3.2.2. NSC culture in 2D

ReNcell VM (EMD Millipore, Burlington, MA, USA) was passaged in a complete NSC medium (ReNcell NSC maintenance medium, EMD Millipore) supplemented with 20 ng/mL epidermal growth factor (EGF, EMD Millipore), 20 ng/mL basic fibroblast growth factor (bFGF, EMD Millipore), and 1% (v/v) penicillin/streptomycin (P/S, Thermo Fisher, Waltham, MA, USA) on laminin-coated, tissue culture-treated, T-75 flasks in a humidified 5% CO_2 incubator at 37°C. The complete NSC medium was replaced every 2 d with a freshly-prepared complete medium until the cells reached 90% confluency, after which they were detached with Accutase™ (EMD Millipore), suspended in ReNcell NSC maintenance medium, and centrifuged at 300 g for 4 min. The resulting cell pellet was

resuspended in the complete NSC medium to determine cell density using a Moxi cell counter (ORFLO Technologies, MXZ001), and then 1.5×10^6 cells were seeded on freshly prepared laminin-coated T-75 flasks.

3.2.3. NSC culture in 3D on a 384-pillar plate

For 3D culture of ReNcell VM, 384-pillar plates (MBD, Suwon, South Korea) were coated with 0.01% (w/v) poly(maleic anhydride *alt*-1-octadecene) (PMA-OD) and dried for at-least 4-6 h at room temperature. A mixture of 0.0033% (w/v) poly-L-lysine (PLL) and 25 mM calcium chloride ($CaCl_2$) was prepared in sterile deionized water and printed on top of the PMA-OD-coated 384-pillar plates at a volume of 2 μL with a microarray spotter (S+ Microarrayer, Samsung Electro Mechanics Co. or SEMCO, Suwon, South Korea). NSC medium plates were prepared by dispensing the complete NSC medium into 384-well plates (Corning) at a volume of 50 μL per 384-well and incubated in the 5% CO_2 incubator at 37°C for later use. For 3D NSC culture on the 384-pillar plate, the suspension of ReNcell VM was mixed with 3% (w/v) low-viscosity alginate (Sigma-Aldrich) and 15 mg/mL growth factor reduced (GFR) Geltrex® (ThermoFisher) to achieve a final cell concentration of 2×10^6 cells/mL in 0.75% (w/v) alginate and 2.5 mg/mL Geltrex and stored on ice until printing. The suspension of ReNcell VM in the alginate-Geltrex mixture was then printed on top of dried PLL/$CaCl_2$ spots at a volume of 2 μL (4,000 cells per 384-pillar) while maintaining the slide deck at 7°C to prevent water evaporation during printing (**Figure 3.2**). The 384-pillar plates were left on the chilling slide deck for 4 min for gelation and then sandwiched with the 384-well plates containing 50 μL of the complete NSC medium per 384-well. The sandwiched 384-pillar/well plates were incubated in the 5% CO_2 incubator at 37°C.

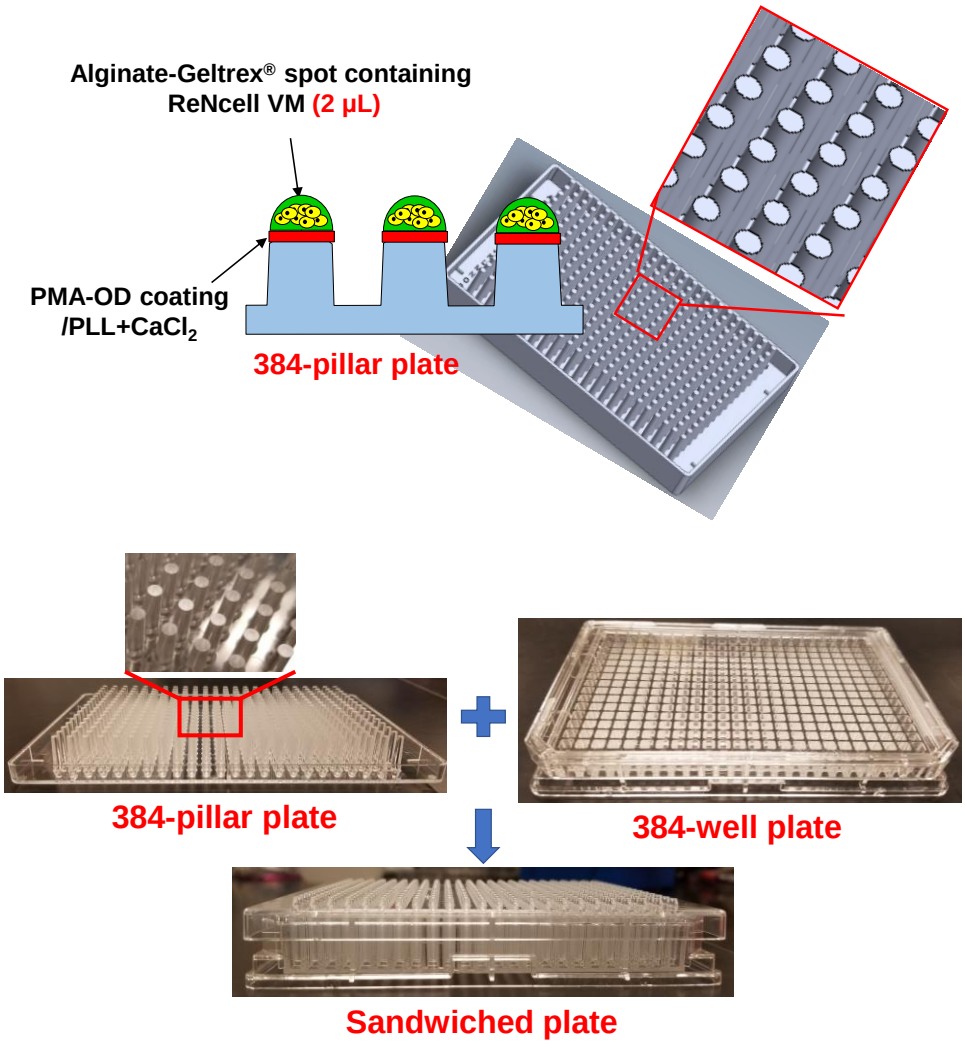

Figure 3.2. Schematics and pictures of the 384-pillar plate with NSCs encapsulated in hydrogel spots. ReNcell VM was suspended in a mixture of 0.75% (w/v) alginate and 2.5 mg/mL GFR Geltrex at a final density of 2×10^6 cells/mL and printed at a volume of 2 µL on the 384-pillar plate coated with PMA-OD and PLL+$CaCl_2$ layers.

3.2.4. Establishment of ion channel assays in 2D- and 3D-cultured ReNcell VM

Potassium ion channel assay

FluxOR™ potassium ion channel assay kit (ThermoFisher) was used to establish high-throughput potassium ion channel assays in 2D- and 3D-cultured ReNcell VM. For the 2D cell assay, ReNcell VM suspension at 10,000 cells/well was seeded in a 96-well plate and

incubated in the 5% CO_2 incubator at 37°C for 48 h. All the buffer solutions, including the loading buffer containing the FluxOR™ reagent, the assay buffer, and the stimulus buffer containing thallium sulfate, were prepared according to the manufacturer's protocol. Powerload™ concentrate and water-soluble probenecid were used as directed by the kit protocol to enhance the dye solubility and retention. Stock solutions of model compounds, such as XE-991 and fluoxetine (both from Sigma-Aldrich), were prepared in DMSO at a concentration of 25 mM and 50 mM, respectively. The cells in the 96-well plate were treated with the loading buffer for 60 min at room temperature, after which the loading buffer was removed and replaced with the assay buffer. Baseline reading was obtained with a microtiter plate reader (Synergy H1, BioTek) at 475 nm excitation and 530 nm emission, and then the assay buffer was removed. XE-991 and fluoxetine were diluted in the stimulus buffer at six different concentrations including a stimulus buffer only control and added to the 96-well plate with the cells, which was immediately followed by kinetic reading of the fluorescent intensity in the microtiter plate reader.

For the 3D cell assay, ReNcell VM encapsulated in 0.75% (w/v) alginate and 2.5 mg/mL GFR Geltrex on the 384-pillar plate was incubated in the complete NSC medium for 4 d prior to performing the FluxOR™ assay. The loading buffer was dispensed into a 384-well plate at 50 μL/well, and 3D-cultured ReNcell VM on the 384-pillar plate was incubated with the loading buffer in the 384-well plate for 60 min at room temperature. After incubation with the loading buffer, the cells on the 384-pillar plate were washed once with a dye-free assay buffer in a 384-well plate before treating with XE-991 and fluoxetine in the stimulus buffer. XE-991 and fluoxetine were diluted in the stimulus buffer at six dosages including the control and added to a 384-well plate. The cells were incubated with

the stimulus buffer contatining the two potassium ion channel blockers, immediately followed by kinetic reading of thallium-sensitive fluorescence intensity from the microtiter plate reader.

Store-operated calcium ion channel assay

Fluo-4 Direct calcium channel assay (ThermoFisher) was used to establish high-throughput calcium channel assays in ReNcell VM culture. The stock solution of 2X Fluo-4 Direct calcium reagent was prepared in 10 mL of Fluo-4 Direct calcium assay buffer according to the manufacturer's protocol. The stock solution of 2-aminoethyldiphenyl borinate (2-APB) (Sigma-Aldrich) was prepared in DMSO at a concentration of 100 mM. Fluo-4 Direct reagent was diluted in the NSC medium at 1:1 ratio to obtain the final concentration of the reagent with 5 mM of Probenecid in the final solution. Six concentrations of 2-APB were prepared in Fluo-4 Direct assay buffer. For the 2D cell assay, ReNcell VM suspension was seeded at 10,000 cells/well in a 96-well plate and incubated with the complete NSC medium in the 5% CO_2 incubator at 37°C for 48 h prior to the assay. On the day of the assay, the cells in the 96-well plate were loaded with Fluo-4 Direct reagent and incubated for 60 min at room temperature, after which the cells were treated with six dosages of 2-APB. Kinetic reading of fluorescence intensity was performed over a period of 1 h with 10 min interval with the microtiter plate reader at 494 nm excitation and 516 nm emission.

For the 3D cell assay, ReNcell VM encapsulated in 0.75% (w/v) alginate and 2.5 mg/mL GFR Geltrex on the 384-pillar plate was incubated in the complete NSC medium in a 384-well plate for 4 d prior to performing the Fluo-4 Direct assay. The stock solution of Fluo-4 Direct reagent was diluted in the NSC medium to obtain the final concentration and added to a 384-well plate at a volume of 50 μL/well. The cells on the 384-pillar plate

were incubated with the reagent in a 384-well plate for 60 min at room temperature, after which the cells were exposed to six dosages of 2-APB including a no compound control. The changes in fluorescence intensity were monitored with the microtiter plate reader over time.

Measuring ion channel activities in ReNcell VM

The changes in fluorescence intensity for both the FluxOR potassium ion channel assay and the Fluo-4 Direct calcium ion channel assay were obtained from the microtiter plate reader. The intensity reading was normalized with control conditions (i.e., stimulus buffer without XE-991 and fluoxetine for the potassium ion channel assay and the Fluo-4 Direct assay buffer without 2-APB for the calcium ion channel assay) and dose response curves were obtained using GraphPad Prism (GraphPad Software, San Diego, CA).

3.2.5. Establishment of transporter assays in 2D- and 3D-cultured ReNcell VM

Identification and evaluation of fluorescent substrates and transporter inhibitors

Inhibitors specific to three major ABC-transporters including verapamil for ABCB1/MDR1, MK-571 and probenecid for ABCCs/MRPs, and novobiocin for ABCG2/BCRP (all from Sigma-Aldrich) were selected from literature search. Optimum concentrations of these inhibitors were determined based on their effect on viability of 2D-cultured ReNcell VM. Briefly, ReNcell VM was seeded in a laminin-coated, 96-well plate at 10,000 cells/well and incubated in the 5% CO_2 incubator at 37°C for 48 h. After 48 h of incubation, the cells were exposed to six dosages of the ABC transporter inhibitors such as verapamil (0.8 - 200 μM), MK-571 (1.6 - 400 μM), probenecid (0.8 - 200 μM), and novobiocin (1.6 - 400 μM) for 2 h, stained with calcein AM at 0.25 μM for 30 min, and

then scanned with an automated fluorescent microscope (S+ scanner, SEMCO) to assess cell viability. The fluorescent cell images were obtained with a green filter (XF404 from Omega Optical), a red filter (TxRed-4040C from Semrock), and a blue filter (DAPI-5060C from Semrock) at 4× magnification with the Olympus UPLFLN 4× (numerical aperture (NA) 0.13, f-number 26.5, and depth of field (DOF) ~ 32.3 μm) (Olympus, Tokyo, Japan). Cell images obtained from the 384-pillar plates were batch-processed using ImageJ (NIH) to extract fluorescence intensity from the entire cell spots and were analyzed using SigmaPlot software ver. 12 (Systat Software Inc., San Jose, CA, USA).

Calcein AM and Hoechst 33342 were evaluated for their application as fluorescent substrates of the three ABC-transporters. Briefly, ReNcell VM seeded in two 96-well plates at 10,000 cells/well and cultured in the 5% CO_2 incubator at 37°C for 48 h was exposed to six dosages of the ABC-transporter inhibitors, including verapamil (0.8 - 200 μM) for MDR1, MK-571 (0.4 - 100 μM) and probenecid (0.8 - 200 μM) for MRP1, and novobiocin (1.6 - 400 μM) for BCRP, all prepared in two complete NSC media containing either 0.25 μM calcein AM or 10 μM Hoechst 33342. After removing old NSC media, inhibitor solutions containing either calcein AM or Hoechst 33342 were added to the 96-well plates with the cells. The cells were incubated at 37°C for 45 min, after which the inhibitor solutions were removed, and the 96-well plates were rinsed with cold D-PBS before fluorescence reading. The changes in fluorescence intensity in the 96-well plates were determined by the microtiter plate reader at 490 nm excitation and 520 nm emission for green fluorescence from calcein AM and at 350 nm excitation and 461 nm emission for blue fluorescence from Hoechst 33342.

Establishing high-throughput ABC-transporter assays in 3D-cultured ReNcell VM

To establish high-throughput ABC transporter assays on the 384-pillar plate with 3D-cultured ReNcell VM, Hoechst 33342 was used to measure activities of MDR1, MRP1, and BCRP in the presence and absence of specific inhibitors of the three transporters, including verapamil for MDR1, probenecid for MRP1, and novobiocin for BCRP. Briefly, ReNcell VM encapsulated in 0.75% (w/v) alginate and 2.5 mg/mL GFR Geltrex on the 384-pillar plate was sandwiched with the complete NSC medium in a 384-well plate and cultured in the 5% CO_2 incubator at 37°C for 4 d to ensure 3D spheroid formation. Varying concentrations of verapamil (0.8 - 200 μM), probenecid (0.8 - 200 μM), and novobiocin (1.6 - 400 μM) were prepared in the complete NSC medium containing 10 μM Hoechst 33342. 3D-cultured ReNcell VM on the 384-pillar plate was exposed to the inhibitors in the 384-well plate for 60 min, after which the inhibitors were removed, and the 384-pillar plate was rinsed with a cold saline solution. The changes in blue fluorescence intensity was determined by the microtiter plate reader and fluorescent cell images were acquired by the S+ scanner.

Assessment of ABC transporter activities in 3D-cultured ReNcell VM

Hoechst 33342 was used to measure the activity of the ABC transporters by blocking MDR1, MRP1, and BCRP in 3D-cultured ReNcell VM using verapamil, probenecid, and novobiocin. Fluorescence intensity was obtained to determine the transporter activity factor (TAF) of the ABC transporters using the following equation:

$$\mathbf{TAF = [(F_n - F_{cntrl}) / F_n] \times 100}$$

where, F_n is the fluorescence intensity from inhibitor-treated ReNcell VM and F_{cntrl} is the fluorescence intensity from the untreated control sample.

3.3. Results

3.3.1. Expression of ion channels in ReNcell VM

Since RNA-Seq can provide alternatively spliced variant of each gene, the splice variant with the highest abundance was selected. From RNA-Seq analysis, we found that there are low expression levels of all voltage-gated sodium ion channels, voltage-gated calcium ion channels, and major chloride ion channels in undifferentiated ReNcell VM. Interestingly, voltage-gated potassium channels including KCNQ2 (Kv 7.2) and KCND3 (Kv 4.3) were expressed at relatively high levels as compared to other voltage-gated and non-voltage gated potassium ion channels **(Figure 3.3)**. In addition, store-operated calcium channels (SOCCs) showed higher expression levels as compared to other types of calcium ion channels (**Figure 3.4**). Thus, we focused on these potassium and calcium ion channels in the follow-up experiments.

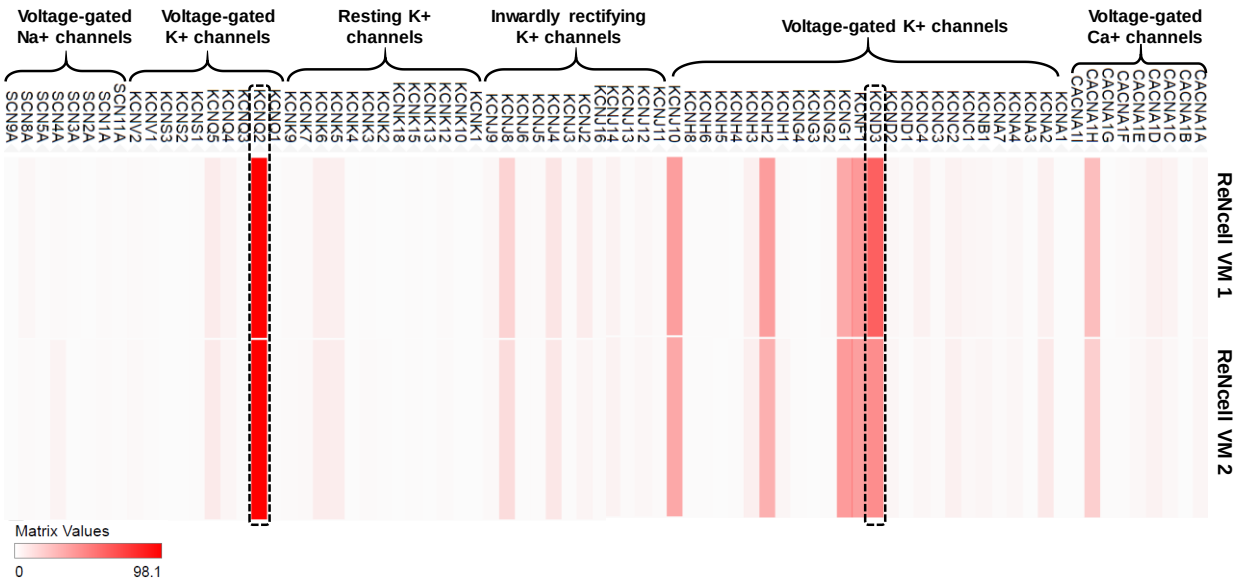

Figure 3.3. Gene expression level of major ion channels in ReNcell VM visualized in Clustergrammer after processing RNA-Seq data obtained from the RNA-Seq workflow. Only few voltage-gated potassium ion channels are well expressed in ReNcell VM as compared to other potassium ion channels, sodium ion channels, and calcium ion channels.

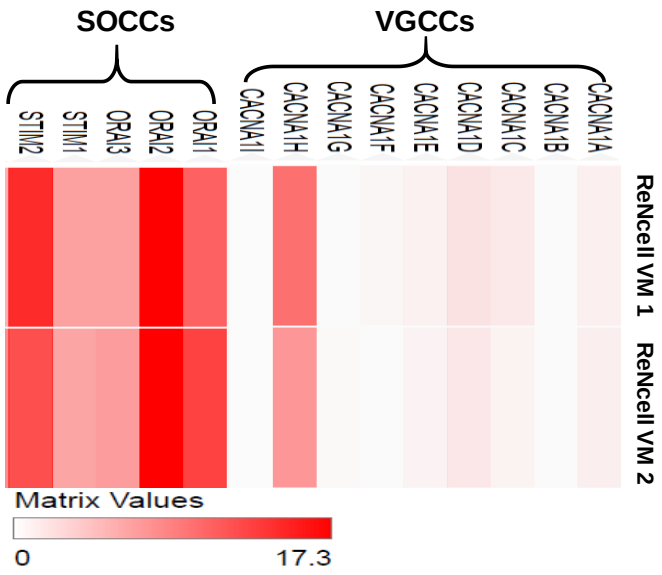

Figure 3.4. Gene expression level of voltage-gated calcium channels (VGCCs) and store-operated calcium channels (SOCCs) in ReNcell VM visualized in Clustergrammer. Only SOCCs are well expressed in ReNcell VM in comparison to VGCCs.

3.3.2. Viability of 3D-cultured NSC on 384-pillar plate

The ability of self-renewal and differentiation into neurons and glial cells makes ReNcell VM human neural progenitor cell line a suitable NSC model for DNT studies (Breier et al. 2010; Kim et al. 2015). ReNcell VM viability and spheroid formation in 3D culture on the 384-pillar plate were assessed over time (days 2, 4, 6, and 14) with calcein AM and ethidium homodimer-1 staining. In chapter 2, we demonstrated improved viability and spheroid formation of ReNcell VM in the mixture of 0.75% (w/v) alginate and 1 mg/mL GFR Matrigel on a micropillar chip with 60 nL of cell spots. However, the micropillar chip was small (25 mm × 75 mm) for easy maneuverability and incompatible with HTS instruments used widely. Thus, we have established 3D-cultures of ReNcell VM on a 384-pillar plate, which contains 16 × 24 pillar arrays (i.e., 384 pillars) and compatible with conventional 384-well plates and HTS instruments. This is the first demonstration of HCI

assays on 3D-cultured ReNcell VM on the 384-pillar plate for the assessment of DNT. GFR Matrigel was replaced with GFR Geltrex because Geltrex is free from lactate dehydrogenase-elevating virus (LDEV) and has less lot-to-lot variation in protein composition although both Geltrex and Matrigel are purified from basement membrane extract of Engelbreth-Holm-Swarm mouse sarcoma cells and have similar compositions. High viability of ReNcell VM in a mixture of 0.75% (w/v) alginate and 2.5 mg/mL GFR Geltrex was maintained over a period of two weeks as evidenced by the increased size of spheroids and the increased fluorescence intensity from the ReNcell VM images at days 2, 4, 6, and 14 (**Figure 3.5**). The green-colored dots represent live cells stained with calcein AM. The 3D-cultured ReNcell VM on the 384-pillar plate was maintained further over a period of two months to establish long-term cell culture on the 384-pillar plate with calcein AM staining at day 14, and H&E staining after two months, to monitor changes in cell viability and morphology (**Figure 3.6**). ReNcell VM formed large spheroids of nearly 400 μm in average diameter and maintained high viability as indicated by the green color in **Figure 3.5A**. In addition, H&E staining after two months revealed compact hydrogel spots filled completely with 3D spheroids as seen in **Figure 3.6**.

(A)

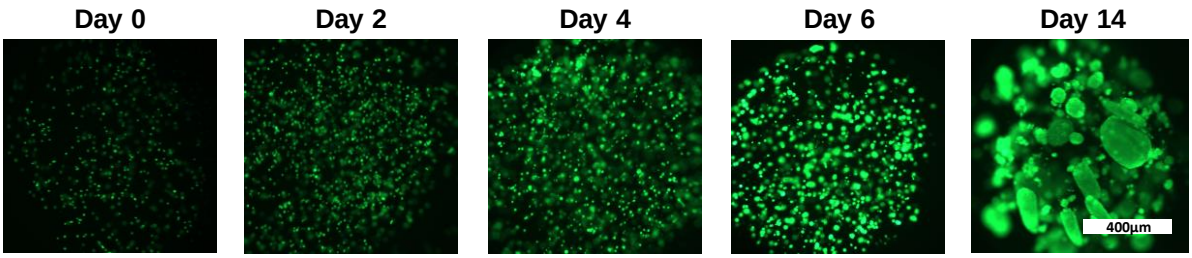

(B)

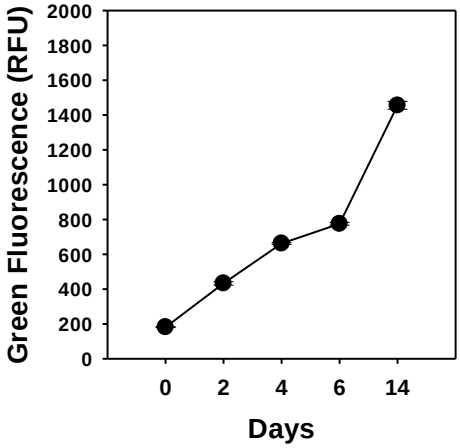

Figure 3.5. Viability and growth of 3D-cultured ReNcell VM on the 384-pillar plate. **(A)** ReNcell VM cells mixed with 0.75% (w/v) alginate and 2.5 mg/mL GFR Geltrex, printed on the 384-pillar plate, incubated for 14 days, and stained with Live/Dead® viability/cytotoxicity kit at day 2, 4, 6, and 14. Green dots represent live cells stained with 0.25 µM calcein AM. Spheroid formation can be observed from day 6. The scale bar is 400 µm. **(B)** Changes in green fluorescence intensity in 3D-cultures of ReNcell VM over 2 weeks.

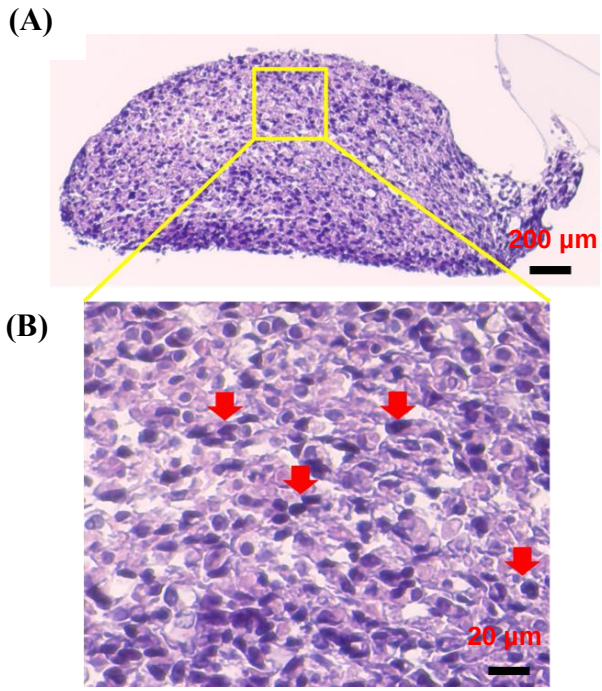

Figure 3.6. Long-term (2-months) 3D culture of ReNcell VM on the 384-pillar plate. **(A)** Cross-sectional image of a single ReNcell spot (2 µL) after two months of incubation on the 384-pillar plate. The cell spot containing ReNcell spheroids was fixed with 4% paraformaldehyde and embedded in the paraffin cassette to make slices. To observe ReNcell spheroids, the cross-sectioned slice on the glass slide was stained with hematoxylin and eosin. Scale bar: 200 µm. **(B)** The blown-up image of the ReNcell spheroids. The red arrows indicate nuclei stained with hematoxylin. The entire hydrogel spot was packed with ReNcell spheroids, which remained viable and exhibited normal 3D morphology. Scale bar: 20 µm.

3.3.3. Ion channel activities in 2D- and 3D-cultured ReNcell VM

ReNcell VM-based potassium channel assays were established in 2D and 3D culture using FluxOR™ potassium ion channel assay kit containing a membrane-permeable FluxOR™ reagent that is transformed into a fluorogenic thallium-sensitive indicator inside the cells. When thallium ions are added to the cells by opening potassium ion channels with a stimulus buffer, the thallium-sensitive dye binds to thallium ions and generates a green fluorescent signal. To measure the activity of the specific voltage-gated potassium channels highly expressed in ReNcell VM, we selected inhibitors specifically binding to each

channel (i.e., XE-991 for Kv 7.2 channel and fluoxetine for Kv 4.3 channel). Six dosages of XE-991 (0.4 - 100 µM) and fluoxetine (0.4 - 100 µM), including a no compound control, were prepared in the stimulus buffer to observe inhibition of specific potassium ion channel activity. Nearly 30% inhibition of Kv 7.2 channel and 20% inhibition of Kv 4.3 channel were observed in both 2D- and 3D-cultured ReNcell VM at the highest dosage of XE-991 and fluoxetine, respectively **(Figure 3.7)**.

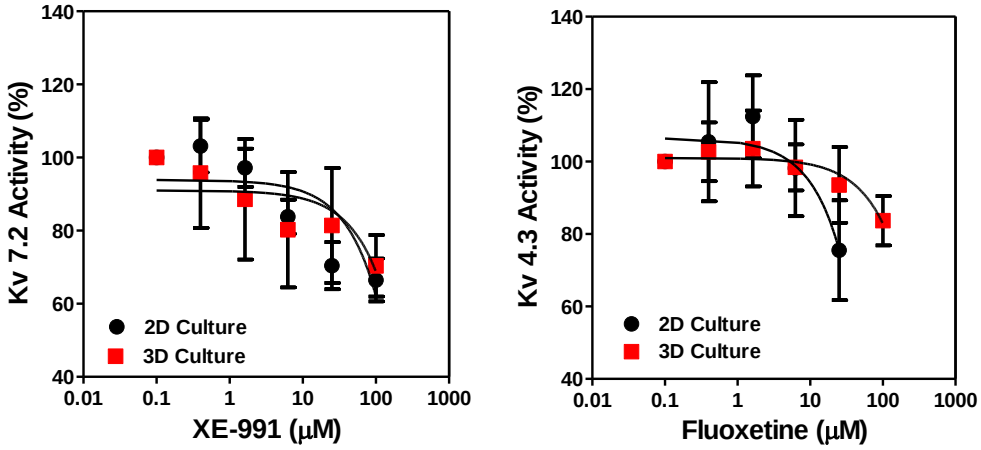

Figure 3.7. Potassium channel activity in 2D- and 3D-cultured ReNcell VM. For the 2D cell assay, ReNcell VM was seeded in the 96-well plate with 10,000 cells/well and incubated for 2 d before performing the assay (n=6). ReNcell VM was encapsulated in a mixture of 0.75% (w/v) alginate and 2.5 mg/mL GFR Matrigel and cultured for 4 d for 3D cell culture before performing the potassium ion channel assay (n=12). On the day of the assay, the cells were loaded with thallium-sensitive FluxOR reagent and treated with XE-991 (Kv 7.2 channel blocker) and fluoxetine (Kv 4.3 channel blocker) along with thallium stimulus to observe the activity of the potassium ion channels.

From the RNA-Seq analysis, we also found that voltage-gated calcium ion channels are not expressed in ReNcell VM. Therefore, we focused on non-voltage gated calcium ion channels such as SOCCs that were shown to be expressed in ReNcell VM (**Figure 3.4**) and selected 2-APB, which is a widely used SOCC modulator. To measure the SOCC activity in 3D-cultured ReNcell VM, a cell-based calcium channel assay was established using Fluo-4 Direct calcium ion channel assay kit. The kit contains a membrane-permeable Fluo-

4 Direct reagent, which is hydrolyzed by esterases inside the cells into a calcium-sensitive fluorescence reagent. When calcium ions enter inside the cells or are released from endoplasmic reticulum (ER) due to SOCC activity, green fluorescence is observed. The cells were loaded with Fluo-4 Direct reagent for 1 h, after which the cells were exposed to six dosages (0.4 – 100 µM) of 2-APB including a no compound control, and the fluorescence intensity reading was obtained. The highest activation of SOCC was observed at 6.25 µM from both 2D- and 3D-cultured ReNcell VM (**Figure 3.8**). Inhibition of the SOCC activity was observed beyond that concentration (i.e., 25 - 100 µM), which is correlated well with literature [174], [175].

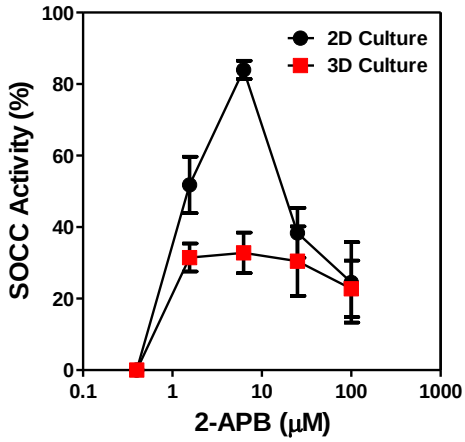

Figure 3.8. Store-operated calcium channel (SOCC) activity in 2D- and 3D-cultured ReNcell VM. For the 2D cell assay, ReNcell VM was seeded in the 96-well plate with 10,000 cells/well and incubated for 2 d before performing the assay (n=6). For the 3D cell assay, ReNcell VM was encapsulated in a mixture of 0.75% (w/v) alginate and 2.5 mg/mL GFR Matrigel and cultured for 4 d before performing the calcium channel assay (n=12). Both cells were loaded with Fluo-4 Direct reagent and treated with 2-APB (SOCC modulator) to observe the changes in the activity of calcium channels over time. The 2-APB exhibited biphasic behavior by activating SOCCs at lower concentrations (1.56 - 6.25 µM) and inhibiting the channels at higher concentrations (25 -100 µM), which is well correlated with the mechanism of 2-APB action.

3.3.4. ABC transporter activities in ReNcell VM

The concentrations of transporter inhibitors which are nontoxic to ReNcell VM were selected to accurately measure transporter activity. Verapamil at 200 µM and MK-571 above (**Figure 3.9**). Calcein AM has been widely known as a fluorescent substrate for MDR and MRP transporters, but the inhibition of MDR1 and MRP1 transporters in ReNcell VM with verapamil and probenecid, did not lead to increase in green fluorescence. On the other hand, Hoechst 33342 widely used as a fluorescence substrate for BCRP and MDR1 transporters, was found to be a useful substrate for MRP1 transporter as well as indicated by the increase in fluorescence with probenecid (**Figure 3.10**). We further found that MK-571 did not selectively inhibit the MRP transporter for both fluorescent substrates, calcein AM and Hoechst 33342.

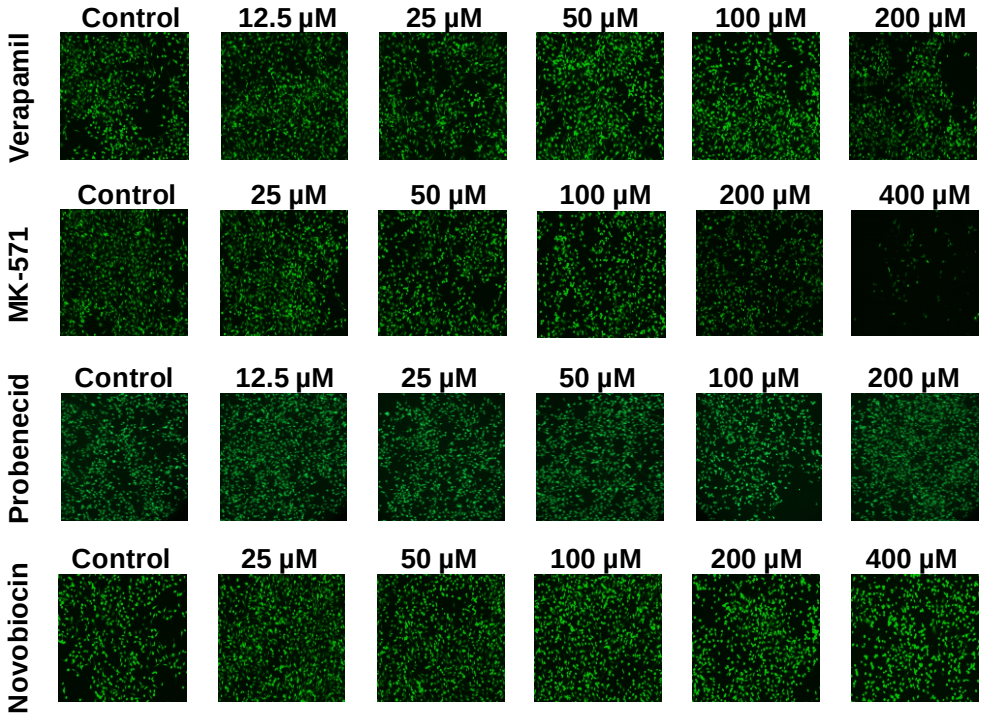

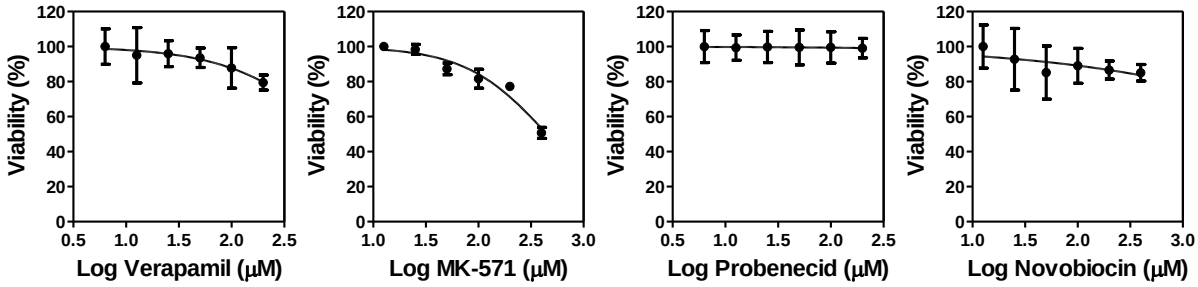

Figure 3.9. Basal toxicity of ReNcell VM with the transporter inhibitors. ReNcell VM seeded in the 96-well plate was treated with various concentrations of verapamil, MK-571, probenecid, and novobiocin and stained with 0.25 μM calcein AM to determine the non-cytotoxic ranges of the inhibitors for accurate assessment of transporter activity (n = 6).

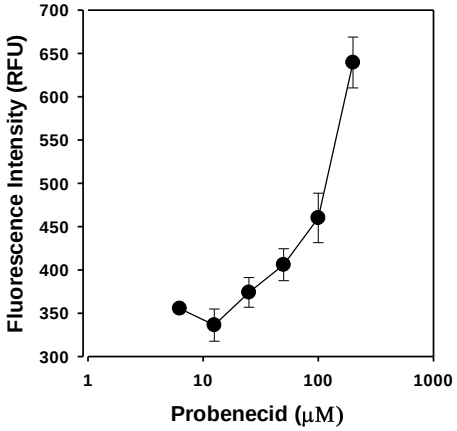

Figure 3.10. Hoechst 33342 used to determine MRP1 transporter inhibition with probenecid. ReNcell VM seeded in the 96-well plate was treated with 12.5 - 200 μM of probenecid and 10 μM of Hoechst 33342 for 30 min and rinsed with ice cold D-PBS, followed by fluorescence intensity reading from the microtiter plate reader (n=6). Increase in blue fluorescence intensity indicated that there is an accumulation of Hoechst 33342 in ReNcell VM due to the inhibition of MRP1 transporter by probenecid.

Therefore, we selected verapamil, probenecid, and novobiocin as selective inhibitors of MDR1, MRP1, and BCRP to determine the transporter activity in 3D-cultured ReNcell VM. Blocking of these transporters with the inhibitors could result in accumulation of Hoechst 33342, the fluorescent transporter substrate, inside the cells, leading to an increase in blue fluorescence intensity with increasing concentrations of the inhibitors (**Figure 3.11**). Thus, transporter activity was determined based on the increase in blue fluorescence

intensity of inhibitor-treated ReNcell VM at varying concentrations of the inhibitors. The TAF of ABC transporters in ReNcell VM was determined at the highest concentration of the inhibitors (i.e., 200 µM verapamil, 200 µM probenecid, and 400 µM novobiocin). Relatively high TAFs (30% and 22%) were observed for MDR1 and MRP1 as compared to BCRP, demonstrating that MDR1 and MRP1 transporter activities are increased in 3D-cultured ReNcell VM (**Figure 3.12**). Interestingly, there was significant difference between 2D- and 3D-cultured ReNcell VM in terms of MDR1 activity. The TAF of MRP1 was high (30% and 22%) for both 2D- and 3D-cultured ReNcell VM, which was well correlated with the result of RNA-Seq analysis where high expression of MRP1 transporter was observed as compared to the expression level of MDR1 and BCRP transporters (**Figure 3.13**).

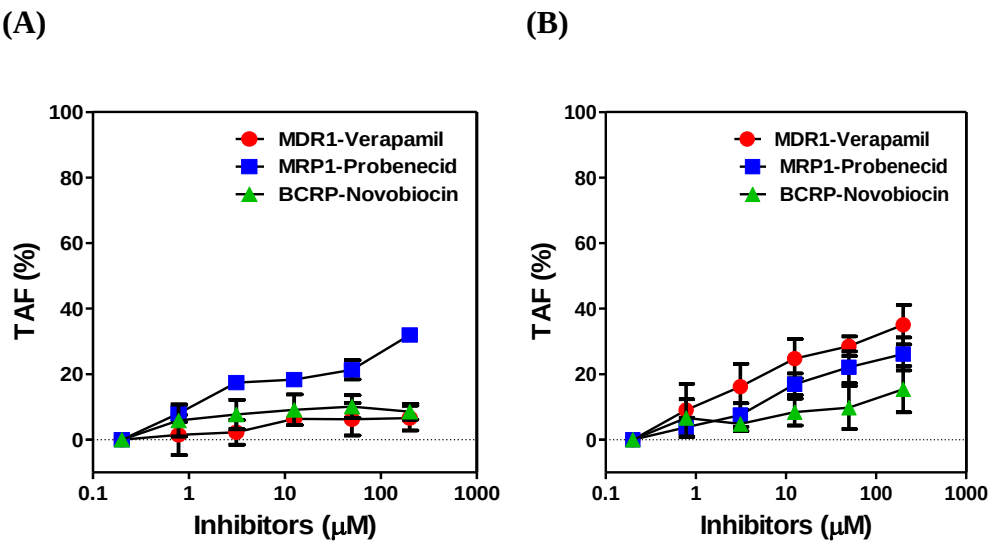

Figure 3.11. Inhibition of MDR1, MRP1, and BCRP transporters in (A) 2D- and (B) 3D-cultured ReNcell VM with varying concentrations of specific inhibitors. ReNcell VM in both 2D **(n=6)** and 3D culture **(n=12)** were exposed to six concentrations of verapamil, probenecid, and novovbiocin for the inhibition of MDR1, MRP1, and BCRP transporters with 10 µM of Hoechst 33342, the fluorescent transporter substrate.

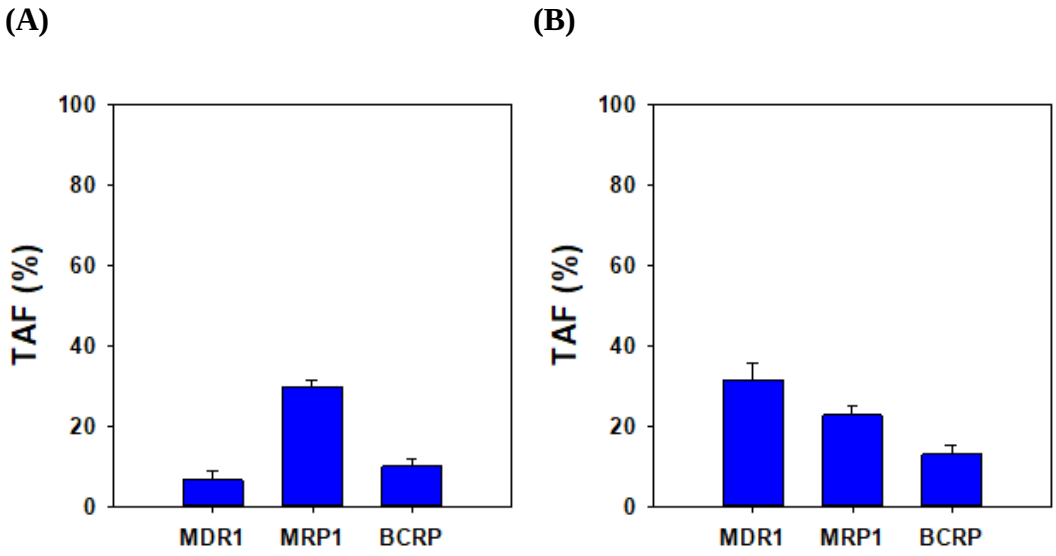

Figure 3.12. Average TAF of MDR1, MRP1, and BCRP transporters in (A) 2D- and (B) 3D-cultured ReNcell VM. The accumulation of Hoechst 33342 in ReNcell VM was determined using the highest concentration of verapamil (200 µM), probenecid (200 µM), and novobiocin (400 µM), respectively. Unlike the other transporters, there might be MDR1 overexpressed in 3D-cultured ReNcell VM.

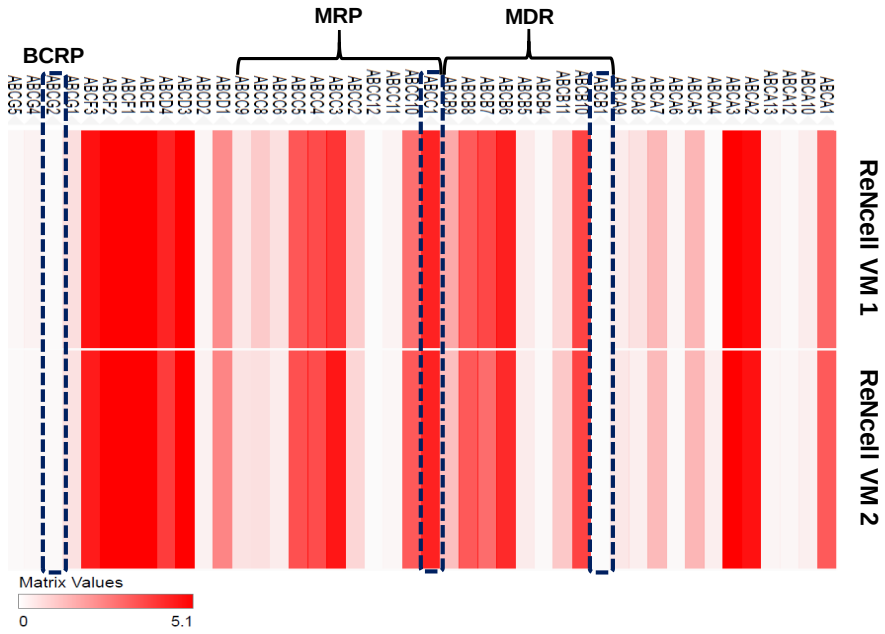

Figure 3.13. Gene expression levels of major ABC transporters in ReNcell VM visualized in Clustergrammer after processing RNA-Seq data. Among the three transporters tested, only MRP1 was expressed higly as compared to the expression level of MDR1 and BCRP, which is consistent with what we discovered in Figure 3.10A.

3.4. Discussion

Ion channels and ABC-transporters have emerged as attractive drug targets in modern drug discovery [167], [176]–[179]. In this study, we established high-throughput fluorescent assays for the assessment of ion channel and transporter activities in 3D-cultured ReNcell VM on a 384-pillar plate. We implemented RNA-Seq analysis to identify gene expression levels of ion channels and transporters in ReNcell VM. RNA-Seq enables the discovery, quantification, and profiling of RNAs, thereby providing information on the expression level of each gene in a cell. The expression level of mRNA in a cell is indicative of the potential expression levels of proteins in the cell. Therefore, depending on the relative gene expression levels of major ion channels and ABC-transporters from RNA-Seq, we were able to select specific inhibitors/blockers as test compounds to measure the activity of ion channels and transporters in ReNcell VM and establish high-throughput, 3D NSC-based, ion channel and efflux transporter assays.

The minimal expression of voltage-gated ion channels and major efflux transporters in ReNcell VM observed from RNA-Seq was consistent with literature [180]–[185] where minimal expression of functional channels such as voltage-gated sodium and calcium channels or receptors in progenitor cells from the nervous system has been reported when grown under proliferative conditions. This can be attributed to the fact that proliferation and functional expression of ion channels or receptors may not occur at the same time [180]. This may be the reason why voltage-gated sodium channels are not expressed in embryonic human neural progenitor cells and neonatal neural progenitor cells [181]. In addition, the expression of voltage-gated potassium channels and the absence of voltage-gated sodium channels in ReNcell VM discovered from our study are consistent with

literature. For example, Cho *et al.* reported the expression of both tetraethylammonium (TEA)-sensitive delayed rectifying potassium channel and inwardly rectifying potassium channel with no expression of sodium channel in human NSC cell line [182]. Likewise, Piper *et al.* found that cultured human NPCs express 4-aminopyridine (4-AP)-sensitive and delayed-rectifier type potassium currents with no observed expression of sodium channel currents under non-differentiating conditions. On the other hand, the majority of them expressed inward tetrodotoxin-sensitive and resistant sodium currents, sustained calcium currents, inwardly rectifying potassium currents) and outward time- and voltage-dependent currents and neuronal markers upon differentiating the cells [183]. Thus, the absence of sodium currents combined with the presence of voltage-activated potassium currents might be one of the characteristic features of NSCs/NPCs [182], [183].

Fluorescent assays enable functional readout of ion channel activity over time in high-throughput platforms [186]. The assays that measure intracellular ionic concentrations are widely used in research and for HTS of ion channel modulators [162]. We initially focused on establishing a high-throughput potassium ion channel assay in 3D-cultured ReNcell VM with FluxOR potassium channel assay kit because of the expression levels of voltage-gated potassium channels (Kv) and the important role of Kv channels in various physiological processes. The FluxOR assay relies on measuring changes in ion concentrations in the intracellular compartment, resulting from potassium ion channel activity. Thallium ions can permeate potassium ion channels and have been substituted for potassium ions in the assay to provide an enhanced signal-to-background ratio [187]–[189]. Kv channels are generally involved in the regulation of membrane potential, cell volume, proliferation, and apoptosis in a wide range of cells [181]. In addition, disruption of even a subtype of

potassium ion channels can result in neurodegenerative diseases such as Alzheimer's and Parkinson's diseases. Due to this important physiological role played by potassium ion channels, it has been used as a therapeutic target for various diseases. The high expression levels of Kv 4.3 and Kv 7.2 in ReNcell VM from RNA-Seq analysis in our study were correlated well with other studies, indicating that they are highly expressed in the human brain [190]. The inhibitor of KCNQ2 channel, XE-991, has been extensively used to block the Kv 7.2/KCNQ2 channel in several *in vitro* and *in vivo* studies even though there has been no clinical trials conducted for this compound [191]–[193]. On the other hand, fluoxetine is a selective serotonin reuptake inhibitor used for treating depression with relatively few side effects [194]–[196]. The effects of fluoxetine on voltage-gated channels have been widely studied [197], [198]. Jeong *et al.* investigated the effects of fluoxetine on cloned Kv4.3 channels expressed in CHO cells using the whole-cell patch-clamp technique and reported that fluoxetine blocked Kv4.3 in a concentration-dependent manner with IC_{50} of 11.8 μM [198]. Our result was correlated with the literature, with more than 20% inhibition observed at 100 μM. In addition, the concentration of fluoxetine in the brain seems to be 20 times higher than the corresponding blood level because of high lipophilicity of the drug [198], [199].

The function of store-operated calcium channels (SOCCs) indicates the inverse relation of calcium ion concentrations in the endoplasmic reticulum (ER) with the rate at which calcium ions cross the plasma membrane and enter the cell [174]. Given the neuroectodermal lineage and non-excitable nature of neural stem/progenitors cells, SOCCs play an important role for neurodevelopmental processes including neurogenesis, proliferation, and migration [200]. Fluorescence-based measurement of calcium ions is

shown to be robust for monitoring the activity of SOCCs [201]. Fluo-4 Direct calcium assay, in particular, allows direct addition of the fluorescence reagent in microtiter well plates, without the need for medium removal and wash steps, and is commonly used for high-throughput assessment of calcium channel activities [202], [203]. 2-APB is one of the most widely studied compound for SOCC modulation, which acts as both the activator and the inhibitor of SOCCs [174], [201], [204]. The biphasic response from 2-APB observed in 2D- and 3D-cultured ReNcell VM is in line with literature that have shown the biphasic action of 2-APB in SOCCs where lower concentration ranges in 1 - 20 μM enhanced store-operated entry whereas higher concentration range in 25 - 100 μM blocked SOCCs [174], [201], [204]. In addition, this complex pharmacological action of 2-APB has not only been shown to be related to applied concentrations but also in the pH levels and cell types [205]. For example, Takahasi *et al.* reported that 2-APB at 100 μM inhibited SOCCs at pH 7.4 whereas it enhanced the store-operated calcium entry at pH 6.5, indicating the dual mode action of 2-APB dependent on external pH [206], [207]. Likewise, in many cell types, the activation of phospholipase C through G protein-coupled receptors liberates calcium ions from the lumen of the ER, resulting in the activation of SOCCs [175].

Efflux transporters including MDR1, MRP1, and BCRP from the ABC transporter family play a major role in drug disposition, limiting the uptake of drugs in target cells and tissue barriers such as the blood-brain barrier [208]. Traditionally, the identification of substrates and inhibitors of ABC efflux transporters and the assessment of their activities has been performed using membrane-based assays, which are prepared from cells expressing ABC transporters [171]. However, these assays are low throughput and do not represent the native transporter expression in the human brain. Therefore, the 3D NSC-based transporter

assay established on the 384-pillar plate is not only high throughput but also provides functional readout of transporter activities and transporter/substrate interactions [171].

RNA-Seq analysis of ReNcell VM revealed minimal expression of ABCB1 (MDR1) and ABCG2 (BCRP) genes and some levels of expression of ABCC1 (MRP1) gene in our study. This result is in contrary to previous studies where higher levels of ABCB1 and ABCG2 gene expression in human neural stem/progenitor cells have been reported [209]–[211]. On the other hand, ABCC1 (MRP1) was found to be expressed highly as compared to the expression levels of the other two efflux transporters. ABCC1 (MRP1) transporters are known to be expressed in the human brain and are involved in removal of endogenous substances and toxic organic anions [184], [185]. In our study, MK-571 did not selectively inhibit the MRP1 transporter for both calcein AM and Hoechst 33342 fluorescent substrates, indicating that MK-571 is a non-selective inhibitor of ABC transporters commonly used to inhibit over-expressed MRP transporters [168]. Probenecid on the other hand, has been shown to be a selective inhibitor of MRP1 transporter [212]. The TAF enabled the comparison of the activity of efflux transporters including MDR1, MRP1, and BCRP among different samples or cell lines [172], [213]. In addition, the TAF of the three ABC-transporters in our study was correlated with the mRNA expression level of those transporters in ReNcell VM identified from RNA-Seq analysis. As the TAF is unitless, the theoretical range is considered to be between 0 to 100 where TAF values > 25 are considered clinically relevant and the cells/specimens are regarded as multi-drug resistance positive whereas with TAF values < 25, the cells/specimens are considered multi-dug resistance negative [172], [213]. In positive control cells, the TAF values can go up to 95 - 98 [214].

3.5. Conclusions

We have successfully established fluorescence-based assays on a 384-pillar plate with 3D-cultured ReNcell VM for high-throughput compound screening for ion channels and transporters. RNA-seq analysis was used to identify ion channels and transporters expressed in ReNcell VM. Only few ion channels and one major ABC transporter was found to be expressed comparatively higher than other functional channels and transporters. Voltage-gated potassium channel and store-operated calcium channel assay was established, and activity of those channels were measured in 3D-cultured ReNcell VM using the known inhibitors of the respective channels. Similarly, ABC-transporter assay was established and TAF was measured for the respective transporter in 3D-cultured ReNcell VM. It is important to develop 3D cell models on HTS systems that can offer highly predictive information at low costs. In the future, we will investigate the effect of unknown compounds on the modulation of ion channels and transporters, and their influence on physiological functions of 3D-cultured NSCs such as proliferation, differentiation, and migration. Rapid, direct, and reliable measurement of compound effects on ion channels and transporters can be used for drug discovery and environmental toxicant screening.

CHAPTER IV

ESTABLISHMENT OF HIGH-CONTENT IMAGING (HCI) ASSAYS IN 3D-CULTURED NSC MICROARRAYS FOR THE ASSESSMENT OF MECHANISTIC NEUROTOXICITY

Pranav Joshi, Soo-Yeon Kang, Kyeong-Nam Yu, Chandrasekhar Kothapalli, and Moo-Yeal Lee*

Department of Chemical and Biomedical Engineering, Cleveland State University

Submitted (March 2019) in Archives of Toxicology

4.1. Introduction

Neurodevelopmental disorders including autism, attention deficit hyperactivity disorder, dyslexia, and other cognitive impairments have been increasing in recent years [215]. Environmental toxicants including heavy metals, pesticides, and herbicides accumulated in the body presumably play an important role in developmental neurotoxicity (DNT). However, only a limited number of compounds have been tested for DNT among a large number of chemicals available in the market [2], [10], [62]. Out of 80,000 – 100,000 chemicals in the market, only about 150 chemicals have been subjected to international DNT guidelines [10], [13], [62]. The lack of information and studies can be attributed to

the current guidelines for DNT which are based entirely on *in vivo* experiments. *In vivo* studies for each chemical requires approximately 700 rodents, costs nearly $1 million, and could take more than a year, making it not only expensive and time-consuming but also ethically questionable [10], [11], [13]. In addition, due to the species-specific difference and the lack of knowledge on pharmaco-/toxicodynamics between rodents and humans, the predictivity of DNT in humans from *in vivo* animal studies is uncertain [7], [14], [15]. Therefore, alternative *in vitro* test methods which are cost-effective, high-throughput, and predictive, based on human-specific toxicity pathways, are required to close the gap [11], [20]. Mechanism-based, target-specific endpoints are required to predict the neurotoxicity of compounds including drug candidates and environmental toxicants in humans [216].

High-throughput screening (HTS) systems implemented for DNT testing of a large number of chemicals should be capable of analyzing the adverse effects on cell and organelle levels [55], [215], [217]. High-content imaging (HCI) assays are indispensable when it comes to high-throughput assessment of DNT as they provide multi-parametric information on cellular functions that play pivotal roles in DNT [62]. HCI analyzes target-specific endpoints (e.g., mitochondrial membrane potential, intracellular glutathione level, oxidative stress, apoptosis/necrosis), morphological changes, and reporter signals thereby improving understanding of the mechanism of action of drug candidates and environmental toxicants. However, HCI assays performed on two-dimensional (2D) cell monolayers limit the predictability of *in vivo* toxicity due to inaccurate representation of *in vivo* tissue structure. Cells in 2D cultures are restricted in various aspects of cell-cell and cell- matrix interactions that are crucial for maintaining regular cell functions, and lack *in vivo* phenotypic and genotypic characteristics [218].

On the other hand, three-dimensional (3D) cell cultures better mimic the physiology of human tissues. Therefore, HCI assays performed on 3D-culture cells can potentially provide better understanding of its morphological and functional features. This further aids in the evaluation of toxicity of drug candidates and environmental toxicants *in vivo.* However, current 3D cell culture systems lack the throughput required for screening DNT against a large number of chemicals [219]. To overcome these limitations, we have developed miniature 3D neural stem cell (NSC) cultures on a unique 384-pillar plate that allows high-throughput, HCI assays to better predict DNT in humans. Stem cells including embryonic stem cells and induced pluripotent stem cells have been used as cellular models for drug discovery and toxicology studies [130]. Among the stem cell models, human neural stem/progenitor cells are suggested as a highly predictive cellular model for neurotoxicity testing [7], [62], [220], due to their ability to proliferate and differentiate into multiple neural lineages from different regions of developing brains [182], [221], [222].

We have recently developed a 384-pillar plate that can be coupled with standard 384-well plates for high-throughput, 3D cell-based, metabolism-induced toxicity assays [223]. Our goal in this study is to demonstrate the HCI capability of the 384-pillar plate using 3D-cultured ReNcell VM for assessing DNT of compounds. Four model compounds have been evaluated against multiple parameters, including mitochondrial membrane impairment, intracellular glutathione levels, cell membrane integrity, DNA damage, and apoptosis, using dyes such as tetramethyl rhodamine methylester (TMRM), monochlorobimane (mBCl), calcein AM, Hoechst 33342, and YO-PRO-1, respectively. Finally, IC_{50} values have been calculated from the dose-response curves obtained to establish 3D HCI assays on the 384-pillar plate.

4.2. Materials and Methods

4.2.1. Human neural stem cell (NSC) culture

ReNcell VM, a human NSC line (EMD Millipore, Burlington, MA, USA) was passaged in complete NSC medium (ReNcell NSC maintenance medium, EMD Millipore) supplemented with 20 ng/mL epidermal growth factor (EGF, EMD Millipore), 20 ng/mL basic fibroblast growth factor (bFGF, EMD Millipore), and 1% (v/v) penicillin/streptomycin (Thermo Fisher, Waltham, MA, USA) on laminin-coated, tissue culture-treated, T-75 flasks in a humidified 5% CO_2 incubator at 37°C. The medium was replaced every two days with freshly-prepared complete NSC medium until the cells reached 90% confluency, after which they were detached with Accutase™ (EMD Millipore), suspended in ReNcell NSC maintenance medium, and centrifuged at 300 *g* for 4 min. The resulting cell pellets were resuspended in 1 mL of complete NSC medium. The density of ReNcells was determined using a Moxi cell counter (ORFLO Technologies, MXZ001), and 1.5×10^6 cells were seeded on freshly-prepared, laminin-coated, T-75 flasks.

4.2.2. Establishment of 3D-cultured NSC on 384-pillar plate

For 3D NSC culture, 384-pillar plates (MBD, South Korea) were coated with 0.01% (w/v) poly(maleic anhydride *alt*-1-octadecene) (PMA-OD) and dried for at-least 4-6 h at room temperature. A mixture of 0.0033% (w/v) poly-L-lysine (PLL) and 25 mM calcium chloride ($CaCl_2$) was prepared in sterile deionized water and printed on top of the PMA-OD-coated 384-pillar plates at a volume of 2 µL with a microarray spotter (S+ Microarrayer from Samsung Electro Mechanics Co. or SEMCO, Suwon, South Korea). NSC medium plates were prepared by dispensing complete NSC medium into 384-well plates (Corning)

at a volume of 50 µL per 384-well and incubated in the 5% CO_2 incubator at 37°C for later use. For 3D NSC culture on the 384-pillar plate, the suspension of ReNcell VM was mixed with 3% (w/v) low-viscosity alginate (Sigma-Aldrich) and 15 mg/mL growth factor reduced (GFR) Geltrex® (ThermoFisher) to achieve a final cell concentration of 2×10^6 cells/mL in 0.75% (w/v) alginate and 2.5 mg/mL Geltrex and stored on ice until printing. The suspension of ReNcell VM in the alginate-Geltrex mixture was then printed on top of dried PLL/$CaCl_2$ spots at a volume of 2 µL (4,000 cells per 384-pillar) while maintaining the slide deck at 7°C to prevent water evaporation during printing. The 384-pillar plates were left on the chilling slide deck for 4 min for gelation and then sandwiched with the 384-well plates containing 50 µL of complete NSC medium per 384-well. The sandwiched 384-pillar/well plates were incubated in the 5% CO_2 incubator at 37°C.

4.2.3. Compound treatment on 3D-cultured NSC

Four model compounds including rotenone, 4-aminopyridine, digoxin, and topotecan (all from Sigma-Aldrich) with different mechanisms of action were selected to demonstrate high-throughput assessment of mechanistic neurotoxicity on the 384-pillar plate platform. These compounds were selected based on previous information of their ability to induce cell death through various mechanisms (**Table 2**). A powder form of each compound was dissolved in DMSO to prepare compound stock solutions. Five concentrations of each compound with 4-fold serial dilution, and one DMSO-alone control, were prepared to obtain dose response curves and calculate IC_{50} values. The concentration ranges of the compounds used were as follows: rotenone (0.16 – 40 µM), 4-aminopyridine (19.5 – 5,000 µM), digoxin (0.04 – 10 µM), and topotecan (0.08 – 20 µM). The dosage range of these compounds were selected based on their known IC_{50} values obtained from literature. The

compounds at five dosages and one control were dispensed at a volume of 50 µL/384-well with 12 replicates per concentration in a 384-well plate. For the assessment of mechanistic neurotoxicity, the 384-pillar plate pre-incubated for 72 h was sandwiched with the 384-well plate containing compounds, and then incubated in the 5% CO_2 incubator for 24 h at 37°C.

Table 2. The four model compounds with their classifications and concentration ranges used in this study.

Compound	Classification	Mechanisms of action [Reference]	Test conc. (µM)
Rotenone	Pesticide, insecticide, and piscicide	AP, MI, OS [224], [225]	0.16 – 40
4- Aminopyridine (4-AP)	Vertebrate pesticide	MI, OS, PCB, (Glover 1982; Jensen et al. 2014; Soares et al. 2018)	19.5 – 5,000
Digoxin	Inotropic agents	AP, OS [229], [230]	0.04 – 10
Topotecan	Chemotherapeutic drug	AP, TI [231]–[233]	0.08 – 20

Abbreviations: mitochondrial impairment (MI), oxidative stress (OS), apoptosis (AP), potassium channel blocking (PCB), and topoisomerase inhibition (TI).

4.2.4. HCI assays of 3D-cultured NSC on 384-pillar plate

Multiple endpoints including mitochondrial impairment with TMRM, DNA damage with Hoechst 33342, decrease in intracellular glutathione level with mBCl, cell membrane integrity with calcein AM, and apoptosis with YO-PRO-1, were evaluated for the determination of mechanisms of compound-induced neurotoxicity. Stock solutions of fluorescent dyes were prepared in DMSO at the following concentrations: 0.5 mM TMRM, 10 mM Hoechst 33342, 200 mM mBCl, 1 mM calcein AM, and 1 mM YO-PRO-1. After

24 h incubation with the model compounds, the 384-pillar plate with 3D-cultured ReNcell VM was rinsed twice for 5 min each by sandwiching it with a 384-well plate containing 50 µL of the saline solution, followed by staining with 50 µL per 384-well of the fluorescent dye solutions in a 384-well plate for 1 h at room temperature. Final working concentrations of fluorescent dyes (0.5 µM TMRM, 10 µM Hoechst 33342, 200 µM mBCl, 0.25 µM calcein AM, and 10 µM YO-PRO-1) were obtained by diluting the dyes in the saline solution containing 140 mM of NaCl and 20 mM $CaCl_2$ in sterile deionized water. After 1 h incubation, excess dyes in the cell spots were removed by rinsing it twice with the saline solution in 384-well plates for 10 min. Apoptosis was assessed with YO-PRO-1 staining after 6, 12, and 24 h of incubation with the compounds.

4.2.5. Image acquisition of 3D-cultured NSC on 384-pillar plate

Images of 3D-cultured ReNcell on the 384-pillar plate were acquired in high-throughput with an automated fluorescence microscope (S+ scanner from SEMCO, South Korea). The S+ scanner contains four filter channels for detecting multicolor, blue, green, and red fluorescent dyes, individually or simultaneously. Fluorescent images stained with different fluorescent dyes were obtained with appropriate filters: TMRM stained cells with the red filter, Hoechst 33342 and mBCl stained cells with a blue filter (DAPI-5060C from Semrock), and calcein AM and YO-PRO-1 stained cells with the green filter. A 4× objective lens (UPLFLN 4X, Olympus, Japan) was used to obtain the image of the entire cell spots from the 384-pillar plate. Exposure times for the filter channels were adjusted based on histogram to obtain optimum fluorescence intensity and prevent photobleaching of the fluorescent dyes.

4.2.6. Image processing and data analysis

Images obtained from the HCI assays were processed using a batch processing macro developed in ImageJ for the extraction of fluorescence intensity, following the method published previously [131]. The intensity data were further analyzed using GraphPad Prism (GraphPad Software, San Diego, CA), except for the intensity data obtained from the apoptosis assay, to determine the concentration-dependent effect of the four model compounds. The data obtained from the apoptosis assay was analyzed using SigmaPlot software to measure both concentration- and time-dependent effects of the compounds on ReNcell VM apoptosis. Changes in fluorescence intensity from TMRM, Hoechst 33342, mBCl, and calcein AM were evaluated to determine mitochondrial impairment, DNA damage, intracellular glutathione level, and cell membrane integrity, respectively. Since the background fluorescence of completely dead ReNcell VM (following treatment with 70% methanol for 1 h) was negligible due to background subtraction, the percentage of live ReNcell VM was calculated using the following equation:

$$\% \textbf{ Live cells} = \left[\frac{F_{Reaction}}{F_{Max}}\right] \textbf{x } 100$$

where $F_{Reaction}$ is the fluorescence intensity of the spot exposed to the compounds and F_{Max} is the fluorescence intensity of fully viable cells. The fluorescent intensities of all the cell spots were normalized with respect to the fluorescent intensity of fully viable cells (i.e., cell spots in control) to generate sigmoidal dose-response curves with response values ranging from 0 to 100% plotted against the logarithm of test concentrations. The sigmoidal dose-response curves and IC_{50} values (concentration of the compound where 50% of cellular mechanism is inhibited) were obtained using the following equation:

$$\mathbf{Y = Bottom + \left[\frac{Top - Bottom}{1 + 10^{(LogIC_{50} - X) \times H}}\right]}$$

where IC_{50} is the midpoint of the curve, X is the log concentration of test compound, H is the hill slope, and Y is the cellular response (% live cells), starting from the top plateau (*Top*) of the sigmoidal curve to the bottom plateau (*Bottom*) [223].

4.2.7. Calculation of the Z' factor and the coefficient of variation (CV)

Robustness and reproducibility of HCI assays on the 384-pillar plate was established by calculating the Z′ factor and the coefficient of variation (CV). The Z′ factor was calculated using the following equation:

$$\mathbf{Z' = \frac{(Avg_{Max} - 3SD_{Max}) - (Avg_{Min} + 3SD_{Min})}{Avg_{Max} - Avg_{Min}}}$$

where Avg_{Max} is the average of all maximum fluorescence intensity from fully viable ReNcell VM on the 384-pillar plate, SD_{Max} is the standard deviation of maximum fluorescence intensity, Avg_{Min} is the average of all minimum fluorescence intensity from the dead cells affected by the highest dose of highly cytotoxic compound (topotecan), and SD_{Min} is the standard deviation of minimum fluorescence intensity. The reproducibility of HCI assays on the 384-pillar plate was measured using the coefficient of variation (CV) which is the ratio of the standard deviation (*SD*) to the average (*Avg*).

$$\mathbf{CV = \frac{SD}{Avg} \times 100}$$

It represents variability in relation to the average signal strength, therefore the inverse of the signal-to-noise ratio [223].

4.2.8. Statistical analysis

To investigate the main mechanism of toxicity for the model compounds, statistical analysis was performed with GraphPad Prism. One-way analysis of variance (ANOVA) was used to compare the mean IC_{50} values of the test compounds obtained from 3D-cultured ReNcell VM. Statistically significant IC_{50} difference among the HCI assays was indicated by * for $p < 0.05$, ** for $p < 0.01$, and *** for $p < 0.001$.

4.3. Results

4.3.1. Robustness of high-content imaging (HCI) assays on 384-pillar plate

HCI assays of 3D-cultured ReNcell VM on the 384-pillar plate were assessed for robustness and reproducibility by calculating Z′ factors and the coefficient of variation (CV: ratio of the standard deviation and the overall mean), prior to testing mechanisms of action of the model compounds. Briefly, ReNcell VM cells printed on the 384-pillar plate were incubated with complete NSC medium for 72 h and treated with the four model compounds for 24 h, followed by cell staining with the fluorescent dyes. To calculate Z′ factors, Avg_{Max} was obtained from control samples exposed to no compound, whereas Avg_{Min} was obtained from the cell spots exposed to the highest dose of highly cytotoxic compound (topotecan). The calculated Z′ factors from topotecan for TMRM, mBCl, and calcein AM staining were 0.59, 0.61, and 0.58 respectively. Since, Hoechst 33342 stained cells showed increase in blue fluorescence intensity due to condensed nuclei, indicating apoptosis, we could not calculate the Z′ factor for Hoechst 33342. Since $0.5 \leq Z' \leq 1$ is considered highly robust for an assay, the HCI assays we performed on the 384-pillar plate platform are robust and suitable for accurately identifying mechanisms of compound toxicity. In addition, the coefficient of variation (CV) was calculated from control samples

exposed to no compound to measure reproducibility of cell printing and the HCI assays on the 384-pillar plate. The fluorescence intensity obtained from staining 3D-cultured ReNcell VM on the 384-pillar plate exposed to no compound was used to calculate CV values for cell printing and day-to-day variability **(Figure 4.1A**). Experimental errors determined by the CV value less than 25% are considered acceptable and reproducible. The overall CV values obtained at different days for the TMRM, calcein AM, mBCl, and Hoechst 33342 assays were 12.4%, 11.8%, 11.3%, and 10.8% respectively, indicating that the HCI assay performed on the 384-pillar plate platform was highly reproducible **(Figure 4.1B)**.

(A)

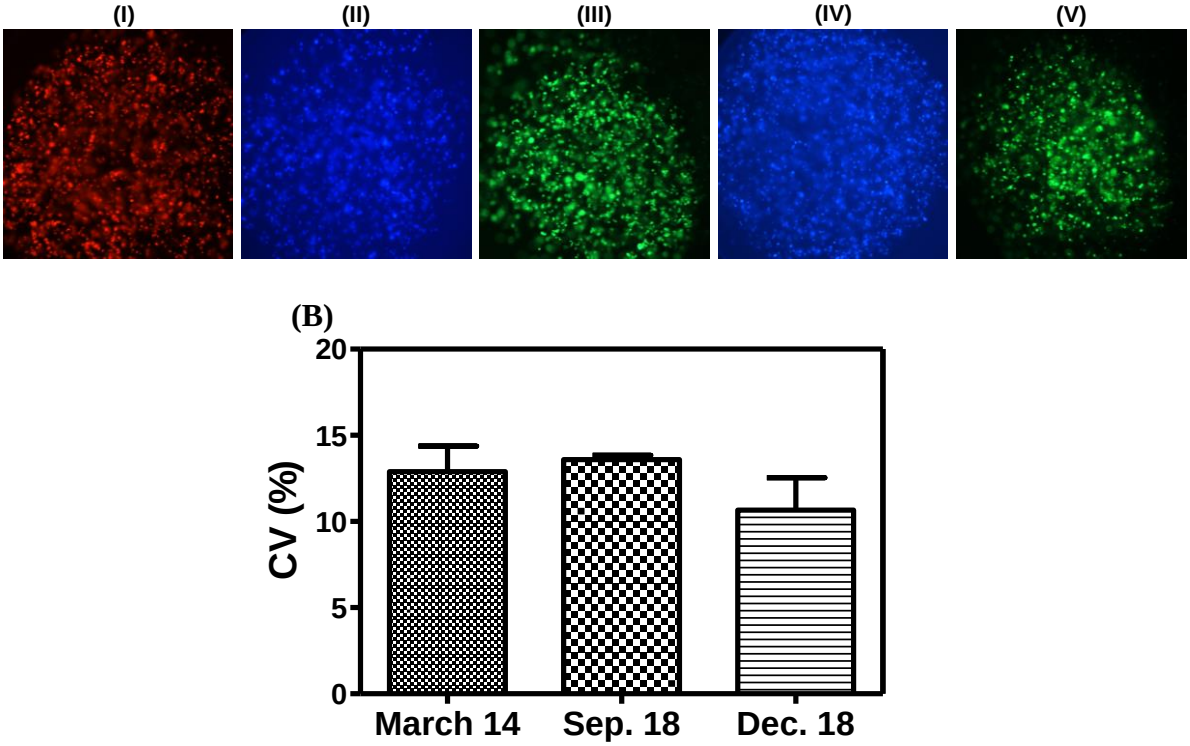

Figure 4.1. (A) Representative fluorescent images of 3D-cultured ReNcell VM at day 4 stained with multiple fluorescent dyes: **(I)** Tetramethyl rhodamine methylester (TMRM), **(II)** monochlorobimane (mBCl), **(III)** Calcein AM, **(IV)** Hoechst 33342, and **(V)** YO-PRO-1. **(B)** Day-to-day variability of CV values determined by TMRM staining for mitochondrial membrane potential. Triplicate 384-pillar plates with each plate containing 12 replicates of each test condition were stained and analyzed on March 14, September 18, and December 18, 2018. The mean CV values obtained at different days were 12.9, 13.6,

and 10.7, respectively. Thus, the overall CV value was 12.4%, indicating high reproducibility of the assay performed on the 384-pillar plate.

4.3.2. Mechanisms of compound toxicity on 3D-cultured NSC

Mechanistic toxicity of the four model compounds was assessed by treating 3D-cultured ReNcell VM on the 384-pillar plate with rotenone, 4-aminopyridine, digoxin, and topotecan, followed by cell staining with the four fluorescent dyes. Fluorescent images were obtained by using the S+ scanner, and fluorescence intensity from cell images was quantified using the ImageJ plugin (**Figure 4.2**). Dose-response curves of the compounds for the four mechanisms of toxicity were plotted by using the normalized fluorescent intensity method (**Figure 4.3**). IC_{50} values were calculated for each compound and assay, in which 50% inhibition of the assessed mechanism of toxicity was observed (**Table 3**). For example, more than 90% impairment in mitochondrial membrane potential (MMP) was observed from the highest concentration of both digoxin and topotecan, whereas only 60% inhibition was observed from the highest concentration of 4-aminopyridine. TMRM is a cell permeable fluorescent dye and its accumulation in the mitochondrial matrix space is dependent on MMP. Since MMP is regarded as a key indicator of mitochondrial health, a decrease in TMRM fluorescence is an indicator of mitochondrial impairment [234]–[236].

Monochlorobimane is a non-fluorescent cell permeable dye that emits blue fluorescence only after conjugation with intracellular glutathione. Intracellular glutathione acts as an antioxidant in mammalian cells and is subjected to depletion by the reactive oxygen species (ROS) generated by toxic compounds [237] [238]. Therefore, a decrease in intracellular glutathione level is an indicator of oxidative stress by the compound. Both

topotecan and digoxin reduced nearly 60% of intracellular glutathione levels in 3D-cultured ReNcell VM. Calcein AM was used to evaluate cell membrane integrity as a measure for cell viability [239]. Calcein AM is a hydrophobic fluorescent dye that permeates live cells and is hydrolyzed by the intracellular esterases to calcein which emits green fluorescence. Calcein is a hydrophilic compound that remains trapped inside the cytosol of intact membranes. The IC_{50} values of topotecan in our study from the calcein AM assay were comparable to those obtained from spheroids of glioma stem cells by *Zhang et al.* [240]. As compared to major changes in MMP after compound exposure, there were minor changes in cell membrane integrity observed at the highest dosage after 24 h incubation with 4-aminopyridine, digoxin, and topotecan. This could be because the cells go through apoptosis with intact cell membrane, as evidenced by YO-PRO-1 staining at different time points. Likewise, Hoechst 33342 which binds to nucleic acid and is widely used to assess condensed pyknotic nuclei in apoptotic cells showed an increase in blue fluorescence intensity, indicating condensed nuclei due to apoptosis [241].

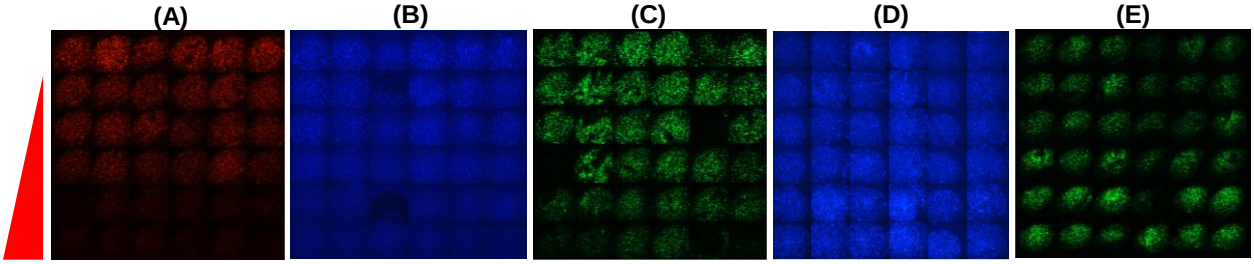

Figure 4.2. Images of 3D-cultured ReNcell VM arrays on the 384-pillar plate exposed to varying concentrations of topotecan (0.08 – 20 µM) for 24 h and stained with four fluorescent dyes: **(A)** TMRM for mitochondrial membrane potential (MMP), **(B)** mBCl for intracellular glutathione (ICG) levels, **(C)** Calcein AM for cell membrane integrity (MI), **(D)** Hoechst 33342 for DNA damage (DD), and **(E)** YO-PRO-1 for apoptosis. A decrease in fluorescence intensity in (A), (B), and (C) and an increase in fluorescence intensity in (D) with increasing compound dosages (from top to bottom) was observed from 3D-cultured ReNcell VM arrays.

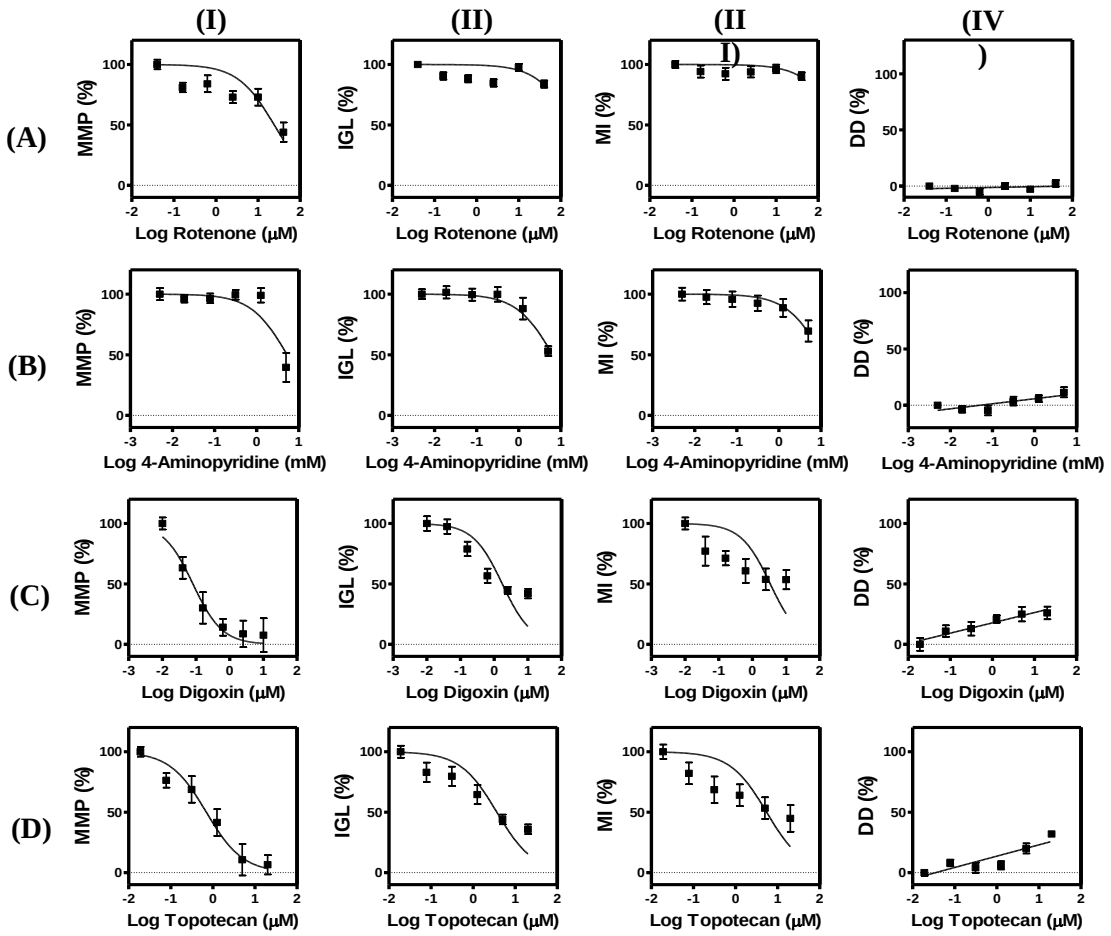

Figure 4.3. Dose response curves of **(A)** Rotenone, **(B)** 4-aminopyridine, **(C)** Digoxin, and **(D)** Topotecan obtained from four HCI assays: **(I)** TMRM for mitochondrial membrane potential (MMP), **(II)** mBCl for intracellular glutathione level (IGL), **(III)** Calcein AM for membrane integrity (MI), and **(IV)** Hoechst 33342 for DNA damage (DD). The array of 3D-cultured ReNcell VM on the 384-pillar plate was exposed to rotenone (0.16 – 40 μM), 4-aminopyridine (19.5 – 5000 μM), digoxin (0.04 – 10 μM), and topotecan (0.08 – 20 μM), for 24 h and stained with TMRM, mBCl, calcein AM, and Hoechst 33342 to obtain dose-response curves and IC_{50} values.

Table 3. Summary of IC_{50} values of four compounds obtained from the HCI assays on 384-pillar plate.

Compound	HCI assays (Endpoints)			
	TMRM (MMP)	**mBCl (IGL)**	**Calcein AM (MI)**	**Hoechst 33342 (DD)**
Rotenone	31.52 ± 7.33	Nontoxic	Nontoxic	NA
4-aminopyridine	4.9 ± 0.45	5.9 ± 0.5	Nontoxic	NA
Digoxin	0.16 ± 0.08	2.06 ± 0.3	3.4 ± 0.8	NA
Topotecan	0.69 ± 0.01	4.24 ± 0.6	6.5 ± 1.0	NA

Abbreviations: mitochondrial membrane potential (MMP), intracellular glutathione level (IGL), membrane integrity (MI), DNA damage (DD), and not applicable (NA).

Apart from indirect assessment of apoptosis *via* condensed nuclei with Hoechst 33342, apoptosis in 3D-cultured ReNcell VM was assessed directly from YO-PRO-1 staining. As apoptosis is a dynamic process, 3D-cultured ReNcell VM on the 384-pillar plate was treated with the four compounds for 6, 12, and 24 h, and then stained with YO-PRO-1 for 1 h. As a result, dose- and time-dependent effects on apoptosis were observed from the compounds (**Figure 4.4**). For example, nearly 50 % increase in apoptosis was observed after 12 and 24 h incubation with 5 μM topotecan as compared to the controls (no compound). Interestingly, the percentage of apoptosis dropped at the highest concentration of 20 μM topotecan at all the time points, possibly indicating that necrosis could have been induced at that concentration. Similarly, digoxin demonstrated both dose- and time-dependent effects on apoptosis. There was a slow and gradual increase in apoptotic cells with increasing digoxin concentration after 6 h incubation, whereas more rapid increase in apoptosis was observed after longer incubation (12 h and 24 h). Necrosis was observed at ≥ 3.125 μM digoxin after 24 h incubation, as evidenced by a decrease in

green fluorescence intensity.

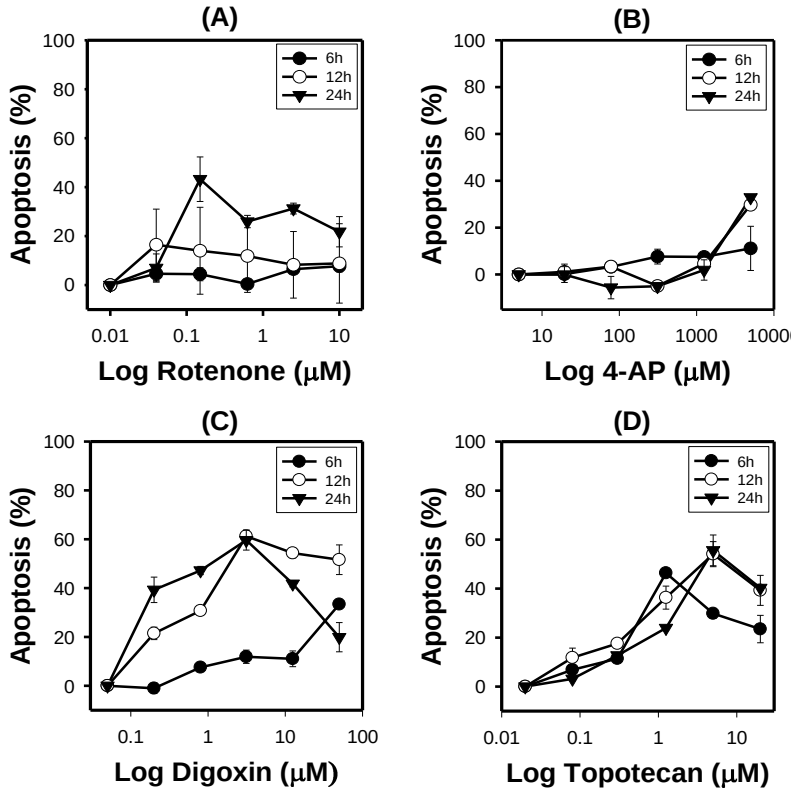

Figure 4.4. Dose-response curves of **(A)** rotenone, **(B)** 4-aminopyridine, **(C)** digoxin, and **(D)** topotecan, obtained from the YO-PRO-1 assay for apoptosis. The array of 3D-cultrued ReNcell VM on the 384-pillar plate was treated with varying concentrations of the four compounds for 6, 12, and 24 h, and stained with 10 μM YO-PRO-1 for an hour to obtain the dose-response curves.

Apoptosis was measured by the increase in fluorescence intensity relative to the control condition. The response of each concentration of a compound was calculated from 12 replicates on a 384-pillar plate, with three independent replicates of the experiment (n = 36 in total). The IC_{50} values of all four compounds obtained from different assays were compared to evaluate the effect of compounds on 3D NSC culture on the 384-pillar plate. Among the five assays/endpoints studied, changes in MMP was found to be the most sensitive mechanism of toxicity based on the IC_{50} values compared to other assays (**Fig.**

4.5). For all the four compounds, changes in MMP was found to be the most sensitive compared to changes in IGL, MI, and DD. Therefore, MMP could be considered as an initiator of the mechanism of toxicity.

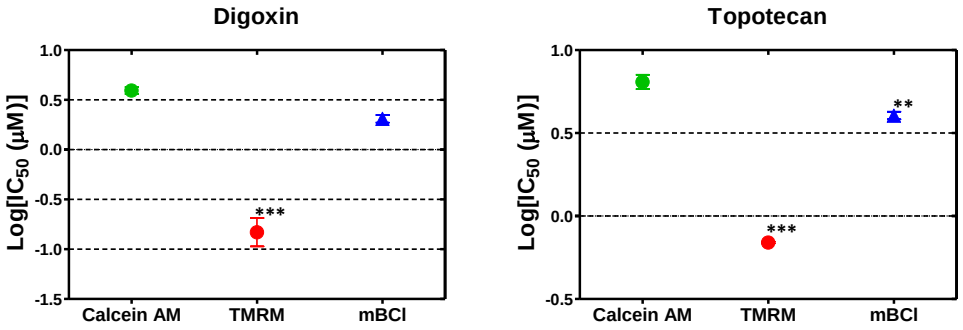

Figure 4.5. One-way ANOVA analysis of IC_{50} values obtained from 3D-cultured ReNcell VM pre-incubated for 72 h, exposed to digoxin and topotecan for 24 h, and stained with calcein AM, TMRM, and mBCl (n=3 independent repeats, $^{**}p < 0.01$, $^{***}p < 0.001$). Statistically significant difference in IC_{50} values of digoxin was observed from TMRM staining, indicating that the main mechanism of toxicity for digoxin is MMP. Statistically significant difference in IC_{50} values of topotecan was observed from TMRM and mBCl staining, indicating that the main mechanism of topotecan toxicity is MMP and IGL.

4.4. Discussion

There is an unmet need among pharmaceutical companies and regulatory agencies to develop a highly predictive *in vitro* cell-based assay platform for early stage detection of neurotoxicity. High-throughput, cell-based assay systems capable of analyzing the adverse effect on human cells are inevitable when it comes to screening a large number of drug candidates and potentially toxic chemicals for DNT testing [6], [9], [53], [130]. Therefore, our goal in this study was to establish 3D-cultured NSCs on a unique 384-pillar plate and demonstrate high-throughput HCI capability for predictive assessment of neurotoxicity. ReNcell VM was selected as a cell model for human NSCs as the progenitor cell line demonstrates the typical features of NSCs, such as the ability to proliferate, self-renew, and

differentiate into neurons, astrocytes, and oligodendrocytes, which represent the lineages from different regions of developing brains. ReNcell VM is a commercially available human neural progenitor cell line obtained from the midbrain region of a 10-week human fetus and immortalized by retroviral transduction with v-myc oncogene [133], [216], [242].

The 3D-cultured ReNcell arrays on the 384-pillar plate established in this study are robust and high-throughput for studying mechanistic compound toxicity. The automated cell printing on the 384-pillar plate combined with 3D cell culture in the 384-well plate ensured highly reproducible outcomes for HCI assays with compounds. The mixture of alginate and Geltrex for cell encapsulation was easily printable and biomimetic for 3D NSC culture. Alginate is biologically inert and provides structural rigidity for cell encapsulation and culture, while Geltrex being bioactive promotes cell-ECM interactions to support cell growth and spheroid formation [136]. For optimum cell-cell interactions, seeding density of 2×10^6 cells/mL was used on the 384-pillar plate, resulting in ~4000 cells per 384-pillar in a 2 µL cell spot. The 384-pillar plate offers several unique advantages in terms of mimicking cell-ECM interactions, ease of media change, high-throughput compound screening, and rapid *in situ* cell imaging as compared to other 3D cell culture systems such as spheroid culture in ultra-low attachment (ULA) plates, microfluidic systems, transwell inserts, and hanging droplet plates. For example, media changing in ULA plates and hanging droplet plates without disturbing the cell aggregates inside is challenging and often time-consuming, leading to damage of those aggregates. Long-term culture and assays of 3D spheroids in hanging droplet plates require transferring the spheroids into a different plate, thus making it cumbersome and low-throughput [243]. In addition, spheroid cultures in ULA plates and hanging droplet plates often lack cell-ECM interactions which are vital

for organotypic 3D cell cultures [244]. Moreover, most of the existing 3D cell cultures such as ExVive™ 3D bioprinted human tissues from Organovo require cryo-sectioning of the spheroids for imaging. Therefore, we envision that the 384-pillar plate and its cell printing technology can be adopted in an industry setting for high-throughput, predictive compound screening, critical for pharmaceutical and chemical companies.

The importance of 3D cell culture models in assessing mechanisms of action of pharmaceutical drug candidates and environmental chemicals for neurotoxicity have been highlighted earlier [6], [131], [216], [245]–[247]. In a recent study, Koo *et al.* established a 3D brain on a chip model with multiple immortalized neuronal cells and reported the correlation of the effect of organophosphates on *in vitro* 3D culture with *in vivo* data [245]. Similarly, Pamies *et al.* reported that a 3D spheroid model of NSCs recapitulates human brain development and demonstrated the reproducible result of neurotoxicity with test compounds for cell viability, ROS generation, and mitochondrial dysfunction [247]. Sirenko *et al.* performed HCI assays on 3D spheroid neural cultures in a 384-well plate with multiple fluorescent dyes to assess cytotoxicity and mitochondrial toxicity of several compounds, demonstrating 3D cultures as a biologically-relevant model system to study neurotoxicity of pharmaceutical drugs and environmental toxicants [246].

Recently, our group has demonstrated the application of this 384-pillar plate platform for the first time in metabolism-induced toxicity assays, using combinations of HEK293 cells and drug metabolizing enzymes [223]. The current study is the first demonstration of high-throughput, HCI capability on the 384-pillar plate with 3D-cultured ReNcell VM for the assessment of compound-induced acute neurotoxicity. Multiple fluorescent dyes such as TMRM, mBCl, calcein AM, Hoechst 33342, and YO-PRO-1, were

used to establish HCI assays and understand various mechanisms of cell death in 3D-cultured ReNcell VM by evaluating the changes in mitochondrial membrane potential, intracellular glutathione levels, cell membrane integrity, DNA damage, and apoptosis, respectively. In particular, apoptosis is an important mechanism of cell death in the developing nervous systems as neural stem/progenitor cells in an early development phase systematically undergo apoptosis during the process of proliferation and differentiation into neurons and glial cells [248], [249]. Due to the high expression of pro-apoptosis activating proteins such as p53 in NSCs, these cells may be even more sensitive to apoptosis than fully differentiated lineages [250]. Therefore, establishing HCI assays for the assessment of apoptosis in NSCs through direct and indirect measures is important for DNT tests *in vitro*. Considering these factors, we investigated the adverse effect of the compounds on various mechanisms of cell death in 3D-cultured ReNcell VM. Studies have shown that the formation of reactive oxygen species (ROS) by toxic compounds leads to a decrease in antioxidant levels, reducing the level of intracellular glutathione [238]. A decrease in the glutathione level further increases the accumulation of ROS, thereby damaging mitochondria and nucleus, and eventually resulting in cell death [88]. In addition, the formation of ROS has been known to induce specific cell death mechanisms such as apoptosis and necrosis [224], [251], [252]. In particular, mitochondria are highly susceptible to oxidative damage as it is a major source of ROS production and thus a primary target for the large amounts of ROS. Mitochondrial intermembrane space houses pro-apoptotic factors such as cytochrome c and apoptosis-inducing factor (AIF) which act in caspase-dependent and caspase-independent manners, respectively [253]. When mitochondrial membranes are disrupted, cytochrome c is released to cytosol, which binds

to Apaf-1 and induces caspase activation in the presence of ATP [254], whereas AIF when released from mitochondria enters the nucleus and activates nuclear endonucleases, leading to chromatin condensation and DNA degradation and ultimately resulting in cell death [224]. Therefore, MMP is a highly sensitive assay to study the mechanism of cell death in neurotoxicity. Undoubtedly, the MMP assay was shown to be the most sensitive assay among the other HCI assays tested for all four compounds.

The mechanisms of toxic action identified through HCI assays are defined as biologically relevant series of key events/endpoints that ultimately lead to adverse outcomes *in vivo* [255]. Therefore, DNT-specific *in vivo* processes can be linked to the changes in various cellular processes such as apoptosis, necrosis, differentiation, and proliferation due to the mechanisms of toxic action that occur at cellular and organelle levels, and thus can be recapitulated with various *in vitro* endpoints. [6], [82]. For example, inhibition of mitochondrial complex I leading to mitochondrial dysfunction has been known to induce motor deficit disorder [82]. Moreover, the brain is known to be highly sensitive to oxidative stress due to low levels of antioxidants and high levels of oxygen consumption. Various opioids and psychostimulant drugs have been shown to trigger oxidative stress and apoptosis *via* mitochondrial dysfunction. These evidences further bolster the need for *in vitro* assays which identify various mechanisms of toxicity to predict the effect of toxic chemicals in human brains [256].

The four model compounds used in this study were selected to demonstrate various mechanisms of toxicity. Rotenone, a common insecticide and pesticide, is known to inhibit the mitochondrial respiratory chain at the complex I site and cause ROS generation. As discussed earlier, accumulation of ROS decreases the glutathione level, resulting in

oxidative stress and disrupting the mitochondrial membrane. This damage in the mitochondrial membrane has been shown to release cytochrome c and induces apoptotic cell death [225]. However, some studies have reported the inhibition of respiratory chain reactions by rotenone-induced necrotic cell death as characterized by intact chromatin and loss of plasma membrane integrity [224], [257]. Therefore, rotenone-induced cell death is variable and depends on multiple factors such as concentration, duration of exposure, and cell type [224]. Jin *et al.* reported rotenone-induced mitochondrial damage in dopaminergic cells *via* caspase-3 activation [225], whereas Li *et al.* reported caspase 9/3-independent cell death in human NSCs by rotenone [224]. Interestingly, we observed a high level of apoptosis in 3D-cultured ReNcells exposed to rotenone for 24 h even at relatively low concentrations, which was comparable to the results of digoxin and topotecan. The effect of rotenone on the other assays was not noticeable as compared to other highly toxic compounds used in this study.

4-Aminopyridine was initially developed as an avicide (Avitrol®) in 1960s. It causes birds to emit distress calls and has been reported to only kill about 1% of the animals when used within the dosage range [258], [259]. However, in the later years it gained wide applications as a treatment for multiple sclerosis. It is a potent potassium channel blocker that protects nerve conduction in demyelinated nerve fibers and improves motor function by enhancing the neuromuscular synaptic transmission [226], [227]. Blocking of voltage-gated potassium channels has been shown to have little to no effect on apoptosis of stem cells [260], which correlated well with our observation in this study. For example, Benı´tez-Rangel *et al.* observed nearly 40% reduction in caspase activity, which is known to be the initiator of apoptosis, in the presence of 4-aminopyridine and other potassium channel

blockers [261]. On the other hand, Soares *et al.* demonstrated the effect of 4-aminopyridine on mitochondrial activity and oxidative stress in *Drosphilia melanogaster* [228]. Based on our observations, 4-aminopyridine seems to be relatively nontoxic with less than 50% inhibition of MMP and IGL, as compared to the other model compounds with relatively high toxicity on 3D-cultured ReNcell VM.

Both digoxin and topotecan were highly toxic with IC_{50} values blow μM ranges for the sensitive assays such as MMP and IGL. Digoxin is a member of the cardiac glycoside family of naturally derived compounds, commonly used for the treatment of heart failure and atrial arrhythmia [229]. Cardiac glycosides have been known to induce apoptosis *via* release of cytochrome c and activation of caspase cascade by the increase in Ca^{2+} concentration. Digoxin is known to inhibit Na^+/K^+ pumps causing increase in intracellular Na^+ levels by decreasing the rate of Na^+ influx through the Na^+/Ca^{2+} exchanger, which in turn inhibits Ca^{2+} efflux through the Na^+/Ca^{2+} exchanger, thereby increasing the Ca^{2+} concentration [262]. Various mechanisms such as calcium-dependent activation of caspases, generation of ROS, and topoisomerase inhibition have been suggested as the mechanisms of cell death by digoxin [229], [230]. Prassas *et al.* reported that digoxin induces caspase-dependent apoptosis in multiple cell lines [229]. In our study, digoxin demonstrated both dose- and time-dependent apoptosis with reduction in MMP as its primary mechanism of toxicity.

Topotecan, a semi-synthetic derivative of camptothecin, is an inhibitor of DNA topoisomerase I and has been approved for the treatment of various cancer types [263]. Inhibition of DNA topoisomerase I results in inhibition of DNA replication and transcription that eventually leads to apoptotic cell death [231]–[233]. Studies in multiple

neuroblastoma cell lines reported that cytotoxic activity of topotecan is highly dependent on exposure time. For example, Chernov *et al.* demonstrated decreasing IC_{50} values for cell viability with Presto Blue with increasing exposure time for various neuroblastoma cell lines [233]. Similarly, Zhang *et al.* showed dose- and time-dependent effects of topotecan on glioma stem cell viability and apoptosis [240]. Topotecan demonstrated both dose- and time-dependent apoptosis in 3D-cultured ReNcell VM over a period of 24 h in our study. In addition, we observed dose-dependent effects of topotecan on all the assays evaluated, with the MMP assay being the most sensitive of all. Overall, our high-throughput 3D cell culture platform was suitable for HCI assays to evaluate various mechanisms of cell death in human NSCs from model compounds, which can be implemented for large-scale screening of neurotoxicity.

4.5. Conclusions

We have successfully demonstrated HCI capability in 3D NSC culture on 384-pillar plate for the first time for the assessment of predictive neurotoxicity. The 3D-cultured ReNcell VM on the 384-pillar plate with five HCI assays, including TMRM, mBCl, calcein AM, Hoechst 33342, and YO-PRO-1 for the evaluation of mitochondrial impairment, intracellular glutathione level, cell membrane integrity, DNA damage, and apoptosis, respectively, generated reproducible data for the assessment of DNT. The HCI assays performed on 3D NSC culture on the 384-pillar plate may need further validation with many model compounds to calculate sensitivity and specificity. With additional DNT-specific endpoints such as proliferation, migration, neurite outgrowth, and synapse formation, our high-throughput, 3D cell culture platform can be implemented for large-scale screening of drug candidates and environmental toxicants in an industry setting.

CHAPTER V

HIGH-THROUGHPUT ASSESSMENT OF METABOLISM-MEDIATED NEUROTOXICITY BY COMBINING 3D-CULTURED NEURAL STEM CELLS AND LIVER CELL SPHEROIDS

5.1. Introduction

Systematic testing of developmental neurotoxicity (DNT) is not mandatory for the regulatory assessment of chemicals in the USA and EU. It is only performed when there is clear evidence of neurotoxicity in systemic acute toxicity or repeated dose studies or based on chemical structure similarity with previously known toxicants [6]. Testing of chemicals for their potential to cause DNT is primarily based on guidelines that require *in vivo* animal studies. In addition, these *in vivo* animal studies do not generate mechanistic data required for scientifically based human-risk assessment. Therefore, significant efforts have been made for validating *in vitro* and *in silico* methods in predicting the neurotoxicity of chemicals in humans, ultimately for reducing the use of animals [6], [223]. To this end, a wide range of *in vitro* systems have been developed to study the effects of neurotoxicants on various cellular functions relevant to the events in humans [264].

High-throughput screening (HTS) with two-dimensional (2D) cell monolayers and preclinical evaluations with animal models are often inaccurate due to the lack of

correlations between *in vitro* cell models and *in vivo* animal models and differences in genetic makeups between animals and humans. In addition, the poor predictivity of *in vitro* models to *in vivo* models can be attributed in part due to the lack of multicellular models with biotransformation capability. Chemicals can be transformed into their metabolites by drug-metabolizing enzymes (DMEs) in the liver, some of which can be severely toxic to organs including the brains [16], [265]. Therefore, it is important to maintain physiologically relevant levels of DMEs in HTS assays and understand the roles of these enzymes in human toxicology [223]. However, despite the knowledge of biotransformation playing an important role in the augmented toxicity of chemicals, relatively little efforts have been made to incorporate biotransformation into an *in vitro* neurotoxicity testing system. Conventional *in vitro* systems for neurotoxicity tests lack the capability of investigating the qualitative and quantitative differences between parent chemicals and their metabolites in the human body [265].

To the best of our knowledge, no high-throughput, *in vitro* methods for evaluating metabolism-mediated neurotoxicity of chemicals have been developed and validated, emphasizing the urgent need for predictive *in vitro* neurotoxicity test systems [264]. Existing *in vitro* hepatotoxicity test models including liver microsomes, recombinant DMEs, primary hepatocytes, isolated liver slices, and transformed hepatic cell lines (e.g., THLE2, HepG2, Hep3B, etc.) are limited to testing neurotoxicity [264], [266]–[268]. For examples, isolated enzymes such as liver microsomes and recombinant DMEs lack the correlation of metabolic activity with *in vivo* metabolism [269], liver slices are difficult to obtain in consistent quantities and qualities and rapidly deteriorated [267], [268], hepatic cell lines express low levels of DMEs [270], and primary hepatocytes have limited lifespan

and are difficult to maintain high DME activity [269], [271]. In addition, there is lack of hepatic and neural cell co-culture systems that can be easily adopted in HTS of chemicals.

Therefore, there is an urgent need to develop an *in vitro* toxicity screening system that can incorporate hepatic biotransformation of chemicals and predict the susceptibility of their metabolites to induce neurotoxicity [272]. Co-cultures of metabolically competent hepatic cells with neural cells can be of critical importance for screening test compounds susceptible to cytochrome P450 enzymes (CYP450s) metabolism [272]. However, simulating metabolism-mediated neurotoxicity *in vitro* is a challenging task due to reduction in activities of specific DMEs in the *in vitro* system as compared to their activities found in the liver. To address these issues, we adopted 3D cultures of metabolically competent and consistent hepatic cells such as a HepaRG cell line with neural stem cells (NSCs) such as ReNcell VM and established a high-throughput, metabolism-mediated neurotoxicity testing system. Spheroids of HepaRG cells were generated in an ultra-low attachment (ULA) 384-well plate and 3D-cultured ReNcell VM was established by printing ReNcell VM in hydrogel on a 384-pillar plate with 4 sidewalls and 4 slits (384PillarPlate). To demonstrate the proof of concept of metabolism-mediated neurotoxicity, model compounds were added in the ULA 384-well plate with HepaRG spheroids, which was coupled with the 384PillarPlate with 3D-cultured ReNcell VM. This simple and straightforward approach allows us to generate metabolites *in situ* by HepaRG cells and systematically test them against ReNcell VM by incorporating high-content imaging (HCI) assays for various cellular functions. We envision that this approach can be widely adopted in pharmaceutical and chemical industries for HTS of compounds and their metabolites for the assessment of neurotoxicity.

5.2. Materials and Methods

5.2.1. HepaRG spheroid culture in ULA 384-well plate

HepaRG complete base medium with supplements (MH100, Lonza, Basel, Switzerland) and the thawing additive (MHTAP, Lonza) were warmed in a 37°C water bath for 30 min. A complete thawing medium was prepared by adding 11.8 mL of MHTAP in 100 mL of MH100. NoSpin HepaRG™ cells (Lonza) were transferred into a 50 mL conical tube containing 7.5 mL of the warm thawing medium. HepaRG cell suspension at 1 million cells/mL was prepared by gently pipetting the solution up and down and seeded in an ultra-low attachment (ULA) 384-well plate (Corning, USA) **(Figure 5.1B)** at 5000 cells/384-well by dispensing 50 µL/384-well. The ULA 384-well plate was incubated for 24 h in a humidified 5% CO_2 incubator (ThermoFisher, Waltham, MA, USA) at 37°C to form HepaRG aggregates **(Figure 5.1D)**. After 24 h incubation, the thawing medium was replaced with a warm maintenance medium prepared by adding the maintenance additive (MHMET, Lonza) in MH100. The medium was changed by taking out 30 µL of the thawing medium from each 384-well and then adding 30 µL of the fresh maintenance medium followed by medium change every 2 days.

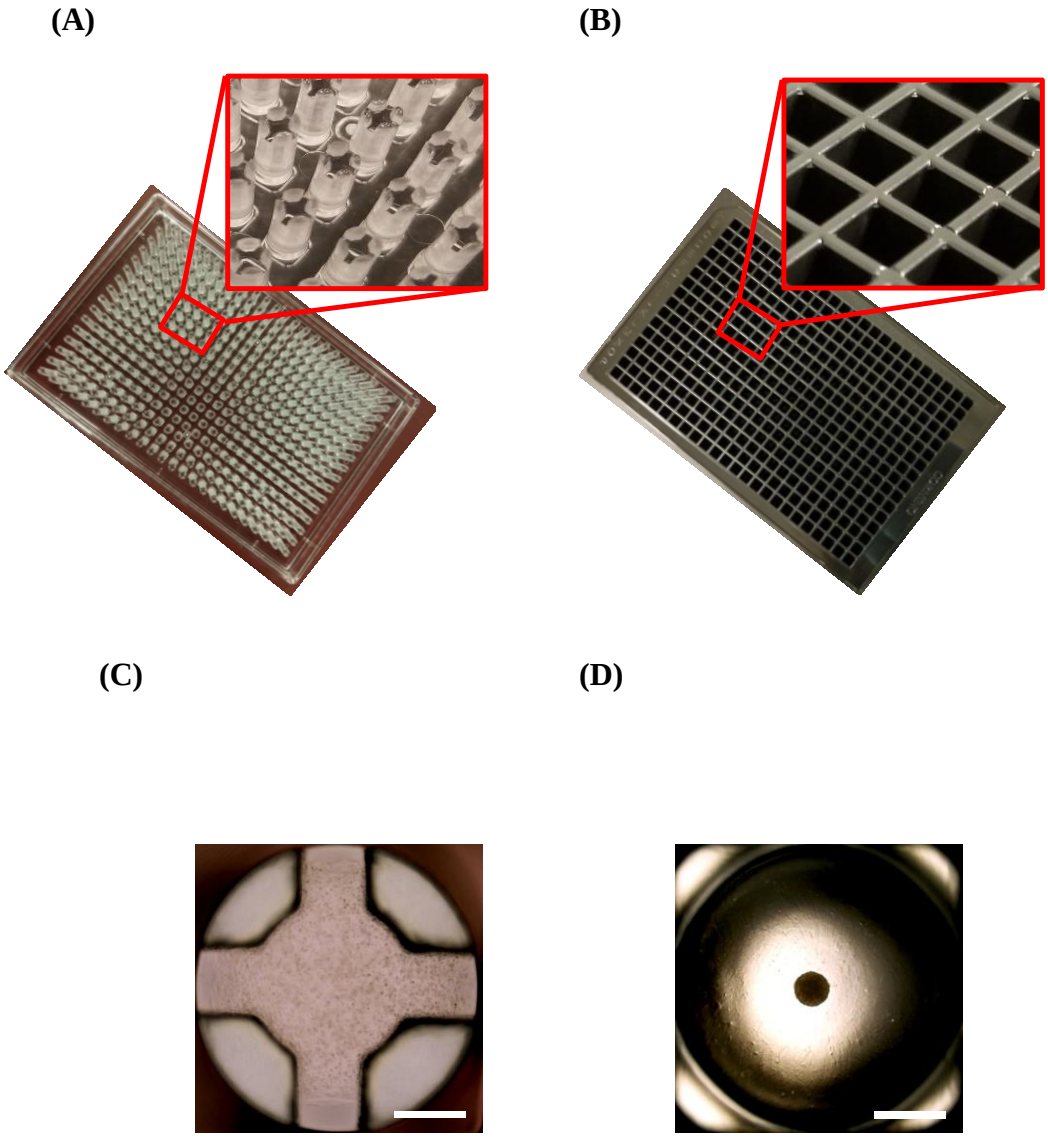

Figure 5.1. Pictures of **(A)** the 384PillarPlate and **(B)** the ULA 384-well plate as well as brightfield images of **(C)** 3D-cultured ReNcell VM on the 384PillarPlate and **(D)** HepaRG spheroids in the ULA 384-well plate. (Scale bar: 700 µm)

5.2.2. Viability of hepatic spheroids in ULA 384-well plate

Viability of HepaRG spheroids in the ULA 384-well plate was assessed at day 3 and day 7 using CellTiter-Glo® assay kit (Promega). Briefly, an equal volume of CellTiter-Glo reagent was added to the 384-wells containing HepaRG spheroids in the maintenance medium and incubated for 10 min at room temperature on an orbital shaker (Fisher

Scientific) to induce cell lysis. The lysate was transferred to an opaque white luminometer plate (Corning) and incubated further for 10 min at room temperature to stabilize luminescent signals. Control wells containing the maintenance medium without the spheroids were prepared to measure background luminescence. Luminescence intensity was measured at 560 nm with an integration time of 0.25 - 1 s using a microtiter plate reader (Synergy H1, BioTek).

5.2.3. Human neural stem cell (NSC) culture

ReNcell VM, a human NSC line (EMD Millipore, Burlington, MA, USA) was passaged in a complete NSC medium (ReNcell NSC maintenance medium, EMD Millipore) supplemented with 20 ng/mL epidermal growth factor (EGF, EMD Millipore), 20 ng/mL basic fibroblast growth factor (bFGF, EMD Millipore), and 1% (v/v) penicillin/streptomycin (ThermoFisher) on laminin-coated, tissue culture-treated, T-75 flasks in the 5% CO_2 incubator at 37°C. The medium was replaced every 2 days with freshly-prepared complete NSC medium until the cells reached 90% confluency, after which they were detached with Accutase™ (EMD Millipore), suspended in ReNcell NSC maintenance medium, and centrifuged at 300 *g* for 4 min. The resulting cell pellets were resuspended in 1 mL of complete NSC medium. The density of ReNcell VM was determined using a Moxi cell counter (ORFLO Technologies, MXZ001), and 1.5×10^6 cells were seeded on freshly-prepared, laminin-coated, T-75 flasks.

5.2.4. Establishment of 3D-cultured NSCs on 384PillarPlate

For 3D NSC culture, 384PillarPlates **(Figure 5.1A)** were coated with 0.01% (w/v) poly(maleic anhydride *alt*-1-octadecene) (PMA-OD) and dried for at-least 4-6 h at room temperature. A mixture of 0.0033% (w/v) poly-L-lysine (PLL) and 25 mM calcium

chloride ($CaCl_2$) was prepared in sterile deionized water and printed on top of the PMA-OD-coated 384PillarPlates at a volume of 3 μL with a microarray spotter (ASFA™ spotter, MBD Korea, Suwon, South Korea). NSC medium plates were prepared by dispensing complete NSC medium into deep well 384-well plates (Corning) at a volume of 130 μL per 384-well and incubated in the 5% CO_2 incubator at 37°C for later use. For 3D NSC culture on the 384PillarPlate, the suspension of ReNcell VM was mixed with 3% (w/v) low-viscosity alginate (Sigma-Aldrich) and 15 mg/mL growth factor reduced (GFR) Geltrex® (ThermoFisher) to achieve a final cell concentration of 2×10^6 cells/mL in 0.75% (w/v) alginate and 2.5 mg/mL Geltrex and stored on ice until printing. The suspension of ReNcell VM in the alginate-Geltrex mixture was then printed on top of dried PLL/$CaCl_2$ spots at a volume of 3 μL (6,000 cells per pillar) while maintaining the slide deck at 7°C to prevent water evaporation during printing. The 384-pillar plates were left on the deck for 4 min for gelation and then sandwiched with the deep well 384-well plates containing 130 μL of complete NSC medium per 384-well **(Figure 5.1C)**. The sandwiched 384Pillar/well plates were incubated in the 5% CO_2 incubator at 37°C.

5.2.5. Viability of 3D-cultured NSCs on 384PillarPlate

The viability of 3D-cultured ReNcell VM on the 384PillarPlate was measured over a period of 10 days using a Live/Dead® viability/cytotoxicity kit for mammalian cells (ThermoFisher). In addition, to simulate the effect of HepaRG and ReNcell VM co-culture in HepaRG maintenance medium, viability of 3D-cultured ReNcell VM at day 7 was assessed using the Live/Dead assay kit after exposing ReNcell VM to HepaRG maintenance medium for 3 days. Briefly, the 384PillarPlate with 3D-cultured ReNcell VM was separated from the 384-well plate with complete NSC medium and rinsed with a saline

solution containing 140 mM NaCl and 20 mM $CaCl_2$. The 3D-cultured ReNcell VM on the 384PillarPlate after exposing to HepaRG maintenance medium for 3 days was stained with a mixture of 0.25 μM calcein AM and 1 μM ethidium homodimer-1 from the kit in a 384-well plate for 1 h at room temperature. The 384PillarPlate was rinsed twice with the saline solution to remove excess dyes, and fluorescent images were acquired in high throughput with an automated fluorescent microscope (S+ scanner from Samsung Electro-Mechanics, Co., Suwon, South Korea). The fluorescent cell images were obtained with a green filter (XF404 from Omega Optical) and a red filter (TxRed-4040C from Semrock) at 4× magnification with the Olympus UPLFLN 4× (numerical aperture (NA) 0.13, f-number 26.5, and depth of field (DOF) ~ 32.3 μm) (Olympus, Tokyo, Japan). Cell images obtained from the 384PillarPlate were batch-processed using ImageJ (NIH) to extract fluorescence intensity from the entire cell spots and were analyzed using SigmaPlot software ver. 12 (Systat Software Inc., San Jose, CA, USA).

5.2.6. Measurement of drug-metabolizing enzyme (DME) activities in HepaRG spheroids

CYP3A4 activity

Among representative DMEs, CYP3A4 activity in HepaRG spheroids was measured using P450-Glo™ assay kit (Promega). Briefly, lyophilized luciferin detection reagent and the reconstitution buffer solution were brought to room temperature and mixed together several times to achieve a homogeneous solution. Luminogenic substrate was prepared by diluting the luciferin-PFBE in HepaRG maintenance medium at 1: 40 dilution. For the CYP3A4 assay, the medium was removed from the 384-wells of the ULA plate and 40 μL of the luminogenic substrate solution was added. The cells were then incubated in the CO_2

incubator at 37°C for 3.5 h after which 25 μL/384-well of the luminogenic substrate solution from the ULA plate was transferred into a 384-well opaque white luminometer plate. An equal volume of reconstituted luciferin detection reagent (LDR) was added into the wells containing the luminogenic substrate and incubated for 20 min at room temperature, followed by luminescence measurement at 560 nm with the microtiter plate reader.

Glutathione-S-transferase (GST) activity

The activity of GSTs in HepaRG spheroids was measured using a GST assay kit (Sigma-Aldrich). Briefly, HepaRG spheroids in the ULA plate were rinsed with DPBS and incubated with 40 μL of Cell Lytic™ MT (Sigma-Aldrich) for 20 min at room temperature on the orbital shaker. The cell lysate was collected from each 384-well into a cold microcentrifuge tubes and centrifuged for 10 min at 16,000 *g* to remove cell debris. The protein-containing supernatant was transferred to a chilled microcentrifuge tube and kept on ice until use. For the GST assay, 200 mM of L-glutathione (GSH) solution was kept on ice while DPBS and 100 mM of 1-chloro-2,4-dinitrobenzene (CDNB) solution were kept at room temperature. A substrate master mix was prepared by adding 200 mM of GSH and 100 mM of CDNB in DPBS to achieve a final concentration of 2 mM GSH and 1 mM CDNB. GST control was prepared by diluting the GST solution 50-fold in a sample buffer. The substrate master mix was dispensed in a new 384-well plate at 45 μL, followed by dispensing 5 μL of the sample per 384-wells and 5 μL of GST control in control wells. Blank control was prepared by dispensing 50 μL of the substrate master mix into the 384-well plate. Absorbance was measured at 340 nm using the microtiter plate reader over a

period of 30 min immediately after preparing the reaction test. GST activity was determined by using the following equation.

$$\frac{\frac{\Delta A_{340}}{min} \times V(mL) \times dil}{\varepsilon_{mM} \times V_{enz}(mL)} = \frac{\mu mol}{mL \times min}$$

Where

$$\frac{\Delta A_{340}}{min} = \frac{A_{340\,(final)} - A_{340\,(initial)}}{reaction\ time\ (\text{min})}$$

V = reaction volume (0.05 mL)

V_{enz} = volume of the enzyme sample tested (0.005 mL)

dil = dilution factor of the original sample

ε_{mM} = extinction coefficient of CDNB conjugate at 340 nm (3.6 $mM^{-1}cm^{-1}$ for a path length of 0.37 cm of the 384-well plate) [4]

UDP glucuronosyltransferase (UGT) activity

Luminescence-based UGT-Glo™ assay kit (Promega) was used to measure UGT activity in HepaRG spheroids. All the reagents were prepared and diluted according to the manufacturer's protocol. Briefly, 40 µL of the HepaRG maintenance medium was aspirated out from the ULA 384-well plate, 5 µL/384-well of 16 mM UDPGA solution and the HepaRG medium were added into sample wells and control wells, respectively. The UGT reaction mixture was added at 10 µL/384-well to all wells including the control wells. The ULA 384-well plate was incubated in the 5% CO_2 incubator at 37°C for 2 h, which was followed by adding 20 µL of reconstituted luciferin detection reagent with D-cysteine

into all wells and incubated for 20 min at room temperature. Luminescence was measured using the microtiter plate reader at 560 nm with an integration time of 0.25 - 1 s.

Albumin secretion

Albumin secretion from HepaRG spheroids was measured using human albumin (ALB) Elisa kit (ThermoFisher). Before performing the assay, all the reagents were brought to room temperature and prepared according to the manufacturer's protocol. Supernatants were collected from the ULA 384-well plate and stored at -80°C until use. Samples and standards were added into appropriate wells of anti-human albumin precoated 96-well strip plate and incubated for 2.5 h at room temperature with gentle shaking. The 96-well plate was rinsed with 1x wash buffer and incubated with biotinylated antibody for 1h followed by washing and incubation with streptavidin-HRP solution for 45 min at room temperature with gentle shaking. After incubation with streptavidin-HRP solution, 3,3',5,5'-tetramethylbenzidine (TMB) substrate was added and incubated for 30 min at room temperature in the dark with gentle shaking, which was followed by adding the stop solution. Absorbance was measured with the microtiter plate reader at 450 nm and 550 nm. The absorbance values at 550 nm was subtracted from the values obtained at 450 nm to correct for optical imperfections in the microplate.

5.2.7. Compound treatment for metabolism-mediated neurotoxicity

Metabolism-sensitive model compounds including acetaminophen, cyclophosphamide, and 3,3'-iminodipropionitrile (IDPN) (all from Sigma-Aldrich) were selected to investigate metabolism-mediated neurotoxicity in the HepaRG and ReNcell VM co-culture system. A powder form of each compound was dissolved in DMSO to prepare compound stock solutions. Five concentrations of each compound with 4-fold serial dilution and one

DMSO-alone control were prepared in HepaRG maintenance medium to obtain dose response curves and calculate IC_{50} values. The concentration ranges of the compounds used were as follows: acetaminophen (0.1 - 25 mM), cyclophosphamide (0.1 - 25 mM), and IDPN (0.02 - 4 mM). The dosage range of these compounds were selected based on their known IC_{50} values obtained from literature. The compounds at five dosages and one control were dispensed at a volume of 40 µL/well in the ULA 384-well plate containing 7 day-cultured HepaRG spheroids. For the assessment of metabolism-mediated neurotoxicity, the 384PillarPlate with 7 day-cultured ReNcell VM was sandwiched with the ULA 384-well plate containing compounds and HepaRG spheroids, and the sandwiched plates were incubated for 48 h in the 5% CO_2 incubator at 37°C **(Figure 5.2)**. As a control, 3D-cultured ReNcell VM was exposed to the test compounds in the absence of HepaRG spheroids in a deep-well 384-well plate.

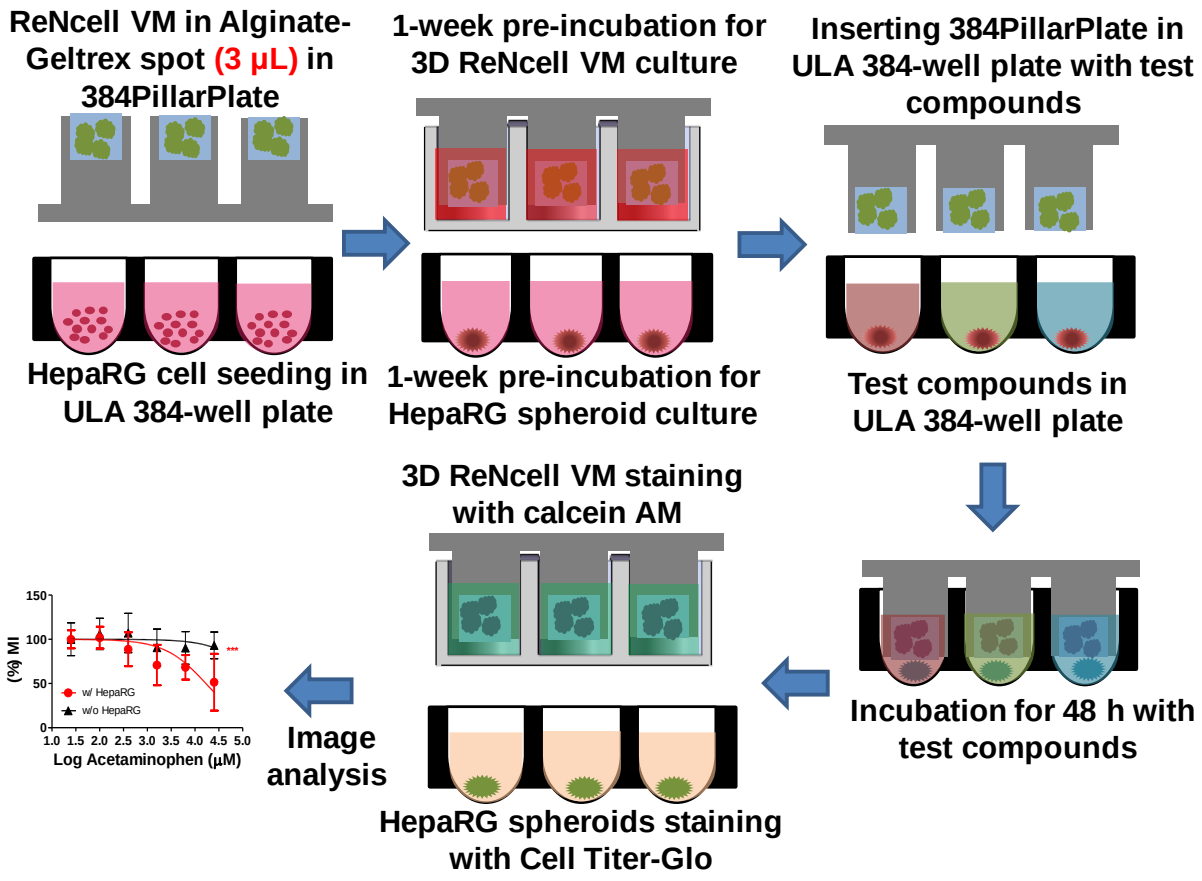

Figure 5.2. Schematic of experimental procedures for metabolism-mediated neurotoxicity. Metabolism-induced neurotoxicity of compounds was assessed with 3D-cultured ReNcell VM on the 384PillarPlate coupled with HepaRG spheroids and test compounds in the ULA 384-well plate. ReNcell VM was encapsulated in 0.75% (w/v) alginate and 2.5 mg/mL Geltrex and cultured in 3D on the 384PillarPlate for 7 days. HepaRG cells were incubated for 7 days to form spheroids and maintain high hepatic functions prior to compound exposure. Compound exposure in the ReNcell VM and HepaRG co-culture system was performed for 2 days.

5.2.8. Assessment of metabolism-mediated neurotoxicity

Viability of 3D-cultured ReNcell VM on the 384PillarPlate after exposure to metabolites generated by HepaRG spheroids in the ULA plate was measured by calcein AM staining for cell membrane integrity. Briefly, a stock solution of 1 M calcein AM was prepared in DMSO. A final working concentration of the fluorescent dye (0.25 µM calcein AM) was

obtained by diluting the dye stock solution in the saline solution containing 140 mM of NaCl and 20 mM of $CaCl_2$ in sterile deionized water. After 48 h compound exposure with HepaRG spheroids, the 384PillarPlate with 3D-cultured ReNcell VM was rinsed twice for 5 min each by sandwiching it with a 384-well plate containing 50 µL of the saline solution, followed by staining with 50 µL/384-well of 0.25 µM calcein AM in a 384-well plate for 1 h at room temperature. After 1 h incubation, excess dye in the cell spots was removed by rinsing it twice with the saline solution in 384-well plates for 10 min. Viability of HepaRG spheroids in the ULA 384-well plate after compound exposure was measured using the CellTiter-Glo assay as described above. Green fluorescent images of 3D-cultured ReNcell VM on the 384PillarPlate were acquired rapidly with the S+ scanner. Exposure times for the filter channels were adjusted based on histogram to obtain optimum fluorescence intensity and prevent photobleaching of the fluorescent dye.

5.2.9. Image processing and data analysis

Image processing and data analysis were performed according to the published methods [131], [223]. Briefly, green fluorescent images obtained from calcein AM staining of ReNcell VM on the 384PillarPlate were processed using a batch processing macro in ImageJ for the extraction of fluorescence intensity. The intensity data were plotted using GraphPad Prism 8 (GraphPad Software, San Diego, CA) to determine the concentration-dependent effect of the test compounds. Since the background fluorescence of completely dead ReNcell VM (following treatment with 70% methanol for 1 h) was negligible due to background subtraction, the percentage of live ReNcell VM was calculated using the following equation:

$$\% \textbf{ Live cells} = \left[\frac{F_{Reaction}}{F_{Max}}\right] \textbf{x } 100$$

where $F_{Reaction}$ is the fluorescence intensity of the spot exposed to the compounds and F_{Max} is the fluorescence intensity of fully viable cells. The fluorescent intensities of all the cell spots were normalized with respect to the fluorescent intensity of fully viable cells (i.e., cell spots in control) to generate sigmoidal dose-response curves with response values ranging from 0 to 100% plotted against the logarithm of test concentrations. The sigmoidal dose-response curves and IC_{50} values (concentration of the compound where 50% of cellular mechanism is inhibited) were obtained using the following equation:

$$\mathbf{Y = Bottom} + \left[\frac{Top - Bottom}{1 + 10^{(LogIC_{50} - X)\times H}}\right]$$

where IC_{50} is the midpoint of the curve, X is the log concentration of test compound, H is the hill slope, and Y is the cellular response (% live cells), starting from the top plateau (*Top*) of the sigmoidal curve to the bottom plateau (*Bottom*).

5.2.10. Statistical Analysis

To investigate the effect of compound biotransformation on toxicity, statistical analysis was performed with GraphPad Prism 8. The data are presented as the means ± standard deviation (SD). Students' t-tests were conducted at the same concentration of a test compound in the presence and absence of HepaRG spheroids. Statistically significant difference between no HepaRG control and HepaRG test conditions was indicated by * for $p < 0.05$ and *** for $p < 0.001$.

5.3. Results

5.3.1. Viability of 3D-cultured ReNcell VM and HepaRG spheroids

The viability of ReNcell VM encapsulated in alginate-Geltrex on the 384PillarPlate and cultured in complete NSC medium was measured at days 1, 4, 7, and 10 with calcein AM and ethidium homodimer-1 staining. In addition, the viability of 3D-cultured ReNcell VM was also assessed after 24 h and 72 h of culture in HepaRG maintenance medium. High viability of ReNcell VM in the mixture of 0.75% (w/v) alginate and 2.5 mg/mL GFR Matrigel on a regular 384-pillar plate with a flat surface has been reported previously in chapter 2. Similarly, we have observed high viability of 3D-cultured ReNcell VM in the mixture of 0.75% (w/v) alginate and 2.5 mg/mL Geltrex on the 384PillarPlate. Formation of ReNcell VM spheroids on the 384PillarPlate was observed over a period of 10 days as evidenced by the increased size of spheroids (**Figure 5.3A**) and the increased fluorescence intensity from the ReNcell VM images at days 4, 7, and 10 (**Figure 5.3C**). The green-colored dots represent live cells stained with calcein AM. In addition, the viability of 3D-cultured ReNcell VM was maintained even after 3 days of culture in HepaRG maintenance medium, demonstrating the similarity in media compositions between the HepaRG medium and the ReNcell VM medium, and the robustness of 3D-cultured ReNcell VM on the 384PillarPlate (**Figure 5.3B and 5.3D**). On the other hand, the viability of HepaRG spheroids in the ULA plate was measured at day 3 and day 7 with the CellTiter-Glo assay, which measures the ATP level in the cells. We observed that HepaRG spheroids maintained high viability in the HepaRG maintenance medium over a period of 1 week (**Figure 5.3E**).

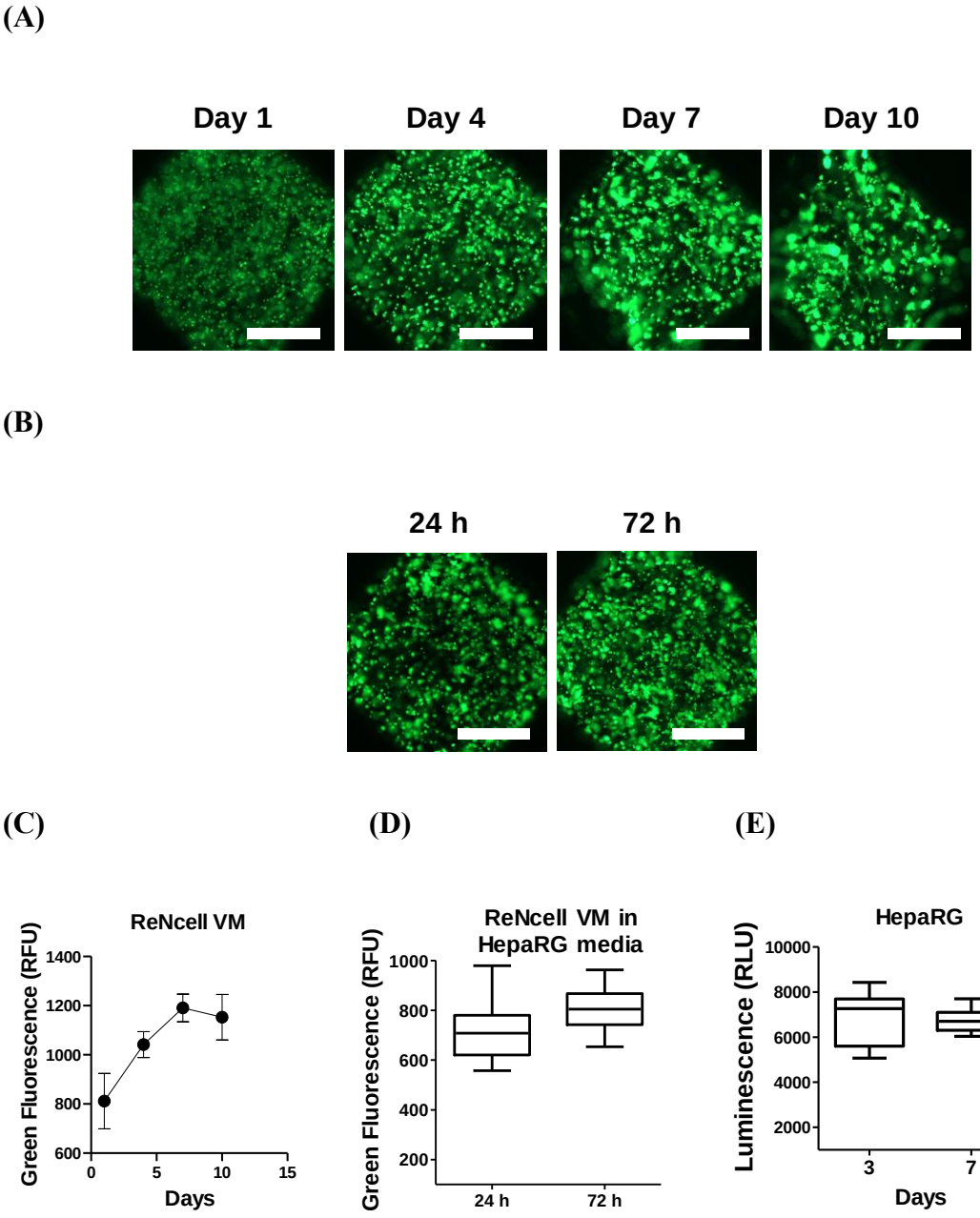

Figure 5.3. Viability of 3D-cultured ReNcell VM on the 384PillarPlate and HepaRG spheroids in the ULA 384-well plate. (A) Pictures of ReNcell VM encapsulated in 0.75% alginate and 2.5 mg/mL Geltrex on the 384PillarPlate, incubated for 10 days, and stained with the Live/Dead cell viability assay kit (Scale bar: 500 µm). **(B)** ReNcell VM viability assessed after 24 h and 72 h incubation in HepaRG maintenance medium (Scale bar: 500 µm). **(C)** Changes in green fluorescence intensity in 3D-cultured ReNcell VM over 10 days. **(D)** Changes in green fluorescence intensity in 3D-cultured ReNcell VM after incubation for 24 h and 72 h in HepaRG media. **(E)** Changes in luminescence in HepaRG spheroids cultured in the ULA 384-well plate over 1 week to determine cell viability.

5.3.2. Hepatic functions of HepaRG spheroids

HepaRG spheroids in the ULA 384-well plate were tested for several liver functions including representative DME activities and albumin secretion using commercially available cell-based assays. Among the most important DMEs, the activity of CYP3A4 was determined by a non-lytic, cell-based P450-Glo assay, which contains a cell-permeable luminogenic substrate (proluciferin) that is converted to luciferin by intracellular CYP3A4. Luciferin comes out of the cells, reacts with a luciferin detection reagent (LDR), emits light which is proportional to the activity of CYP3A4. CYP3A4 activity in HepaRG spheroids was found to be increased over time at day 5 and 9 in HepaRG maintenance medium as supported by the increase in luminescence (**Figure 5.4A**). One of representative Phase II enzymes, GST activity was also shown to be increased after 5 days of incubation in HepaRG maintenance medium (**Figure 5.4B**). The activity of GSTs increased nearly 9-fold over a period of 9 days from 1 µmol/mL/min to 9 µmol/mL/min. CDNB has been used as a substrate of GSTs, which is conjugated with GSH through the thiol group of GSH by the catalytic activity of GSTs. The GS-CDNB conjugate was detected at 340 nm, and the rate of absorbance increase was directly proportional to GST activity. GST activity was expressed as µmol/mL/min, which indicates the amount of GS-CDNB conjugate generated per min by 1 mL of the reaction solution [273]. Likewise, the activity of UGTs in HepaRG spheroids increased from day 5 as evidenced by the increase in the consumption of luminogenic proluciferin substrate at day 5 determined by the UGT-Glo assay **(Figure 5.4C)**. Since proluciferin was converted into glucuronidated luciferin by UGT enzymes in the presence of UDPGA, there was decrease in luminescence when UGTs were active, whereas native proluciferin reacted with D-cysteine and emitted strong light after

conjugation with the luciferin detection reagent. Therefore, the activity of UGTs in HepaRG spheroids was determined by subtracting the luminescence from the sample with UDPGA from those without UDPGA.

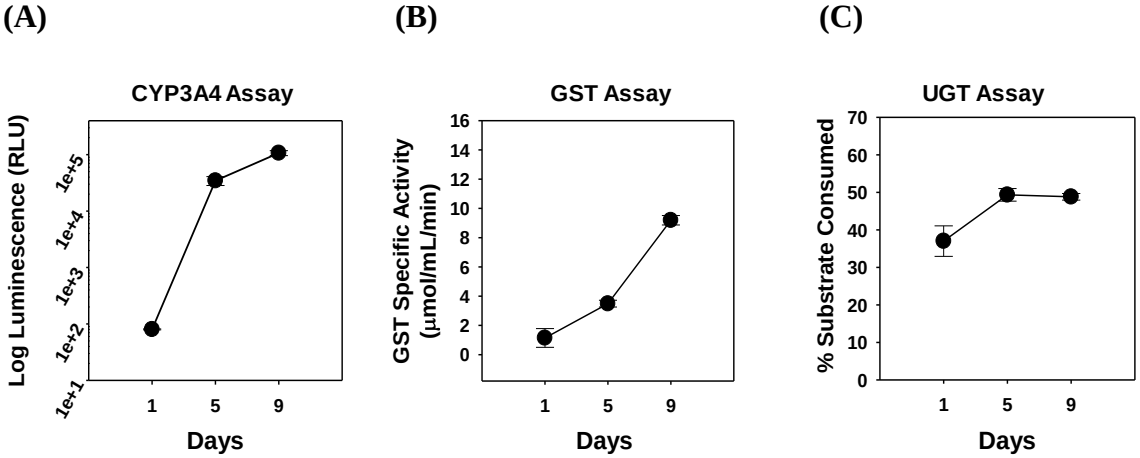

Figure 5.4. Representative DME activities in HepaRG spheroids cultured in the ULA 384-well plate. (A) CYP3A4 activity measured with the P450-Glo assay kit from Promega, **(B)** GST activity measured with the GST assay kit from Sigma-Aldrich, and **(C)** UGT activity measured with the UGT-Glo assay kit from Promega.

In addition, high levels of albumin secretion from HepaRG spheroids were maintained when measured at day 3 and day 7 (**Figure 5.5**). This result correlates well with literature where albumin secretion has been maintained constant over a period of 6 weeks in HepaRG cells [274]. A human albumin ELISA kit was used to measure the level of albumin secretion in HepaRG spheroids. The standard curve of albumin was generated by plotting the average of absorbance difference (i.e., absorbance at 450 nm minus absorbance at 550 nm) on Y-axis as a function of the concentrations of albumin standard on X-axis **(Figure 5.5A)**. The albumin standard solutions were prepared by diluting 1200 ng/mL of albumin with solvent provided in the kit (Assay Diluent C) 2.5-fold serially. The level of albumin secretion at day 3 and day 7 was determined by the sigmoidal standard curve, and the maximum detection limit was approximately 3000 ng/mL (**Figure 5.5B**). These results

demonstrate the utility of HepaRG spheroids as a metabolically-competent cell model for investigating metabolism-mediated neurotoxicity in combination with 3D-cultured ReNcell VM.

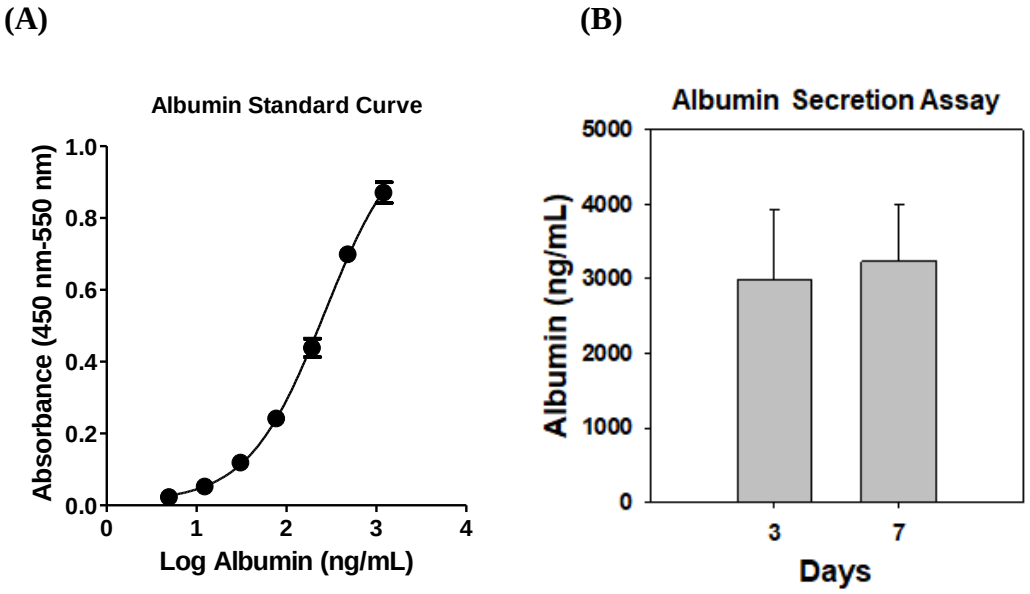

Figure 5.5. The level of albumin secretion by HepaRG spheroids. (A) The sigmoidal standard curve of albumin obtained by plotting absorbance as a function of albumin concentration. **(B)** Albumin secreted by HepaRG spheroids and quantified by the standard curve.

5.3.3. High-throughput, metabolism-mediated neurotoxicity on the 384PillarPlate

Metabolism-mediated neurotoxicity has been demonstrated using metabolism-sensitive compounds such as acetaminophen, cyclophosphamide, and IDPN, all of which are known to be converted into more cytotoxic metabolites in the presence of hepatic DMEs. Metabolites of the compounds were generated by HepaRG spheroids in the ULA 384-well plate and tested against 3D-cultured ReNcell VM on the 384PillarPlate by simply sandwiching the two plates together. The HepaRG maintenance medium was used as a universal medium to maintain high cell viability during the drug exposure for 48 h. The

compounds exposed to 3D-cultured ReNcell VM in the absence of HepaRG spheroids were used as controls. In addition, dose response curves were plotted by normalizing fluorescence intensity obtained from different concentrations of the compounds with those from no compound controls. The metabolism effect on 3D-cultured ReNcell VM by the compounds at the highest concentration due to the presence of metabolically competent HepaRG spheroids was compared with those from the ReNcell VM alone conditions. Statistically significant difference was observed between the ReNcell VM-HepaRG case and the ReNcell VM alone case in terms of metabolism-mediated neurotoxicity.

For example, the viability of ReNcell VM reduced up to 50% when exposed to 25 mM of acetaminophen in the presence of HepaRG spheroids as compared to those in 10% reduction in the absence of HepaRG spheroids. This difference was statistically significant (p value < 0.001) when analyzed by Students' t-test (**Figure 5.6A**). We hypothesized that acetaminophen is transformed into its toxic metabolite, NAPQI [275], in the presence of HepaRG spheroids, which influenced the viability of 3D-cultured ReNcell VM. This hypothesis was supported by high activity of CYP3A4 in HepaRG spheroids (**Figure 5.4A**) and low viability of HepaRG spheroids in the presence of acetaminophen (**Figure 5.7 A**). Similarly, the viability of ReNcell VM reduced approximately 40% when exposed to 25 mM of cyclophosphamide in the presence of HepaRG spheroids as compared to those in 15% reduction in the absence of HepaRG spheroids. This difference was statistically significant (p value < 0.05) (**Figure 5.6B**). The prodrug, cyclophosphamide, is well known to be metabolized by CYP450 isoforms including CYP3A4 and CYP2B6 [276]–[278] into active metabolite, 4-hydroxycyclophosphamide. Therefore, the augmented toxicity of cyclophosphamide in the presence of HepaRG spheroids in our study correlates well with

literature where the cytotoxic effect of 4-hydroxycyclophosphamide has been reported by its metabolism by CYP3A4 [276], [279]. Finally, the viability of ReNcell VM reduced 32% when exposed to 4 mM of IDPN in the presence of HepaRG spheroids whereas there was only 8% reduction in the viability of ReNcell VM in the absence of HepaRG spheroids (**Figure 5.6C**). This difference was statistically significant (p value < 0.05), thereby demonstrating the effectiveness of our co-culture system in assessing metabolism-mediated neurotoxicity of chemicals in high throughput.

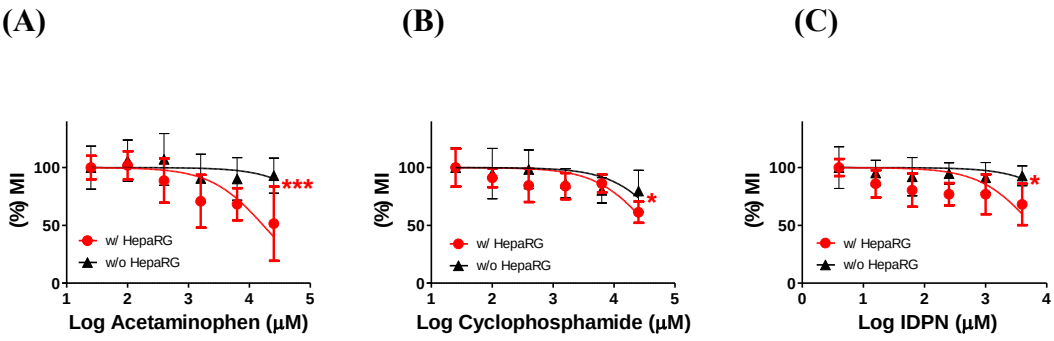

Figure 5.6. Dose response curves of 3D-cultured ReNcell VM on the 384PillarPlate tested with HepaRG spheroids in the ULA 384-well plate in the presence of test compounds: (A) acetaminophen, **(B)** cyclophosphamide, and **(C)** IDPN. For cell viability, membrane integrity of 3D-cultured ReNcell VM was measured with calcein AM staining. * is for $p < 0.05$ and *** is for $p < 0.001$.

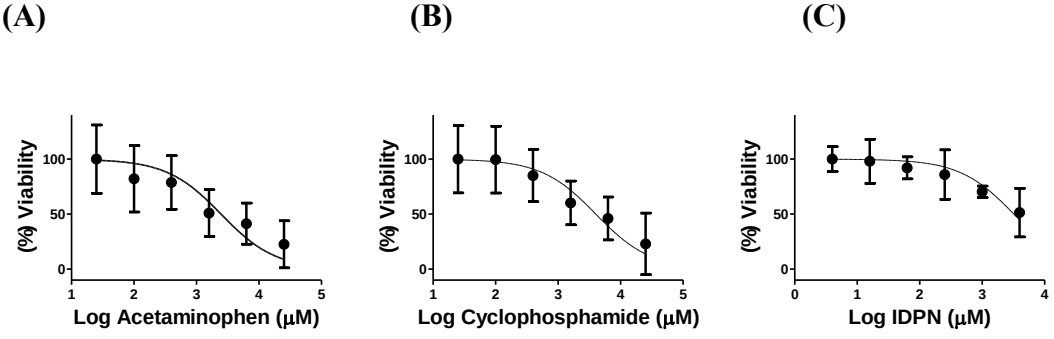

Figure 5.7. Dose response curves of HepaRG spheroids in the ULA 384-well plate tested with the compounds: (A) acetaminophen, **(B)** cyclophosphamide, and **(C)** IDPN. Cell viability was measured by the Cell Titer-Glo assay.

5.4. Discussion

Assessing the toxicity of parent compounds and their metabolites is of critical importance in pharmaceutical and chemical industries for safer product development. To investigate metabolism-mediated effects of potential neurotoxicants *in vitro*, it requires to incorporate hepatic cell culture in neural cell culture [272]. Primary hepatocytes and hepatic cell lines expressing individual or multiple DMEs are primarily used to provide metabolism competence [271], [280]. In our study, we incorporate HepaRG spheroids due to their robustness and user friendliness. Although HepaRG cells are derived from tumors of a female patient suffering from chronic hepatitis C infection and hepatocarcinoma [281]–[283], they have gained enormous popularity as an *in vitro* model system in the field of drug metabolism and toxicology due to its similarity to primary human hepatocytes in terms of DME gene expressions and liver-specific functions as compared to other cells lines [270], [282], [284], [285]. For example, HepaRG cells express similar or higher levels of CYP450 enzymes compared to primary human hepatocytes [270], [274], [283]. CYP450 enzymes, monooxygenases, are a class of DMEs, which play a major role in biotransformation of various compounds including drug candidates and environmental chemicals. Since some of their metabolites are more cytotoxic than parent compounds, CYP450 enzymes are in part responsible for metabolism-induced toxicity [264], [276], [278]. Among dozens of major isoforms of CYP450s, CYP3A4 alone can metabolize almost 50% of known therapeutic drugs [286] and is therefore subjected to a wide range of studies [269], [287], [288]. Formation of reactive metabolites after CYP3A4 metabolism is a critical issue in drug safety screening [289].

Increased activities of CYP450s along with GSTs and UGTs in our HepaRG spheroids correlated well with other HepaRG cell studies where increased expression levels of DMEs and hepatic functions were observed in 2D monolayer cultures and 3D spheroid cultures with hepatic cell culture media supplemented with DMSO [270], [274], [282], [283]. For example, Aninat *et al.* demonstrated increased expression levels of DMEs with longer periods of incubation in 2% DMSO-supplemented media [283]. Similarly, in the study by Hart *et al.*, up-regulation of CYP3A4 and UGTs in HepaRG cells incubated over a period of 2 weeks in the maintenance medium was observed, which was comparable to the levels of the enzymes in primary hepatocytes [270]. In addition, Kanebratt and Andersson showed the increased expression level of CYP3A4 over time in the presence of 2% DMSO [274]. Moreover, albumin secretion from HepaRG spheroids at day 3 and 7 in this study is comparable to the level of albumin secretion obtained by Wang *et al.*, in their study with tethered spheroids of HepaRG cells [290]. In our study, the HepaRG maintenance medium containing DMSO was added after 24 h of HepaRG cell seeding in the ULA 384-well plate, replacing the thawing and plating media. As a result, increased activity of DMEs was observed after 72 h of incubation in the maintenance medium.

Metabolism-sensitive compounds including acetaminophen, cyclophosphamide, and IDPN were selected based on the information of their metabolism by DMEs. For example, acetaminophen is widely used as an analgesic and antipyretic drug and its overdose is known to be one of the most common drug-induced liver injuries [1,2]. Acetaminophen is well known to be metabolized by CYP450s into highly reactive and unstable metabolite, N-acetyl-p-benzoquinone imine (NAPQI), which is primarily responsible for acetaminophen-induced hepatotoxicity. Detoxification of NAPQI occurs

through its binding to the sulfhydryl group of GSH to form acetaminophen-glutathione. However, high dosages of acetaminophen consume intracellular GSH and saturate glucuronidation reaction mediated by UGTs, both of which are the main mechanism of liver protection from toxic compounds, resulting in high levels of NAPQI in the hepatic cells and leading to liver injury [275], [291], [292]. Cyclophosphamide, a widely used chemotherapeutic drug, is known to have severe side effects and metabolism-induced toxicity at high dosages in humans when metabolized into 4-hydroxycyclophosphamide by CYP450s such as CYP3A4 and CYP2B6 [223], [278], [279]. In the study by Yokoyama *et al.*, HepaRG cell viability was reduced to 57% at 25 mM of cyclophosphamide dosage for 48 h, which was alleviated by co-treatment with 100 μM of 1-aminobenzotriazole, a broad CYP inhibitor [278]. In our study, statistically significant, metabolism-mediated hepatoxicity and neurotoxicity were observed at 25 mM of cyclophosphamide dosage, indicating the effect of the reactive metabolite generated by CYP450s in HepaRG spheroids. IDPN that produces profound behavioral abnormalities has been widely explored for its neurotoxic potential in *in vivo* studies [293]–[295]. It has been known to be metabolized by DMEs, specifically flavin-containing monooxygenases (FMOs) to reactive metabolites including N-hydroxy-IDPN that are more neurotoxic than the parent compound [296], [297]. FMOs have been known to be expressed moderately as compared to CYP450s in HepaRG cells [270], [284]. We have explored the metabolism-mediated cytotoxic effect of IDPN with HepaRG spheroids and its downstream effect on 3D-cultured ReNcell VM on the 384PillarPlate for the first time.

Metabolism-mediated neurotoxicity of xenobiotics has been primarily investigated with the CYP enzymes locally expressed in brain [288], [298], [299]. However, considering the

interactions between organs such as liver and brain in the whole organism and its role in determining the accumulation of xenobiotics in the target organ, a single organ cell culture might be insufficient to predict the probable toxic effects of drugs *in vivo* [300]. In addition, the permeability of metabolites through blood brain barrier (BBB) also needs to be considered since, the BBB provides the first line of defense against xenobiotics and regulates the effect of compounds and their metabolites in human brain. The BBB is formed by specialized endothelial cells lining cerebral micro-vessels characterized by high electrical resistance, epithelial-like tight junctions that facilitates the uptake of essential nutrients and efflux of xenobiotics [301], [302]. Thus, understanding the metabolite penetration of the BBB will be critical in considering the co-culture system for metabolism-mediated neurotoxicity. However, modeling the complex interactions between BBB and other cellular components of the CNS *in vitro* is a challenging task. Therefore, it is only recently, that *in vitro* models with BBB has been considered for neurotoxicity studies. For example, Koo et al., recently reported a microfluidic 3D brain culture platform consisting of two membrane-free compartments and an endothelial cell-lined vascular compartment to take into account the penetration of xenobiotics across BBB [245].

Microfluidic tissue-on-chip platforms possess limitations in terms of its adaptation in high-throughput compound screening. On the other hand, the 384PillarPlate is compatible with standard 384-well plates and existing HTS equipment and cell imagers. The unique 384PillarPlate platform offers robust, high-throughput, cost-efficient, 3D cell culture for testing mechanisms of toxicity by various compounds and environmental chemicals. Individual cell spots or multiple cell spots in layers can be printed accurately on the 384PillarPlate using a microarray bioprinter or manually dispensed using multichannel

pipettes for tissue engineering and disease modeling. The 384PillarPlate requires relatively small amounts of cells, hydrogels, extracellular matrices, growth factors, compounds, and reagents for creating and evaluating bioprinted cells/tissues. Cell image acquisition from bioprinted cells/tissues is straightforward because the entire sample depth fits within the focus depth of a normal objective (4x). Although the metabolism-mediated neurotoxicity testing system established in 384PillarPlate/384-well plate combination in this study did not consider BBB for the simplicity and high-throughput testing. Multiple cell types can in fact be cultured in 3D in the ULA 384-well plate and on the 384PillarPlate separately and combined later for compound tests for relatively short periods of time, which reduces critical concerns for developing universal media for co-cultures significantly. Moreover, highly reproducible, high-throughput precision printing allows us to test a variety of cell culture conditions and individual drugs/mixtures of drugs in combination, which makes it well suited for early-stage HTS of compound libraries.

5.5. Conclusions

We successfully established a metabolism-mediated neurotoxicity testing system by combining metabolically competent HepaRG spheroids in the ULA 384-well plate with 3D-cultured neural stem cell line, ReNcell VM on the 384PillarPlate. To the best of our knowledge, the 384PillarPlate coupled with the ULA 384-well plate is the only system that can provide a simple and straightforward method to facilitate two organ-organ communications (e.g., liver metabolism influencing brain developmental toxicity) in high throughput. This system will require validation with several known neurotoxic and non-neurotoxic compounds for their potential to induce neurotoxicity after biotransformation accompanied by high-content imaging assays. Overall, the 384PillarPlate can be used as a

promising tool for predictive human toxicology in pharmaceutical and chemical industries with 3D-cultured human cells.

CHAPTER VI

CONCLUSIONS AND FUTURE DIRECTIONS

6.1. Conclusions

Relatively small numbers of commercially available chemicals have been subjected to international guidelines studies for developmental neurotoxicity, creating a high demand for evaluating the neurotoxicity potential of drug candidates and industrial chemicals. The assessment of neurotoxicity and developmental neurotoxicity (DNT) is based on high-dose animal testing according to OECD test guideline (TG) 426 and TG 443. Adverse effects on neurodevelopment could also result in altered neuronal cell populations in the absence of cell death and thus may not be detected by regular cytotoxicity screening. In addition, there are differences in the brain development of humans and animals, leading to inaccurate assessment of human health risk based on animal data. Significant efforts have been exerted towards the development of mechanism-based, *in vitro* assays using human cells, particularly after the release of the Tox21 vision document (NRC 2007) in 2007. However, the majority of existing *in vitro* systems are still based on 2D cell monolayers which do not provide physiological relevance required for high predictability of neurotoxicity *in vivo*.

This dissertation details the methods for creating 3D-cultured NSCs in high-throughput platforms and demonstrates the feasibility for performing high-throughput neurotoxicity

assessment to predict the toxicity of unknown chemicals *in vivo*. In this study, we successfully established miniaturized 3D-cultured ReNcell VM in biocompatible hydrogels on multiple high-throughput cell culture platforms and constructed a highly-efficient promoter-reporter assay system for rapid assessment of lineage-specific differentiation of human NSCs. We further established various high-content imaging (HCI) assays for the assessment of mechanisms of neurotoxicity and demonstrated rapid assessment of metabolism-mediated neurotoxicity using 3D-cultured ReNcell VM and HepaRG spheroids.

The high-throughput neurotoxicity testing system presented in this work can be implemented in various industrial and academic settings to identify the effects of therapeutic drug candidates and environmental chemicals in NSC morphology, cell function, molecular actions on cell surface receptors, and mechanisms of toxicity, thereby ultimately enhancing the predictability of DNT in vivo. For example, the 3D NSC culture system combined with recombinant lentiviruses developed in Aim 1 can be used to rapidly assess the effect of compounds on viability and differentiation of NSCs. The promoter-reporter assay system developed in this study enabled efficient measurement of cell differentiation and self-renewal by simply comparing green and red fluorescence intensities from the NSCs. The high-throughput ion channel and ABC-transporter assays established in Aim 2 combined with the HCI assays established in Aim 3 will enable researchers to rapidly screen the effect of unknown compounds on various morphological and functional features with high predictability. In addition, our unique demonstration of metabolism-mediated neurotoxicity in the two 3D cell culture systems enabled identification of the toxic effect of compounds and their metabolites. The outcomes from

all the aims can be combined to establish an intensive neurotoxicity testing system with a battery of tests that can ensure rapid assessment of neurotoxicity in a physiologically relevant cellular model. We envision that our high-throughput, 3D NSC platform can be implemented for large-scale screening of drug candidates and environmental toxicants for their potential in causing DNT. Table 4 summarizes the key findings of each aims.

Table 4. Summary of results from individual aims

Aim 1	Aim 2	Aim 3
Demonstrate high neuronal cell functions on 3D NSC microarrays within biomimetic microenvironments in high-throughput on the chip platform	Establish high-throughput ion channel and transporter assays in 3D-cultured NSCs for neurotoxicity assessment	Establish HCI assays on 3D NSC microarrays to investigate mechanistic profiles of toxicity by compounds and their metabolites
• Optimized ReNcell VM encapsulation conditions on the micropillar and microwell chip platform • Established miniaturized 3D ReNcell VM culture in alginate-GFR Matrigel hydrogels with high NSC viability and spheroid formation • Constructed recombinant lentiviruses with dual promoters for measuring transduction efficiency and NSC-specific biomarkers • Infected ReNcell VM with recombinant lentiviruses and demonstrated high	• Identified major ion channels and ABC-transporters expressed in ReNcell VM via RNA-Seq • Established 3D NSC culture on the 384-pillar plate for long-term cell culture • Demonstrated high cell viability and spheroid formation over 2 months • Established high-throughput potassium channel and calcium channel assays in 3D-cultured NSCs with a high signal-to-background ratio • Measured the activity of Kv 7.2, Kv 4.3 and SOCC in 3D-cultured	• Optimized the concentrations of fluorescent dyes to get a high signal-to-background ratio in 3D NSC culture • Established robust and reproducible HCI assays in 3D-cultured NSCs to assess mechanisms of action of test compounds • Investigated the dose-dependent effect of test compounds and determined IC_{50} values from the dose-response curves • Identified mitochondrial impairment as the main mechanism of toxicity among the HCI assays • Established 3D NSC culture on the 384PillarPlate and

neuronal functions in 3D NSC culture • Validated the selectivity of recombinant lentiviruses with differentiation inducers	NSCs with specific inhibitors • Established high-throughput ABC-transporter assays and measured the TAF with specific inhibitors	HepaRG spheroids in the ULA 384-well plate • Demonstrated high DME activities in HepaRG spheroids • Combined 3D NSC culture and HepaRG spheroids for the assessment of metabolism-mediated neurotoxicity with test compounds

6.2. Future Directions

1. Although cell viability and spheroid formation of NSCs were shown to be increased in the mixture of alginate and GFR Matrigel/Geltrex, alginate which is an inert hydrogel did not facilitate cell-ECM interactions. In the future, naturally derived ECM hydrogels should be considered for 3D cell/organoid culture to achieve high cell viability and cell-ECM interactions, mimicking the *in vivo* features.
2. The 3D NSC culture established on the 384PillarPlate platform was a simple proof-of-concept system which needs to be improved by developing brain organoids comprising of all major cell types, including neurons, astrocytes, and oligodendrocytes, which recapitulate the aspects of human brain development and function more closely.
3. Various combinations of growth factors and small molecules should be investigated for efficient differentiation of NSCs into neurons, astrocytes, and oligodendrocytes and compare the effect of test compounds on differentiation of NSCs.

4. Gene expression data for major ion channels and ABC-transporters obtained from RNA-Seq analysis should be validated at protein levels with immunofluorescence assays or western blots.
5. The effect of unknown compounds on the modulation of ion channels and transporters, and their influence on physiological functions of 3D-cultured NSCs such as proliferation, differentiation, and migration should be investigated.
6. We did not investigate the expression of functional ion channels and transporters in differentiated NSCs (excitable neuronal cells). Future studies should consider investigating the differentiated cells for the activities of ion channels and transporters.
7. The HCI assays established in Aim 3.1 need to be validated with a large number of test compounds including neurotoxic compounds and control compounds with no known neurotoxicity.
8. Sensitivity and specificity must be calculated to determine the predictivity of the HCI assays established in Aim 3.1.
9. DNT-specific endpoints such as migration, proliferation, neurite outgrowth, synapse formation must be included to improve the predictability of *in vivo* DNT.
10. In Aim 3.2, we established metabolism-mediated neurotoxicity assays with only three metabolically active test compounds and one assay. To validate the two 3D cell culture systems and ensure high predictability of metabolism-mediated neurotoxicity *in vivo*, a large number of metabolically active compounds along with control compounds must be tested with multiple DNT-specific endpoints.

11. Incorporation of microvasculature and blood-brain barrier in *in vitro* brain organoid models would enable understanding of the expression of efflux and transporter proteins and small molecules and the permeability of reactive metabolites to the brain and provide more accurate predictability of *in vivo* exposure scenarios.

LIST OF PUBLICATIONS

- **Peer-Reviewed Manuscripts**

1. Joshi, P., Kang, S.Y, Yu, K.N, Kothapalli, C.R., and Lee, M.Y., **High-content imaging assays on 3D neural stem cell (NSC) culture for the assessment of mechanistic neurotoxicity,** In review Archives of toxicology (2019)
2. Joshi, P., Yu, K.N., Kang, S.Y., Kwon, S.J., Kwon, P.S., Dordick, J.S., Kothapalli, C.R., and Lee, M.Y**., 3D-cultured neural stem cell (NSC) microarrays on a micropillar chip for high-throughput developmental neurotoxicology**, Experimental Cell Research, 370:680-691 (2018)
3. Joshi, P., Datar, A., Yu, K.N., Kang, S.Y and Lee, M.Y., **Miniaturized high-content imaging assays on 3D cultured cell microarrays for mechanistic toxicity**, Toxicology In Vitro, 50:147-159 (2018)
4. Joshi, P., Kang, S.Y., Datar, A., and Lee, M.Y., **High-throughput assessment of mechanistic toxicity of chemicals in miniaturized 3D cell culture**, Current Protocols in Toxicology, 79:1-22 (2018)
5. Yu, S., Joshi, P., Park, Y.J., Yu, K.N., and Lee, M.Y., **Deconvolution of images from 3D printed cells in layers on a chip**, Biotechnology Progress, 34(2):445-454 (2018)

- **Book Chapters**

1. Lee, M.Y., **Microarray Bioprinting Technology: Fundamentals and Practices**, Springer, ISBN # 978-3-319-46803-7 (2016)
    - **Chapter 5. High content cell staining** (by Yu, K.N., Joshi, P., and Lee, M.Y.)
    - **Chapter 6. 3D-Cultured cell image acquisition** (by Joshi, P., Yu, K.N., Serbinowski, E., and Lee, M.Y.)
    - **Chapter 7. High-content image analysis** (by Yu, S., Joshi, P., Lee, D.W., and Lee, M.Y.)
2. Farrel, K., Joshi, P., Roth, A., Kothapalli, C.R., Lee, M.Y., **High-throughput screening of toxic chemicals on neural stem cells**, Human Stem Cell Toxicology, Royal Society of Chemistry, 31-63 (2016)

- **Review Papers**

1. Joshi, P. and Lee, M.Y., **High content imaging (HCI) on miniaturized three-dimensional (3D) cell cultures**, Biosensors, *5:*768-790 (2015)
2. Datar, A., Joshi, P., and Lee, M.Y., **Biocompatible hydrogels for microarray cell printing and encapsulation**, Biosensors, *5:*647-663 (2015)

REFERENCES

[1] U. S. Epa, "America's Children and the Environment: Neurodevelopmental Disorders," no. October, pp. 1–32, 2015.

[2] P. Grandjean and P. J. Landrigan, "Neurobehavioural effects of developmental toxicity," *Lancet Neurol.*, vol. 13, no. 3, pp. 330–338, 2014.

[3] P. Grandjean and P. J. Landrigan, "Developmental neurotoxicity of industrial chemicals.," *Lancet*, vol. 368, no. 9553, pp. 2167–2178, 2006.

[4] W. R. Mundy *et al.*, "Expanding the test set: Chemicals with potential to disrupt mammalian brain development," *Neurotoxicol. Teratol.*, vol. 52, pp. 25–35, 2015.

[5] M. Aschner *et al.*, "Reference compounds for alternative test methods to indicate developmental neurotoxicity (DNT) potential of chemicals: example lists and criteria for their selection and use.," *ALTEX*, vol. 34, no. 1, pp. 1–32, 2016.

[6] A. Bal-Price, F. Pistollato, M. Sachana, S. K. Bopp, S. Munn, and A. Worth, "Strategies to improve the regulatory assessment of developmental neurotoxicity (DNT) using in vitro methods," *Toxicol. Appl. Pharmacol.*, vol. 354, no. February, pp. 7–18, 2018.

[7] E. Fritsche *et al.*, "Literature review on in vitro and alternative Developmental Neurotoxicity (DNT) testing methods," *EFSA Support. Publ.*, vol. 778, pp. 1–186, 2015.

[8] A. Bal-price and H. T. Hogberg, "In Vitro Developmental Neurotoxicity Testing: Relevant Models and Endpoints," in *In Vitro Toxicology Systems, Methods in Pharmacology and Toxicology*, A. Bal-Price and P. Jennings, Eds. New York: Springer New York, 2014, pp. 125–145.

[9] B. Z. Schmidt *et al.*, "In vitro acute and developmental neurotoxicity screening: an overview of cellular platforms and high-throughput technical possibilities," *Arch. Toxicol.*, vol. 91, pp. 1–33, 2017.

[10] R. Tsuji and K. M. Crofton, "Developmental neurotoxicity guideline study: Issues with methodology, evaluation and regulation," *Congenit. Anom. (Kyoto).*, vol. 52, no. 3, pp. 122–128, 2012.

[11] K. M. Crofton, W. R. Mundy, and T. J. Shafer, "Developmental neurotoxicity testing: A path forward," *Congenit. Anom. (Kyoto).*, vol. 52, no. 3, pp. 140–146, 2012.

[12] C. Van Thriel, R. H. S. Westerink, C. Beste, A. S. Bale, P. J. Lein, and M. Leist, "Translating neurobehavioural endpoints of developmental neurotoxicity tests into in vitro assays and readouts," *Neurotoxicology*, vol. 33, no. 4, pp. 911–924, 2012.

[13] L. Smirnova, H. T. Hogberg, M. Leist, and T. Hartung, "Food for thought...: Developmental neurotoxicity - Challenges in the 21st century and in vitro opportunities," *Altex*, vol. 31, no. 2. pp. 129–156, 2014.

[14] D. C. Dorman *et al.*, "Methods to Identify and Characterize Developmental

Neurotoxicity for Human Health Risk Assessment. III: Pharmacokinetic and Pharmacodynamic Considerations," *Environ. Health Perspect.*, vol. 109, no. SUPPL. 1, pp. 79–91, 2001.

[15] W. Kaufmann, "Current status of developmental neurotoxicity: An industry perspective," *Toxicol. Lett.*, vol. 140–141, pp. 161–169, 2003.

[16] S. Coecke *et al.*, "Workgroup report: incorporating in vitro alternative methods for developmental neurotoxicity into international hazard and risk assessment strategies.," *Environ. Health Perspect.*, vol. 115, no. 6, pp. 924–31, 2007.

[17] C. Hellwig *et al.*, "Culture of human neurospheres in 3D scaffolds for developmental neurotoxicity testing," *Toxicol. Vitr.*, vol. 52, no. June, pp. 106–115, 2018.

[18] H. Olson *et al.*, "Concordance of the toxicity of pharmaceuticals in humans and in animals," *Regul. Toxicol. Pharmacol.*, vol. 32, no. 1, pp. 56–67, 2000.

[19] M. Florio and W. B. Huttner, "Neural progenitors, neurogenesis and the evolution of the neocortex," *Development*, vol. 141, no. 11, pp. 2182–2194, 2014.

[20] K. M. Crofton *et al.*, "Developmental neurotoxicity testing: recommendations for developing alternative methods for the screening and prioritization of chemicals.," *ALTEX*, vol. 28, no. 1, pp. 9–15, 2011.

[21] M. Leist, T. Hartung, and P. Nicotera, "The Dawning of a New Age of Toxicology Doerenkamp-Zbinden Chair for alternative in vitro methods," pp. 103–114, 2008.

[22] L. M. *et al.*, "Consensus report on the future of animal-free systemic toxicity testing," *ALTEX*, vol. 31, no. 3, pp. 341–356, 2014.

[23] M. Leist *et al.*, "Test systems of developmental toxicity: State-of-the art and future perspectives," *Arch. Toxicol.*, vol. 87, no. 12, pp. 2037–2042, 2013.

[24] L. Hölting, "Use of human pluripotent stem cells and their progeny to develop in vitro models for neurotoxicity testing," no. August, 2015.

[25] N. Malik *et al.*, "Compounds with species and cell type specific toxicity identified in a 2000 compound drug screen of neural stem cells and rat mixed cortical neurons," *Neurotoxicology*, vol. 45, pp. 192–200, 2014.

[26] L. Meli *et al.*, "Three dimensional cellular microarray platform for human neural stem cell differentiation and toxicology.," *Stem Cell Res.*, vol. 13, pp. 36–47, 2014.

[27] Y. J. Choi, S. Chae, J. H. Kim, K. F. Barald, J. Y. Park, and S.-H. Lee, "Neurotoxic amyloid beta oligomeric assemblies recreated in microfluidic platform with interstitial level of slow flow.," *Sci. Rep.*, vol. 3, p. 1921, 2013.

[28] M. Zychowicz *et al.*, "Developmental stage dependent neural stem cells sensitivity to methylmercury chloride on different biofunctional surfaces," *Toxicol. Vitr.*, vol. 28, pp. 76–87, 2014.

[29] J. E. Lee, M. S. Lim, J. H. Park, C. H. Park, and H. C. Koh, "Nuclear NF-κB contributes to chlorpyrifos-induced apoptosis through p53 signaling in human

neural precursor cells," *Neurotoxicology*, vol. 42, pp. 58–70, 2014.

[30] F. Liu *et al.*, "Effects of silver nanoparticles on human and rat embryonic neural stem cells," *Front. Neurosci.*, vol. 9, no. April, pp. 1–9, 2015.

[31] M. E. Culbreth, J. a Harrill, T. M. Freudenrich, W. R. Mundy, and T. J. Shafer, "Comparison of chemical-induced changes in proliferation and apoptosis in human and mouse neuroprogenitor cells.," *Neurotoxicology*, vol. 33, no. 6, pp. 1499–510, Dec. 2012.

[32] S.-H. Chang *et al.*, "Methylmercury induces caspase-dependent apoptosis and autophagy in human neural stem cells.," *J. Toxicol. Sci.*, vol. 38, no. 6, pp. 823–31, 2013.

[33] Y.-C. Toh, T. C. Lim, D. Tai, G. Xiao, D. van Noort, and H. Yu, "A microfluidic 3D hepatocyte chip for drug toxicity testing.," *Lab Chip*, vol. 9, no. 14, pp. 2026–2035, 2009.

[34] N. Ye, J. Qin, W. Shi, X. Liu, and B. Lin, "Cell-based high content screening using an integrated microfluidic device.," *Lab Chip*, vol. 7, no. 12, pp. 1696–704, Dec. 2007.

[35] R. Cheong, C. J. Wang, and A. Levchenko, "High content cell screening in a microfluidic device.," *Mol. Cell. Proteomics*, vol. 8, no. 3, pp. 433–42, Mar. 2009.

[36] G. Su, K. E. Sung, D. J. Beebe, and A. Friedl, "Functional Screen of Paracrine Signals in Breast Carcinoma Fibroblasts," *PLoS One*, vol. 7, no. 10, pp. 1–12, 2012.

[37] K. Yang *et al.*, "A microfluidic array for quantitative analysis of human neural stem cell self-renewal and differentiation in three-dimensional hypoxic microenvironment," *Biomaterials*, vol. 34, no. 28, pp. 6607–6614, 2013.

[38] N. Lee *et al.*, "Monitoring the Differentiation and Migration Patterns of Neural Cells Derived from Human Embryonic Stem Cells Using a Microfluidic Culture System," *Mol. Cells*, vol. 37, no. 6, pp. 497–502, 2014.

[39] J. M. Lee, J. E. Kim, J. Borana, B. H. Chung, and B. G. Chung, "Dual-micropillar-based microfluidic platform for single embryonic stem cell-derived neuronal differentiation," *Electrophoresis*, vol. 34, no. 13, pp. 1931–1938, 2013.

[40] S. Han *et al.*, "Three-dimensional extracellular matrix-mediated neural stem cell differentiation in a microfluidic device," *Lab Chip*, vol. 12, no. 13, pp. 2305–8, 2012.

[41] H. Xu and S. C. Heilshorn, "Microfluidic investigation of BDNF-enhanced neural stem cell chemotaxis in CXCL12 gradients," *Small*, vol. 9, no. 4, pp. 585–595, 2013.

[42] K. Wong, A. Ayuso-Sacido, P. Ahyow, A. Darling, J. a Boockvar, and M. Wu, "Assessing neural stem cell motility using an agarose gel-based microfluidic device.," *J. Vis. Exp.*, no. 12, pp. 2–6, 2008.

[43] C. R. Kothapalli *et al.*, "A high-throughput microfluidic assay to study neurite

response to growth factor gradients.," *Lab Chip*, vol. 11, no. 3, pp. 497–507, 2011.

[44] A. R. Dixon and M. a. Philbert, "Morphometric assessment of toxicant induced neuronal degeneration in full and restricted contact co-cultures of embryonic cortical rat neurons and astrocytes: Using m-Dinitrobezene as a model neurotoxicant," *Toxicol. Vitr.*, vol. 29, no. 3, pp. 564–574, 2015.

[45] M.-Y. Lee, R. A. Kumar, S. M. Sukumaran, M. G. Hogg, D. S. Clark, and J. S. Dordick, "Three-dimensional cellular microarray for high-throughput toxicology assays.," *Proc. Natl. Acad. Sci.*, vol. 105, no. 1, pp. 59–63, 2008.

[46] S. J. Kwon *et al.*, "High-Throughput and Combinatorial Gene Expression on a Chip for Metabolism-Induced Toxicology Screening," *Nat. Commun.*, vol. 5, no. 3739, pp. 1–16, 2014.

[47] D. W. Lee *et al.*, "High-throughput screening (HTS) of anticancer drug efficacy on a micropillar/microwell chip platform," *Anal. Chem.*, 2014.

[48] T. G. Fernandes *et al.*, "Three-dimensional cell culture microarray for high-throughput studies of stem cell fate.," *Biotechnol. Bioeng.*, vol. 106, no. 1, pp. 106–18, May 2010.

[49] P. Joshi *et al.*, "3D-cultured neural stem cell microarrays on a micropillar chip for high-throughput developmental neurotoxicology," *Exp. Cell Res.*, no. July, pp. 0–1, 2018.

[50] M. Demir and E. D. Laywell, "Neurotoxic effects of AZT on developing and adult neurogenesis," *Front. Neurosci.*, vol. 9, no. March, pp. 1–15, 2015.

[51] X. Bai, Y. Yan, S. Canfield, M. Y. Muravyeva, and C. Kikuchi, "Ketamine Enhances Human Neural Stem Cell Proliferation and Induces Neuronal Apoptosis Via Reactive Oxygen Species- Mediated Mitochondrial Pathway," *Anesth. Analg.*, vol. 116, no. 4, pp. 869–880, 2013.

[52] D. Rice and S. B. Jr, "Critical Periods of Vulnerability for the Developing Nervous System : Evidence from Humans and Animal Models," *Environ. Heal. Perspect. Suppl.*, vol. 108, no. April, pp. 1–71, 2000.

[53] J. Llorens, A. a. Li, S. Ceccatelli, and C. Suñol, "Strategies and tools for preventing neurotoxicity: To test, to predict and how to do it," *Neurotoxicology*, vol. 33, no. 4, pp. 796–804, 2012.

[54] N. V. Stiegler, A. K. Krug, F. Matt, and M. Leist, "Assessment of chemical-induced impairment of human neurite outgrowth by multiparametric live cell imaging in high-density cultures," *Toxicol. Sci.*, vol. 121, no. 1, pp. 73–87, 2011.

[55] N. M. Radio and W. R. Mundy, "Developmental neurotoxicity testing in vitro: models for assessing chemical effects on neurite outgrowth.," *Neurotoxicology*, vol. 29, no. 3, pp. 361–76, May 2008.

[56] J. M. Breier *et al.*, "Neural progenitor cells as models for high-throughput screens of developmental neurotoxicity: State of the science," *Neurotoxicol. Teratol.*, vol.

32, no. 1, pp. 4–15, 2010.

[57] a. Efthymiou *et al.*, “Functional Screening Assays with Neurons Generated from Pluripotent Stem Cell-Derived Neural Stem Cells,” *J. Biomol. Screen.*, vol. 19, no. 1, pp. 32–43, 2014.

[58] V. Ourednik *et al.*, “Segregation of Human Neural Stem Cells in the Developing Primate Forebrain,” 2001.

[59] F. Doetsch, I. Caillé, D. a Lim, J. M. García-Verdugo, and A. Alvarez-Buylla, “Subventricular zone astrocytes are neural stem cells in the adult mammalian brain.,” *Cell*, vol. 97, no. 6, pp. 703–16, 1999.

[60] D. L. Clarke *et al.*, “Generalized potential of adult neural stem cells.,” *Science (80-.).*, vol. 288, no. 5471, pp. 1660–1663, 2000.

[61] A. K. Bal-Price *et al.*, “Advancing the science of developmental neurotoxicity (DNT): testing for better safety evaluation.,” 2012.

[62] M. R. Schmuck *et al.*, “Omnisphero: a high-content image analysis (HCA) approach for phenotypic developmental neurotoxicity (DNT) screenings of organoid neurosphere cultures in vitro,” *Arch. Toxicol.*, vol. 91, no. 4, pp. 2017–2028, 2017.

[63] A. Bal-Price, F. Pistollato, M. Sachana, S. K. Bopp, S. Munn, and A. Worth, “Strategies to improve the regulatory assessment of developmental neurotoxicity (DNT) using in vitro methods,” *Toxicol. Appl. Pharmacol.*, vol. 354, no. February, pp. 7–18, 2018.

[64] S. Temple, “The development of neural stem cells.,” *Nature*, vol. 414, no. 6859, pp. 112–117, 2001.

[65] C. Tamm, F. Sabri, and S. Ceccatelli, “Mitochondrial-mediated apoptosis in neural stem cells exposed to manganese,” *Toxicol. Sci.*, vol. 101, no. 2, pp. 310–320, 2008.

[66] R. Tofighi *et al.*, “Hippocampal neurons exposed to the environmental contaminants methylmercury and polychlorinated biphenyls undergo cell death via parallel activation of calpains and lysosomal proteases,” *Neurotox. Res.*, vol. 19, no. 1, pp. 183–194, 2011.

[67] F. Pampaloni, E. G. Reynaud, and E. H. K. Stelzer, “The third dimension bridges the gap between cell culture and live tissue.,” *Nat. Rev. Mol. Cell Biol.*, vol. 8, no. 10, pp. 839–45, Oct. 2007.

[68] S. Breslin and L. O’Driscoll, “Three-dimensional cell culture: The missing link in drug discovery,” *Drug Discov. Today*, vol. 18, no. 5–6, pp. 240–249, 2013.

[69] N. Alépée *et al.*, “State-of-the-Art of 3D Cultures (Organs-on-a- Chip) in Safety Testing and Pathophysiology –,” *ALTEX*, pp. 1–42, 2014.

[70] D. W. Lee, S. H. Yi, S. H. Jeong, B. Ku, J. Kim, and M.-Y. Lee, “Plastic pillar inserts for three-dimensional (3D) cell cultures in 96-well plates,” *Sensors Actuators B Chem.*, vol. 177, pp. 78–85, Feb. 2013.

[71] N. Alépée *et al.*, "State-of-the-art of 3D cultures (organs-on-a-chip) in safety testing and pathophysiology," *ALTEX*, vol. 31, no. 4, pp. 441–477, 2014.

[72] A. Astashkina and D. W. Grainger, "Critical analysis of 3-D organoid in vitro cell culture models for high-throughput drug candidate toxicity assessments," *Adv. Drug Deliv. Rev.*, vol. 69–70, pp. 1–18, 2014.

[73] X. Meng, P. Leslie, Y. Zhang, and J. Dong, "Stem cells in a three-dimensional scaffold environment.," *Springerplus*, vol. 3, p. 80, 2014.

[74] M. a Lancaster *et al.*, "Cerebral organoids model human brain development and microcephaly," *Nature*, vol. 501, no. 7467, pp. 1190–1194, 2013.

[75] D. Pamies *et al.*, "A human brain microphysiological system derived from induced pluripotent stem cells to study neurological diseases and toxicity," *ALTEX*, vol. 34, no. 3, pp. 362–376, 2017.

[76] A. M. Paşca *et al.*, "Functional cortical neurons and astrocytes from human pluripotent stem cells in 3D culture," *Nat. Methods*, vol. 12, no. 7, pp. 671–8, 2015.

[77] Y. H. Kim *et al.*, "A 3D human neural cell culture system for modeling Alzheimer's disease," *Nat. Protoc.*, vol. 10, no. 7, pp. 985–1006, 2015.

[78] L. Smirnova *et al.*, "A LUHMES 3D dopaminergic neuronal model for neurotoxicity testing allowing long-term exposure and cellular resilience analysis," *Arch. Toxicol.*, vol. 90, no. 11, pp. 2725–2743, 2016.

[79] J. Haycock, "3D Cell Culture: A Review of Current Approaches and Techniques," in *Methods in Molecular Biology*, vol. 695, 2011, pp. 243–259.

[80] P. Lein, E. Silbergeld, P. Locke, and A. M. Goldberg, "In vitro and other alternative approaches to developmental neurotoxicity testing (DNT)," *Environ. Toxicol. Pharmacol.*, vol. 19, no. 3, pp. 735–744, 2005.

[81] T. J. Shafer *et al.*, "Putative adverse outcome pathways relevant to neurotoxicity," *Crit. Rev. Toxicol.*, vol. 45, no. 1, pp. 83–91, 2015.

[82] A. Bal-Price and M. E. (Bette. Meek, "Adverse outcome pathways: Application to enhance mechanistic understanding of neurotoxicity," *Pharmacol. Ther.*, vol. 179, pp. 84–95, 2017.

[83] C. Dong, C. R. Rovnaghi, and K. J. S. Anand, "Ketamine Affects the Neurogenesis of Rat Fetal Neural Stem Progenitor Cells via the PI3K/Akt-p27 Signaling Pathway," *Birth Defects Res. Part B Dev. Reprod. Toxicol.*, vol. 101, no. 5, pp. 355–363, 2014.

[84] J. Sisnaiske *et al.*, "Acrylamide alters neurotransmitter induced calcium responses in murine ESC-derived and primary neurons," *Neurotoxicology*, vol. 43, pp. 117–126, 2014.

[85] M. W. G. D. M. de Groot and R. H. S. Westerink, "Chemically-induced oxidative stress increases the vulnerability of PC12 cells to rotenone-induced toxicity,"

Neurotoxicology, vol. 43, pp. 102–109, 2014.

[86] F. Zanella, J. B. Lorens, and W. Link, "High content screening: seeing is believing.," *Trends Biotechnol.*, vol. 28, no. 5, pp. 237–45, May 2010.

[87] W. Buchser *et al.*, "Assay Development Guidelines for Image-Based High Content Screening , High Content Analysis and High Content Imaging," in *Assay Guidance Manual*, 2012, pp. 1–69.

[88] L. Tolosa *et al.*, "Development of a Multiparametric Cell-based Protocol to Screen and Classify the Hepatotoxicity Potential of Drugs," *Toxicol. Sci.*, vol. 127, no. 1, pp. 187–198, May 2012.

[89] M. Mioulane, G. Foldes, N. N. Ali, M. D. Schneider, and S. E. Harding, "Development of high content imaging methods for cell death detection in human pluripotent stem cell-derived cardiomyocytes," *J. Cardiovasc. Transl. Res.*, vol. 5, pp. 593–604, 2012.

[90] O. Sirenko, J. Hesley, I. Rusyn, and E. F. Cromwell, "High-content assays for hepatotoxicity using induced pluripotent stem cell-derived cells.," *Assay Drug Dev. Technol.*, vol. 12, no. 1, pp. 43–54, 2014.

[91] S. Fujisawa *et al.*, "Evaluation of YO-PRO-1 as an early marker of apoptosis following radiofrequency ablation of colon cancer liver metastases," *Cytotechnology*, vol. 66, no. 2, pp. 259–273, 2014.

[92] A. R. Ranade, M. S. Wilson, A. M. Mcclanahan, and A. J. Ball, "High Content Imaging and Analysis Enable Quantitative In Situ Assessment of CYP3A4 Using Cryopreserved Differentiated HepaRG Cells," *J. Toxicol.*, vol. 2014, pp. 1–12, 2014.

[93] M. T. Donato, L. Tolosa, N. Jiménez, J. V Castell, and M. J. Gómez-Lechón, "High-content imaging technology for the evaluation of drug-induced steatosis using a multiparametric cell-based assay.," *J. Biomol. Screen.*, vol. 17, no. 3, pp. 394–400, Mar. 2012.

[94] J. J. Xu, P. V Henstock, M. C. Dunn, A. R. Smith, J. R. Chabot, and D. de Graaf, "Cellular imaging predictions of clinical drug-induced liver injury.," *Toxicol. Sci.*, vol. 105, no. 1, pp. 97–105, Sep. 2008.

[95] P. D. Andrews *et al.*, "High-content screening of feeder-free human embryonic stem cells to identify pro-survival small molecules.," *Biochem. J.*, vol. 432, no. 1, pp. 21–33, 2010.

[96] M. S. Wilson, J. R. Graham, and A. J. Ball, "Multiparametric High Content Analysis for assessment of neurotoxicity in differentiated neuronal cell lines and human embryonic stem cell-derived neurons.," *Neurotoxicology*, vol. 42, pp. 33–48, 2014.

[97] J. A. Harrill, B. L. Robinette, and W. R. Mundy, "Use of high content image analysis to detect chemical-induced changes in synaptogenesis in vitro.," *Toxicol. Vitr.*, vol. 25, pp. 368–387, 2011.

[98] J. a. Harrill, T. M. Freudenrich, B. L. Robinette, and W. R. Mundy, "Comparative

sensitivity of human and rat neural cultures to chemical-induced inhibition of neurite outgrowth," *Toxicol. Appl. Pharmacol.*, vol. 256, no. 3, pp. 268–280, 2011.

[99] S. I. Montanez-Sauri, D. J. Beebe, and K. E. Sung, "Microscale screening systems for 3D cellular microenvironments: platforms, advances, and challenges," *Cell. Mol. Life Sci.*, vol. 72, pp. 237–249, 2015.

[100] M. Håkanson, E. Cukierman, and M. Charnley, "Miniaturized pre-clinical cancer models as research and diagnostic tools," *Adv. Drug Deliv. Rev.*, vol. 69–70, pp. 52–66, 2014.

[101] S. Lindström and H. Andersson-Svahn, "Overview of single-cell analyses: microdevices and applications.," *Lab Chip*, vol. 10, pp. 3363–3372, 2010.

[102] T. G. Fernandes, M. M. Diogo, D. S. Clark, J. S. Dordick, and J. M. S. Cabral, "High-throughput cellular microarray platforms: applications in drug discovery, toxicology and stem cell research.," *Trends Biotechnol.*, vol. 27, no. 6, pp. 342–9, Jun. 2009.

[103] P. J. Landrigan, L. Lambertini, and L. S. Birnbaum, "A research strategy to discover the environmental causes of autism and neurodevelopmental disabilities," *Environ. Health Perspect.*, vol. 120, no. 7, pp. 258–260, 2012.

[104] Y. Yi, J. Park, J. Lim, C. J. Lee, and S. H. Lee, "Central Nervous System and its Disease Models on a Chip," *Trends Biotechnol.*, vol. 33, no. 12, pp. 762–776, 2015.

[105] P. McNutt, J. Celver, T. Hamilton, and M. Mesngon, "Embryonic stem cell-derived neurons are a novel, highly sensitive tissue culture platform for botulinum research," *Biochem. Biophys. Res. Commun.*, vol. 405, no. 1, pp. 85–90, 2011.

[106] M. P. Schwartz *et al.*, "Human pluripotent stem cell-derived neural constructs for predicting neural toxicity.," *Proc. Natl. Acad. Sci. U. S. A.*, vol. 112, no. 40, pp. 12516–12521, 2015.

[107] A. K. Krug *et al.*, "Human embryonic stem cell-derived test systems for developmental neurotoxicity: a transcriptomics approach.," *Arch. Toxicol.*, vol. 87, no. 1, pp. 123–43, Jan. 2013.

[108] K. Farrell, P. Joshi, A. Roth, C. Kothapalli, and M.-Y. Lee, "High-throughput Screening of Toxic Chemicals on Neural Stem Cells," in *Human Stem Cell Toxicology*, no. 29, J. L. Sherley, Ed. Royal Society of Chemistry, 2016, pp. 31–63.

[109] L. Meli *et al.*, "Three dimensional cellular microarray platform for human neural stem cell differentiation and toxicology.," *Stem Cell Res.*, vol. 13, no. 1, pp. 36–47, Jul. 2014.

[110] J. P. Capela *et al.*, "The neurotoxicity of hallucinogenic amphetamines in primary cultures of hippocampal neurons," *Neurotoxicology*, vol. 34, no. 1, pp. 254–263, 2013.

[111] F. Cornelissen *et al.*, "Quantitation of chronic and acute treatment effects on neuronal network activity using image and signal analysis: toward a high-content assay.," *J. Biomol. Screen.*, vol. 18, no. 7, pp. 807–19, 2013.

[112] W. R. Mundy, N. M. Radio, and T. M. Freudenrich, “Neuronal models for evaluation of proliferation in vitro using high content screening.,” *Toxicology*, vol. 270, pp. 121–30, 2010.

[113] M. W. G. D. M. de Groot, M. D. M. Kock, and R. H. S. Westerink, “Assessment of the neurotoxic potential of exposure to 50Hz extremely low frequency electromagnetic fields (ELF-EMF) in naïve and chemically stressed PC12 cells.,” *Neurotoxicology*, vol. 44, pp. 358–364, 2014.

[114] N. M. Radio, J. M. Breier, T. J. Shafer, and W. R. Mundy, “Assessment of chemical effects on neurite outgrowth in PC12 cells using high content screening.,” *Toxicol. Sci.*, vol. 105, no. 1, pp. 106–118, 2008.

[115] D. A. Brafman, “Generation, Expansion, and Differentiation of Human Pluripotent Stem Cell (hPSC) Derived Neural Progenitor Cells (NPCs),” in *Methods in Molecular Biology*, no. 1212, New York: Springer New York, 2015, pp. 87–102.

[116] D. Seidel *et al.*, “Impedimetric real-time monitoring of neural pluripotent stem cell differentiation process on microelectrode arrays,” *Biosens. Bioelectron.*, vol. 86, pp. 277–286, 2016.

[117] S. A. Jones, D. M. Jolson, K. K. Cuta, C. N. Mariash, and G. W. Anderson, “Triiodothyronine is a survival factor for developing oligodendrocytes,” *Mol. Cell. Endocrinol.*, vol. 199, pp. 49–60, 2003.

[118] E. Fritsche, J. E. Cline, N.-H. Nguyen, T. S. Scanlan, and J. Abel, “Polychlorinated Biphenyls Disturb Differentiation of Normal Human Neural Progenitor Cells: Clue for Involvement of Thyroid Hormone Receptors,” *Environ. Health Perspect.*, vol. 113, no. 7, pp. 871–876, 2005.

[119] P. G. Franco, L. Silvestroff, E. F. Soto, and J. M. Pasquini, “Thyroid hormones promote differentiation of oligodendrocyte progenitor cells and improve remyelination after cuprizone-induced demyelination,” *Exp. Neurol.*, vol. 212, no. 2, pp. 458–467, 2008.

[120] S. Grade, L. Bernardino, and J. O. Malva, “Oligodendrogenesis from neural stem cells: perspectives for remyelinating strategies.,” *Int. J. Dev. Neurosci.*, vol. 31, no. 7, pp. 692–700, Nov. 2013.

[121] H. El-Tahry, H. Marei, A. Shams, M. El-Shahat, H. Abdelaziz, and M. Abd El-kader, “The effect of triiodothyronine on maturation and differentiation of oligodendrocyte progenitor cells during remyelination following induced demyelination in male albino rat,” *Tissue Cell*, vol. 48, pp. 242–251, 2016.

[122] S. Shin and M. Vemuri, “Culture and Differentiation of Human Neural Stem Cells,” in *Protocols for Neural Cell Culture*, 4th ed., L. C. Doering, Ed. New York: Humana Press, 2010.

[123] B.-Y. Hu *et al.*, “Neural differentiation of human induced pluripotent stem cells follows developmental principles but with variable potency,” *Proc. Natl. Acad. Sci.*, vol. 107, no. 9, pp. 4335–4340, 2010.

[124] R. Santos *et al.*, "Differentiation of Inflammation-Responsive Astrocytes from Glial Progenitors Generated from Human Induced Pluripotent Stem Cells," *Stem Cell Reports*, vol. 8, pp. 1757–1769, 2017.

[125] S. Zhou *et al.*, "Neurosphere based differentiation of human IPSC improves astrocyte differentiation," *Stem Cells Int.*, vol. 2016, 2016.

[126] M. Tio, K. H. Tan, W. Lee, T. T. Wang, and G. Udolph, "Roles of db-cAMP, IBMX and RA in aspects of neural differentiation of cord blood derived mesenchymal-like stem cells," *PLoS One*, vol. 5, no. 2, 2010.

[127] M. W. Mu, Z. Y. Zhao, and C. G. Li, "Comparative study of neural differentiation of bone marrow mesenchymal stem cells by different induction methods.," *Genet. Mol. Res.*, vol. 14, no. 4, pp. 14169–14176, 2015.

[128] A. Shahbazi *et al.*, "Rapid Induction of Neural Differentiation in Human Umbilical Cord Matrix Mesenchymal Stem Cells by cAMP-elevating Agents," *Int. J. Mol. Cell. Med.*, vol. 5, no. 3, pp. 167–177, 2016.

[129] M. J. Pino-Barrio, E. García-García, P. Menéndez, and A. Martínez-Serrano, "V-Myc immortalizes human neural stem cells in the absence of pluripotency-associated traits," *PLoS One*, vol. 10, no. 3, pp. 1–13, 2015.

[130] G. J. Nierode *et al.*, "High-Throughput Toxicity and Phenotypic Screening of 3D Human Neural Progenitor Cell Cultures on a Microarray Chip Platform," *Stem Cell Reports*, vol. 7, pp. 970–982, 2016.

[131] P. Joshi, A. Datar, K.-N. Yu, S.-Y. Kang, and M.-Y. Lee, "High-content imaging assays on a miniaturized 3D cell culture platform," *Toxicol. Vitr.*, vol. 50, pp. 147–159, Aug. 2018.

[132] K. N. Yu *et al.*, "Prediction of metabolism-induced hepatotoxicity on three-dimensional hepatic cell culture and enzyme microarrays," *Arch. Toxicol.*, pp. 1–16, 2017.

[133] R. Donato *et al.*, "Differential development of neuronal physiological responsiveness in two human neural stem cell lines," *BMC Neurosci.*, vol. 8, no. 36, 2007.

[134] C. Lange *et al.*, "Small molecule GSK-3 inhibitors increase neurogenesis of human neural progenitor cells," *Neurosci. Lett.*, vol. 488, pp. 36–40, 2011.

[135] S. Choi *et al.*, "A three-dimensional human neural cell culture model of Alzheimer's disease," *Nature*, vol. 515, pp. 274–278, 2014.

[136] A. Datar, P. Joshi, and M.-Y. Lee, "Biocompatible Hydrogels for Microarray Cell Printing and Encapsulation," *Biosensors*, vol. 5, no. 4, pp. 647–663, 2015.

[137] L. A. Flanagan, L. M. Rebaza, S. Derzic, P. H. Schwartz, and E. S. Monuki, "Regulation of human neural precursor cells by laminin and integrins," *J. Neurosci. Res.*, vol. 83, no. 5, pp. 845–856, 2006.

[138] H. T. Hogberg *et al.*, "Toward a 3D model of human brain development for studying gene/environment interactions.," *Stem Cell Res. Ther.*, vol. 4, no. Suppl 1, pp. 2–7, 2013.

[139] P. de Vos, M. M. Faas, B. Strand, and R. Calafiore, "Alginate-based microcapsules for immunoisolation of pancreatic islets," *Biomaterials*, vol. 27, no. 32, pp. 5603–5617, 2006.

[140] M. Chayosumrit, B. Tuch, and K. Sidhu, "Alginate microcapsule for propagation and directed differentiation of hESCs to definitive endoderm," *Biomaterials*, vol. 31, pp. 505–514, 2010.

[141] G. C. Reilly and A. J. Engler, "Intrinsic extracellular matrix properties regulate stem cell differentiation," *J. Biomech.*, vol. 43, pp. 55–62, 2010.

[142] W. Ma, T. Tavakoli, E. Derby, Y. Serebryakova, M. S. Rao, and M. P. Mattson, "Cell-extracellular matrix interactions regulate neural differentiation of human embryonic stem cells.," *BMC Dev. Biol.*, vol. 8, p. 90, 2008.

[143] A. J. Engler, S. Sen, H. L. Sweeney, and D. E. Discher, "Matrix Elasticity Directs Stem Cell Lineage Specification," *Cell*, vol. 126, no. 4, pp. 677–689, 2006.

[144] F. Guilak, D. M. Cohen, B. T. Estes, J. M. Gimble, W. Liedtke, and C. S. Chen, "Control of Stem Cell Fate by Physical Interactions with the Extracellular Matrix," *Cell Stem Cell*, vol. 5, pp. 17–26, 2009.

[145] C. S. Hughes, L. M. Postovit, and G. A. Lajoie, "Matrigel: a complex protein mixture required for optimal growth of cell culture.," *Proteomics*, vol. 10, no. 9, pp. 1886–1890, 2010.

[146] G. Benton, I. Arnaoutova, J. George, H. K. Kleinman, and J. Koblinski, "Matrigel: From discovery and ECM mimicry to assays and models for cancer research," *Adv. Drug Deliv. Rev.*, vol. 79–80, pp. 3–18, 2014.

[147] G. Sun *et al.*, "The Three-Dimensional Culture System with Matrigel and Neurotrophic Factors Preserves the Structure and Function of Spiral Ganglion Neuron In Vitro," *Neural Plast.*, vol. 2016, pp. 1–15, 2016.

[148] E. E. Capowski *et al.*, "Lentiviral vector-mediated genetic modification of human neural progenitor cells for ex vivo gene therapy," *J. Neurosci. Methods*, vol. 163, no. 2, pp. 338–349, 2007.

[149] N. Israsena, M. Hu, W. Fu, L. Kan, and J. A. Kessler, "The presence of FGF2 signaling determines whether β-catenin exerts effects on proliferation or neuronal differentiation of neural stem cells," *Dev. Biol.*, vol. 268, no. 1, pp. 220–231, 2004.

[150] V. Graham, J. Khudyakov, P. Ellis, and L. Pevny, "SOX2 functions to maintain neural progenitor identity," *Neuron*, vol. 39, no. 5, pp. 749–765, 2003.

[151] S. P. Gupta, *Ion Channels and Their Inhibitors*. 2011.

[152] N. C. Spitzer, "Electrical activity in early neuronal development.," *Nature*, vol. 444,

no. 7120, pp. 707–712, 2006.

[153] A. B. Toth, A. K. Shum, and M. Prakriya, “Regulation of neurogenesis by calcium signaling,” *Cell Calcium*, vol. 59, no. 2–3, pp. 124–134, 2016.

[154] W. J. Moody and M. M. Bosma, “Ion Channel Development, Spontaneous Activity, and Activity-Dependent Development in Nerve and Muscle Cells,” *Physiol. Rev.*, vol. 85, no. 3, pp. 883–941, 2005.

[155] N. Stanslowsky *et al.*, “Calcium, Sodium, and Transient Receptor Potential Channel Expression in Human Fetal Midbrain-Derived Neural Progenitor Cells,” *Stem Cells Dev.*, vol. 27, no. 14, pp. 976–984, Jul. 2018.

[156] L. A. Pardo *et al.*, “Voltage-Gated Potassium Channels in Cell Proliferation Voltage-Gated Potassium Channels in Cell,” pp. 285–292, 2015.

[157] S. Horigane, Y. Ozawa, H. Yamada, and S. Takemoto-, “Calcium signaling : a key regulator of neuronal migration,” *J. Biochem.*, pp. 1–36, 2019.

[158] P. Imbrici, O. Nicolotti, F. Leonetti, D. Conte, and A. Liantonio, “Ion Channels in Drug Discovery and Safety Pharmacology,” in *Computational Toxicology: Methods and Protocols*, vol. 1800, B. Reisfeld and A. N. Mayeno, Eds. Totowa, NJ: Humana Press, 2018.

[159] C. Sun *et al.*, “Association study between inwardly rectifying potassium channels 2.1 and 4.1 and autism spectrum disorders,” *Life Sci.*, vol. 213, no. July, pp. 183–189, 2018.

[160] J. P. Overington, B. Al-Lazikani, and A. L. Hopkins, “How many drug targets are there?,” *Nat. Rev. Drug Discov.*, vol. 5, no. 12, pp. 993–996, Dec. 2006.

[161] S. Talwar, J. W. Lynch, and D. F. Gilbert, “Fluorescence-Based High-Throughput Functional Profiling of Ligand-Gated Ion Channels at the Level of Single Cells,” *PLoS One*, vol. 8, no. 3, pp. 1–11, 2013.

[162] H.-B. Yu, M. Li, W.-P. Wang, and X.-L. Wang, “High throughput screening technologies for ion channels.,” *Acta Pharmacol. Sin.*, vol. 37, no. 1, pp. 34–43, 2016.

[163] O. B. Mcmanus, D. Ph, and M. Bryant, “Ion Channel Screening,” *Assay Guid. Man.*, pp. 1–27, 2012.

[164] J. Dunlop, M. Bowlby, R. Peri, D. Vasilyev, and R. Arias, “High-throughput electrophysiology: An emerging paradigm for ion-channel screening and physiology,” *Nat. Rev. Drug Discov.*, vol. 7, no. 4, pp. 358–368, 2008.

[165] O. B. McManus, “HTS assays for developing the molecular pharmacology of ion channels,” *Curr. Opin. Pharmacol.*, vol. 15, no. 1, pp. 91–96, 2014.

[166] M. Martina and S. Taverna, *Patch-Clamp Methods and Protocols*. 2014.

[167] P. Borst and R. O. Elferink, “Mammalian ABC Transporters in Health and Disease,” *Annu. Rev. Biochem.*, vol. 71, no. 1, pp. 537–592, 2002.

[168] P. Matsson, J. M. Pedersen, U. Norinder, C. A. S. Bergström, and P. Artursson, "Identification of Novel Specific and General Inhibitors of the Three Major Human ATP-Binding Cassette Transporters P-gp, BCRP and MRP2 Among Registered Drugs," *Pharm. Res.*, vol. 26, no. 8, pp. 1816–1831, 2009.

[169] Glavinas H., Krajcsi P., Cserepes J., and Sarkadi B., "The Role of ABC Transporters in Drug Resistance, Metabolism and Toxicity," *Curr. Drug Deliv.*, vol. 1, no. 1, pp. 27–42, 2004.

[170] B. G. Peterson, K. W. Tan, B. Osa-Andrews, and S. H. Iram, "High-content screening of clinically tested anticancer drugs identifies novel inhibitors of human MRP1 (ABCC1)," *Pharmacol. Res.*, vol. 119, pp. 313–326, 2017.

[171] M. Gameiro *et al.*, "Cellular models and in vitro assays for the screening of modulators of P-gp, MRP1 and BCRP," *Molecules*, vol. 22, no. 4, pp. 4–6, 2017.

[172] I. V. Lebedeva, P. Pande, and W. F. Patton, "Sensitive and specific fluorescent probes for functional analysis of the three major types of Mammalian ABC transporters," *PLoS One*, vol. 6, no. 7, 2011.

[173] O. Iamshanova, P. Mariot, V. Lehen'kyi, and N. Prevarskaya, "Comparison of fluorescence probes for intracellular sodium imaging in prostate cancer cell lines," *Eur. Biophys. J.*, vol. 45, no. 7, pp. 765–777, 2016.

[174] J. W. Putney, "Pharmacology of store-operated calcium channels.," *Mol. Interv.*, vol. 10, no. 4, pp. 209–18, 2010.

[175] W. I. DeHaven, J. T. Smyth, R. R. Boyles, G. S. Bird, and J. W. Putney, "Complex actions of 2-aminoethyldiphenyl borate on store-operated calcium entry," *J. Biol. Chem.*, vol. 283, no. 28, pp. 19265–19273, 2008.

[176] P. B. Bennett and H. R. E. Guthrie, "Trends in ion channel drug discovery: Advances in screening technologies," *Trends Biotechnol.*, vol. 21, no. 12, pp. 563–569, 2003.

[177] K. L. R. Brouwer *et al.*, *In vitro methods to support transporter evaluation in drug discovery and development*, vol. 94, no. 1. 2013.

[178] P. Imbrici, O. Nicolotti, F. Leonetti, D. Conte, and A. Liantonio, "Ion Channels in Drug Discovery and Safety Pharmacology," in *Computational Toxicology: Methods and Protocols*, vol. 1800, B. Reisfeld and A. N. Mayeno, Eds. Totowa, NJ: Humana Press, 2018.

[179] Glavinas H., Krajcsi P., Cserepes J., and Sarkadi B., "The Role of ABC Transporters in Drug Resistance, Metabolism and Toxicity," *Curr. Drug Deliv.*, vol. 1, no. 1, pp. 27–42, 2004.

[180] D. W. Y. Sah, J. Ray, and F. H. Gage, "Regulation of voltage- and ligand-gated currents in rat hippocampal progenitor cells in vitro," *J. Neurobiol.*, vol. 32, no. 1, pp. 95–110, 1997.

[181] T. Yasuda and D. J. Adams, "Physiological roles of ion channels in adult neural stem cells and their progeny," *J. Neurochem.*, vol. 114, no. 4, pp. 946–959, 2010.

[182] T. Cho *et al.*, “Human neural stem cells : electrophysiological properties of voltage-gated ion channels,” *Membr. Biophys. Biochem.*, vol. 13, no. 11, pp. 1–7, 2002.

[183] D. R. Piper, T. Mujtaba, M. S. Rao, and M. T. Lucero, “Immunocytochemical and physiological characterization of a population of cultured human neural precursors.,” *J. Neurophysiol.*, vol. 84, no. 1, pp. 534–48, 2000.

[184] T. Lin, O. Islam, and K. Heese, “ABC transporters, neural stem cells and neurogenesis – a different perspective,” *Cell Res.*, vol. 16, no. 11, pp. 857–871, 2006.

[185] A. T. Nies, G. Jedlitschky, H. H. Steiner, and D. Keppler, “EXPRESSION AND IMMUNOLOCALIZATION OF THE MULTIDRUG RESISTANCE PROTEINS , MRP1 – MRP6 (ABCC1 – ABCC6), IN HUMAN,” vol. 129, pp. 349–360, 2004.

[186] Z. Miao, Z. Zhang, H. Wei, J. Gao, and L. Kurgan, “Prediction of Ion Channels and Their Types from Protein Sequences: Comprehensive Review and Comparative Assessment as an original article to Current Drug Targets,” *Curr. Drug Targets*, vol. 19, pp. 579–592, 2018.

[187] S. A. Titus *et al.*, “A new homogeneous high-throughput screening assay for profiling compound activity on the human ether-a-go-go-related gene channel,” *Anal. Biochem.*, vol. 394, no. 1, pp. 30–38, 2009.

[188] C. D. Weaver, D. Harden, S. I. Dworetzky, B. Robertson, and R. J. Knox, “A thallium-sensitive, fluorescence-based assay for detecting and characterizing potassium channel modulators in mammalian cells,” *J. Biomol. Screen.*, vol. 9, no. 8, pp. 671–677, 2004.

[189] O. B. McManus *et al.*, “ Discovery of a Series of 2-Phenyl- N -(2-(pyrrolidin-1-yl)phenyl)acetamides as Novel Molecular Switches that Modulate Modes of K v 7.2 (KCNQ2) Channel Pharmacology: Identification of (S)-2-Phenyl- N -(2-(pyrrolidin-1-yl)phenyl)butanamide (ML252) as a P,” *J. Med. Chem.*, vol. 55, no. 15, pp. 6975–6979, 2012.

[190] D. A. Brown and G. M. Passmore, “Neural KCNQ (Kv7) channels,” *Br. J. Pharmacol.*, vol. 156, no. 8, pp. 1185–1195, 2009.

[191] S. Joshi, P. Balan, and A. M. Gurney, “Pulmonary vasoconstrictor action of KCNQ potassium channel blockers,” *Respir. Res.*, vol. 7, pp. 1–10, 2006.

[192] W. Wang, X. F. Gao, L. Xiao, Z. H. Xiang, and C. He, “KV7/KCNQ channels are functionally expressed in oligodendrocyte progenitor cells,” *PLoS One*, vol. 6, no. 7, pp. 1–10, 2011.

[193] D. L. Greene, S. Kang, and N. Hoshi, “XE991 and Linopirdine Are State-Dependent Inhibitors for Kv7/KCNQ Channels that Favor Activated Single Subunits,” *J. Pharmacol. Exp. Ther.*, vol. 362, no. 1, pp. 177–185, 2017.

[194] D. T. Wong, F. P. Bymaster, and E. A. Engleman, “Prozac (fluoxetine, lilly 110140), the first selective serotonin uptake inhibitor and an antidepressant drug: Twenty years since its first publication,” *Life Sci.*, vol. 57, no. 5, pp. 411–441, 1995.

[195] A. M. Stewart *et al.*, "Aquatic toxicology of fluoxetine: Understanding the knowns and the unknowns," *Aquat. Toxicol.*, vol. 156, pp. 269–273, 2014.

[196] N. O. de Farias *et al.*, "Exposure to low concentration of fluoxetine affects development, behaviour and acetylcholinesterase activity of zebrafish embryos," *Comp. Biochem. Physiol. Part - C Toxicol. Pharmacol.*, vol. 215, no. August 2018, pp. 1–8, 2019.

[197] B. H. Choi *et al.*, "Effects of norfluoxetine, the major metabolite of fluoxetine, on the cloned neuronal potassium channel Kv3.1," *Neuropharmacology*, vol. 41, no. 4, pp. 443–453, 2001.

[198] I. Jeong, J. S. Choi, and S. J. Hahn, "Effects of fluoxetine on cloned Kv4.3 potassium channels," *Brain Res.*, vol. 1500, pp. 10–18, 2013.

[199] C. N. Karson *et al.*, "Human Brain Fluoxetine Concentrations," *J. Neuropsychiatry Clin. Neurosci.*, vol. 5, no. 3, pp. 322–329, 1993.

[200] A. B. Toth, A. K. Shum, and M. Prakriya, "Regulation of neurogenesis by calcium signaling," *Cell Calcium*, vol. 59, no. 2–3, pp. 124–134, 2016.

[201] G. S. Bird, W. I. DeHaven, J. T. Smyth, and J. W. Putney Jr, "Methods for studying store-operated calcium entry," *Methods*, vol. 46, no. 3, pp. 204–212, 2008.

[202] J. Luo, Y. Zhu, M. X. Zhu, and H. Hu, "Cell-based Calcium Assay for Medium to High Throughput Screening of TRP Channel Functions using FlexStation 3.," *J. Vis. Exp.*, no. August, pp. 1–6, 2011.

[203] Y. Lai and W. S. Kisaalita, "Performance evaluation of 3D polystyrene 96-well plates with human neural stem cells in a calcium assay," *J. Lab. Autom.*, vol. 17, no. 4, pp. 284–292, 2012.

[204] X. Xu *et al.*, "2-Aminoethoxydiphenyl Borate Potentiates CRAC Current by Directly Dilating the Pore of Open Orai1," *Sci. Rep.*, vol. 6, no. January, pp. 1–11, 2016.

[205] W. Y. Hu, Z. Y. He, L. J. Yang, M. Zhang, D. Xing, and Z. C. Xiao, "The Ca^{2+} channel inhibitor 2-APB reverses β-amyloid-induced LTP deficit in hippocampus by blocking BAX and caspase-3 hyperactivation," *Br. J. Pharmacol.*, vol. 172, no. 9, pp. 2273–2285, 2015.

[206] K. Takahashi, M. Yokota, and T. Ohta, "Molecular mechanism of 2-APB-induced Ca2+influx in external acidification in PC12," *Exp. Cell Res.*, vol. 323, no. 2, pp. 337–345, 2014.

[207] K. Takahashi and T. Ohta, "Low pH enhances 2-aminoethoxydiphenyl borate-induced cell death of PC12 cells," *Toxicol. Lett.*, vol. 215, no. 3, pp. 161–166, 2012.

[208] J. M. Pedersen, P. Matsson, C. A. S. Bergström, U. Norinder, J. Hoogstraate, and P. Artursson, "Prediction and identification of drug interactions with the human ATP-binding cassette transporter multidrug-resistance associated protein 2 (MRP2; ABCC2)," *J. Med. Chem.*, vol. 51, no. 11, pp. 3275–3287, 2008.

[209] M. O. Islam *et al.*, "Characterization of ABC transporter ABCB1 expressed in human neural stem/progenitor cells," *FEBS Lett.*, vol. 579, no. 17, pp. 3473–3480, 2005.

[210] M. O. Islam *et al.*, "Functional expression of ABCG2 transporter in human neural stem/progenitor cells," *Neurosci. Res.*, vol. 52, no. 1, pp. 75–82, 2005.

[211] A. Yamamoto *et al.*, "ABCB1 is predominantly expressed in human fetal neural stem/progenitor cells at an early development stage," *J. Neurosci. Res.*, vol. 87, no. 12, pp. 2615–2623, 2009.

[212] A.-M. Faussat, J.-Y. Perrot, J.-P. Marie, A. L. Dogan, and O. Legrand, "Evaluation and comparison of MRP1 activity with three fluorescent dyes and three modulators in leukemic cell lines," *Leuk. Res.*, vol. 28, no. 6, pp. 619–622, 2003.

[213] L. Homolya, Z. Holló, M. Müller, E. B. Mechetner, and B. Sarkadi, "A new method for quantitative assessment of P-glycoprotein-related multidrug resistance in tumour cells," *Br. J. Cancer*, vol. 73, no. 7, pp. 849–855, 1996.

[214] A. Krawczenko *et al.*, "Expression and activity of multidrug resistance proteins in mature endothelial cells and their precursors: A challenging correlation," *PLoS One*, vol. 12, no. 2, pp. 1–19, 2017.

[215] I. Druwe, T. M. Freudenrich, K. Wallace, T. J. Shafer, and W. R. Mundy, "Sensitivity of neuroprogenitor cells to chemical-induced apoptosis using a multiplexed assay suitable for high-throughput screening," *Toxicology*, vol. 333, pp. 14–24, 2015.

[216] P. Joshi *et al.*, "3D-cultured neural stem cell microarrays on a micropillar chip for high-throughput developmental neurotoxicology," *Exp. Cell Res.*, vol. 370, no. 2, pp. 680–691, 2018.

[217] M. W. G. D. M. de Groot, R. H. S. Westerink, and M. M. L. Dingemans, "Don't judge a neuron only by its cover: Neuronal function in in vitro developmental neurotoxicity testing," *Toxicol. Sci.*, vol. 132, no. 1, pp. 1–7, 2013.

[218] H. Page, P. Flood, and E. G. Reynaud, "Three-dimensional tissue cultures: current trends and beyond.," *Cell Tissue Res.*, vol. 352, no. 1, pp. 123–31, Apr. 2013.

[219] J. Kriston-Vizi and H. Flotow, "Getting the whole picture: High content screening using three-dimensional cellular model systems and whole animal assays," *Cytom. Part A*, vol. 91, no. 2, pp. 152–159, 2017.

[220] S. N. Bhatia and D. E. Ingber, "Microfluidic organs-on-chips," *Nat. Biotechnol.*, vol. 32, no. 8, pp. 760–772, 2014.

[221] S. Weiss, B. A. Reynolds, A. L. Vescovi, C. Morshead, C. G. Craig, and D. Van Der Kooy, "Is there a neural stem cell in the mammalian forebrain?," *Trends Neurosci.*, vol. 19, no. 9, pp. 387–393, 1996.

[222] J. D. Flax *et al.*, "Engraftable human neural stem cells respond to developmental cues, replace neurons, and express foreign genes," *Nat. Biotechnol.*, vol. 16, no. 11, pp. 1033–1039, 1998.

[223] K. N. Yu, S. Y. Kang, S. Hong, and M. Y. Lee, "High-throughput metabolism-induced toxicity assays demonstrated on a 384-pillar plate," *Arch. Toxicol.*, vol. 92, no. 8, pp. 2501–2516, 2018.

[224] J. Li, M. L. Spletter, D. a. Johnson, L. S. Wright, C. N. Svendsen, and J. a. Johnson, "Rotenone-induced caspase 9/3-independent and -dependent cell death in undifferentiated and differentiated human neural stem cells," *J. Neurochem.*, vol. 92, no. 3, pp. 462–476, 2005.

[225] J. Jin *et al.*, "Identification of novel proteins affected by rotenone in mitochondria of dopaminergic cells.," *BMC Neurosci.*, vol. 8, no. 1, p. 67, 2007.

[226] W. E. Glover, "The Aminopyridines," *Gen. Pharmacol.*, vol. 13, pp. 259–285, 1982.

[227] H. B. Jensen, M. Ravnborg, U. Dalgas, and E. Stenager, "4-Aminopyridine for symptomatic treatment of multiple sclerosis: a systematic review.," *Ther. Adv. Neurol. Disord.*, vol. 7, no. 2, pp. 97–113, 2014.

[228] D. C. S. Soares *et al.*, "Treatment with pentylenetetrazole (PTZ) and 4-aminopyridine (4-AP) differently affects survival, locomotor activity, and biochemical markers in Drosophila melanogaster," *Mol. Cell. Biochem.*, vol. 442, no. 1–2, pp. 129–142, 2018.

[229] I. Prassas, G. S. Karagiannis, I. Batruch, A. Dimitromanolakis, A. Datti, and E. P. Diamandis, "Digitoxin-Induced Cytotoxicity in Cancer Cells Is Mediated through Distinct Kinase and Interferon Signaling Networks," *Mol. Cancer Ther.*, vol. 10, no. 11, pp. 2083–2093, 2011.

[230] I. Prassas and E. P. Diamandis, "Novel therapeutic applications of cardiac glycosides," *Nat. Rev. Drug Discov.*, vol. 7, p. 926, Oct. 2008.

[231] B. L. Staker, K. Hjerrild, M. D. Feese, C. A. Behnke, A. B. Burgin, and L. Stewart, "The mechanism of topoisomerase I poisoning by a camptothecin analog.," *Proc. Natl. Acad. Sci. U. S. A.*, vol. 99, no. 24, pp. 15387–92, 2002.

[232] K. Sterzyńska *et al.*, "The role of matrix gla protein (MGP) expression in paclitaxel and topotecan resistant ovarian cancer cell lines," *Int. J. Mol. Sci.*, vol. 19, no. 10, 2018.

[233] L. Chernov, R. J. Deyell, M. Anantha, N. Dos Santos, R. Gilabert-Oriol, and M. B. Bally, "Optimization of liposomal topotecan for use in treating neuroblastoma," *Cancer Med.*, vol. 6, no. 6, pp. 1240–1254, 2017.

[234] R. C. Scaduto and L. W. Grotyohann, "Measurement of mitochondrial membrane potential using fluorescent rhodamine derivatives.," *Biophys. J.*, vol. 76, no. 1 Pt 1, pp. 469–77, Jan. 1999.

[235] A. Monteith *et al.*, "Imaging of mitochondrial and non-mitochondrial responses in cultured rat hippocampal neurons exposed to micromolar concentrations of TMRM.," *PLoS One*, vol. 8, no. 3, p. e58059, Jan. 2013.

[236] F. Distelmaier *et al.*, "Life cell quantification of mitochondrial membrane potential

at the single organelle level.," *Cytometry. A*, vol. 73, no. 2, pp. 129–38, Feb. 2008.

[237] H. Kamencic, A. Lyon, P. G. Paterson, and B. H. J. Juurlink, "Monochlorobimane fluorometric method to measure tissue glutathione," *Anal. Biochem.*, vol. 286, no. 1, pp. 35–37, 2000.

[238] K. Park, D. P. Williams, D. J. Naisbitt, N. R. Kitteringham, and M. Pirmohamed, "Investigation of toxic metabolites during drug development," *Toxicol. Appl. Pharmacol.*, vol. 207, no. 2 SUPPL., pp. S425-434, 2005.

[239] D. Bratosin, L. Mitrofan, C. Palii, J. Estaquier, and J. Montreuil, "Novel fluorescence assay using calcein-AM for the determination of human erythrocyte viability and aging," *Cytom. Part A*, vol. 66, no. 1, pp. 78–84, 2005.

[240] F. L. Zhang *et al.*, "Topoisomerase I inhibitors, shikonin and topotecan, inhibit growth and induce apoptosis of glioma cells and glioma stem cells," *PLoS One*, vol. 8, no. 11, pp. 1–12, 2013.

[241] L. C. Crowley, B. J. Marfell, and N. J. Waterhouse, "Analyzing cell death by nuclear staining with Hoechst 33342," *Cold Spring Harb. Protoc.*, vol. 2016, no. 9, pp. 778–781, 2016.

[242] S. H. Choi *et al.*, "A three-dimensional human neural cell culture model of Alzheimer's disease.," *Nature*, vol. 515, no. 7526, pp. 274–8, 2014.

[243] B. Larson, "3D Cell Culture: A Review of Current Techniques," *White Pap.*, vol. 6, p. 10, 2015.

[244] P. Joshi and M.-Y. Lee, "High Content Imaging (HCI) on Miniaturized Three-Dimensional (3D) Cell Cultures," *Biosensors*, vol. 5, no. 4, pp. 768–790, 2015.

[245] Y. Koo, B. T. Hawkins, and Y. Yun, "Three-dimensional (3D) tetra-culture brain on chip platform for organophosphate toxicity screening," *Sci. Rep.*, vol. 8, no. 1, pp. 1–7, 2018.

[246] O. Sirenko *et al.*, "Functional and Mechanistic Neurotoxicity Profiling Using Human iPSC–Derived Neural 3D Cultures," *Toxicol. Sci.*, pp. 1–19, 2018.

[247] D. Pamies *et al.*, "Rotenone exerts developmental neurotoxicity in a human brain spheroid model," *Toxicol. Appl. Pharmacol.*, vol. 354, no. February, pp. 101–114, 2018.

[248] D. De Zio, L. Giunta, M. Corvaro, E. Ferraro, and F. Cecconi, "Expanding roles of programmed cell death in mammalian neurodevelopment," *Semin. Cell Dev. Biol.*, vol. 16, no. 2, pp. 281–294, 2005.

[249] A. Jaeger *et al.*, "Characterization of Apoptosis Signaling Cascades During the Differentiation Process of Human Neural ReNcell VM Progenitor Cells In Vitro," *Cell. Mol. Neurobiol.*, vol. 35, no. 8, pp. 1203–1216, 2015.

[250] Y. Geng, K. C. Walls, A. P. Ghosh, R. S. Akhtar, B. J. Klocke, and K. A. Roth, "Cytoplasmic p53 and activated bax regulate p53-dependent, transcription-

independent neural precursor cell apoptosis," *J. Histochem. Cytochem.*, vol. 58, no. 3, pp. 265–275, 2010.

[251] A. Valencia and J. Morán, "Reactive oxygen species induce different cell death mechanisms in cultured neurons," *Free Radic. Biol. Med.*, vol. 36, no. 9, pp. 1112–1125, 2004.

[252] I. C. J. Lang-Rollin, H. J. Rideout, M. Noticewala, and L. Stefanis, "Mechanisms of caspase-independent neuronal death: energy depletion and free radical generation.," *J. Neurosci.*, vol. 23, no. 35, pp. 11015–11025, 2003.

[253] T. Kuwana and D. D. Newmeyer, "Bcl-2-family proteins and the role of mitochondria in apoptosis," *Curr. Opin. Cell Biol.*, vol. 15, no. 6, pp. 691–699, 2003.

[254] D. Acehan, X. Jiang, D. G. Morgan, J. E. Heuser, X. Wang, and C. W. Akey, "Three-Dimensional Structure of the Apoptosome: Implications for Assembly, Procaspase-9 Binding, and Activation," *Mol. Cell*, vol. 9, no. 2, pp. 423–432, 2002.

[255] C. Sonich-Mullin *et al.*, "IPCS conceptual framework for evaluating a mode of action for chemical carcinogenesis," *Regul. Toxicol. Pharmacol.*, vol. 34, no. 2, pp. 146–152, 2001.

[256] T. Cunha-Oliveira, A. C. Rego, and C. R. Oliveira, "Cellular and molecular mechanisms involved in the neurotoxicity of opioid and psychostimulant drugs," *Brain Res. Rev.*, vol. 58, no. 1, pp. 192–208, 2008.

[257] C. Chauvin, F. De Oliveira, X. Ronot, M. Mousseau, X. Leverve, and E. Fontaine, "Rotenone Inhibits the Mitochondrial Permeability Transition-induced Cell Death in U937 and KB Cells," *J. Biol. Chem.*, vol. 276, no. 44, pp. 41394–41398, 2001.

[258] E. W. Schafer, R. B. Brunton, and D. J. Cunningham, "A summary of the acute toxicity of 4-aminopyridine to birds and mammals," *Toxicol. Appl. Pharmacol.*, vol. 26, no. 4, pp. 532–538, 1973.

[259] A. M. King, N. B. Menke, K. D. Katz, and A. F. Pizon, "4-Aminopyridine Toxicity: A Case Report and Review of the Literature," *J. Med. Toxicol.*, vol. 8, no. 3, pp. 314–321, 2012.

[260] S.-Y. Ng *et al.*, "Role of voltage-gated potassium channels in the fate determination of embryonic stem cells," *J. Cell. Physiol.*, no. December 2009, p. n/a-n/a, 2010.

[261] E. Benítez-Rangel, L. García, M. C. Namorado, J. L. Reyes, and a Guerrero-Hernández, "Ion channel inhibitors block caspase activation by mechanisms other than restoring intracellular potassium concentration.," *Cell Death Dis.*, vol. 2, p. e113, 2011.

[262] Å. Svensson, F. Azarbayjani, U. Bäckman, T. Matsumoto, and R. Christofferson, "Digoxin inhibits neuroblastoma tumor growth in mice," *Anticancer Res.*, vol. 25, no. 1 A, pp. 207–212, 2005.

[263] J.-F. HÉRON, "Topotecan : An Oncologist ' s View," *Oncology*, vol. 3, pp. 390–402, 1998.

[264] C. S. *et al.*, "Metabolism and neurotoxicity: The significance of genetically engineered cell lines and new three-dimensional cell cultures," *ATLA Altern. to Lab. Anim.*, vol. 30, no. SUPPL. 2, pp. 115–118, 2002.

[265] S. Coecke *et al.*, "Metabolism: A bottleneck in in vitro toxicological test development," *ATLA Altern. to Lab. Anim.*, vol. 34, no. 1, pp. 49–84, 2006.

[266] E. F. A. Brandon, C. D. Raap, I. Meijerman, J. H. Beijnen, and J. H. M. Schellens, "An update on in vitro test methods in human hepatic drug biotransformation research: Pros and cons," *Toxicol. Appl. Pharmacol.*, vol. 189, no. 3, pp. 233–246, 2003.

[267] R. C. A. Onderwater, J. N. M. Commandeur, and N. P. E. Vermeulen, "Comparative cytotoxicity of N-substituted N′-(4-imidazole-ethyl) thiourea in precision-cut rat liver slices," *Toxicology*, vol. 197, no. 2, pp. 80–90, 2004.

[268] M. Martignoni, M. Monshouwer, R. de Kanter, D. Pezzetta, A. Moscone, and P. Grossi, "Phase I and phase II metabolic activities are retained in liver slices from mouse, rat, dog, monkey and human after cryopreservation," *Toxicol. Vitr.*, vol. 18, no. 1, pp. 121–128, 2004.

[269] R. E. White, "High-Throughput Screening in Drug Metabolism and Pharmacokinetic Support of Drug Discovery," *Annu. Rev. Pharmacol. Toxicol.*, vol. 40, pp. 133–157, 2000.

[270] S. N. Hart, Y. Li, K. Nakamoto, E. A. Subileau, D. Steen, and X. B. Zhong, "A comparison of whole genome gene expression profiles of HepaRG cells and HepG2 cells to primary human hepatocytes and human liver tissues," *Drug Metab. Dispos.*, vol. 38, no. 6, pp. 988–994, 2010.

[271] M.-Y. Lee, C. B. Park, J. S. Dordick, and D. S. Clark, "Metabolizing enzyme toxicology assay chip (MetaChip) for high-throughput microscale toxicity analyses.," *Proc. Natl. Acad. Sci.*, vol. 102, no. 4, pp. 983–7, 2005.

[272] S. Coecke *et al.*, "Metabolism : A Bottleneck in In Vitro Toxicological Test Development," no. January 2004, pp. 49–84, 2006.

[273] L. Moatamedi Pour, A. Farahnak, M. Molaei Rad, T. Golmohamadi, and M. Eshraghian, "Activity Assay of Glutathione S-Transferase (GSTs) Enzyme as a Diagnostic Biomarker for Liver Hydatid Cyst in Vitro.," *Iran. J. Public Health*, vol. 43, no. 7, pp. 994–9, 2014.

[274] K. P. Kanebratt and T. B. Andersson, "Evaluation of HepaRG Cells as an in Vitro Model for Human Drug Metabolism Studies," *Drug Metab. Dispos.*, vol. 36, no. 7, pp. 1444–1452, 2008.

[275] L. L. Mazaleuskaya, K. Sangkuhl, C. F. Thorn, G. A. Fitzgerald, R. B. Altman, and T. E. Klein, "PharmGKB summary: Pathways of acetaminophen metabolism at the therapeutic versus toxic doses," *Pharmacogenet. Genomics*, vol. 25, no. 8, pp. 416–426, 2015.

[276] K. N. Yu, S. Y. Kang, S. Hong, and M. Y. Lee, "High-throughput metabolism-

induced toxicity assays demonstrated on a 384-pillar plate," *Arch. Toxicol.*, vol. 92, no. 8, pp. 2501–2516, 2018.

[277] J. C. Dinh *et al.*, "Potential Contribution of Cytochrome P450 2B6 to Hepatic 4-Hydroxycyclophosphamide Formation In Vitro and In Vivo," *Drug Metab. Dispos.*, vol. 40, no. 1, pp. 54–63, 2011.

[278] Y. Yokoyama *et al.*, "Comparison of drug metabolism and its related hepatotoxic effects in HepaRG, cryopreserved human hepatocytes, and HepG2 cell cultures," *Biol. Pharm. Bull.*, vol. 41, no. 5, pp. 722–732, 2018.

[279] L. Yang *et al.*, "Effects of ketoconazole on cyclophosphamide metabolism: Evaluation of CYP3A4 inhibition effect using the in vitro and in vivo models," *Exp. Anim.*, vol. 67, no. 1, pp. 71–82, 2018.

[280] S. J. Kwon *et al.*, "High-throughput and combinatorial gene expression on a chip for metabolism-induced toxicology screening," *Nat. Commun.*, vol. 5, no. May, pp. 1–12, 2014.

[281] P. Gripon *et al.*, "Infection of a human hepatoma cell line by hepatitis B virus," *Proc. …*, vol. 99, no. 24, pp. 15655–15660, 2002.

[282] T. B. Andersson, K. P. Kanebratt, and J. G. Kenna, "The HepaRG cell line: a unique *in vitro* tool for understanding drug metabolism and toxicology in human," *Expert Opin. Drug Metab. Toxicol.*, vol. 8, no. 7, pp. 909–920, 2012.

[283] and A. ´e G. Caroline Aninat, 1 Am´elie Piton, 1 Denise Glaise, Typhen Le Charpentier, Sophie Langou ¨et, Fabrice Morel, Christiane Guguen-Guillouzo, "EXPRESSION OF CYTOCHROMES P450, CONJUGATING ENZYMES AND NUCLEAR RECEPTORS IN HUMAN HEPATOMA HepaRG CELLS," *Drug Metab. Dispos.*, vol. 34, no. 1, pp. 75–83, 2006.

[284] H. H. J. Gerets *et al.*, "Characterization of primary human hepatocytes, HepG2 cells, and HepaRG cells at the mRNA level and CYP activity in response to inducers and their predictivity for the detection of human hepatotoxins," *Cell Biol. Toxicol.*, vol. 28, no. 2, pp. 69–87, 2012.

[285] K. P. Kanebratt and T. B. Andersson, "HepaRG Cells as an in Vitro Model for Evaluation of Cytochrome P450 Induction in Humans," *Drug Metab. Dispos.*, vol. 36, no. 1, pp. 137–145, 2008.

[286] F. P. Guengerich, "CYTOCHROME P-450 3A4: Regulation and Role in Drug Metabolism," *Annu. Rev. Pharmacol. Toxicol.*, vol. 39, no. 1, pp. 1–17, 2002.

[287] M.-F. Yueh, M. Kawahara, and J. Raucy, "HIGH VOLUME BIOASSAYS TO ASSESS CYP3A4-MEDIATED DRUG INTERACTIONS : INDUCTION AND INHIBITION IN A SINGLE CELL LINE," *Drug Metab. Dispos.*, vol. 33, no. 1, pp. 38–48, 2005.

[288] V. Agarwal *et al.*, "Drug metabolism in human brain: High levels of cytochrome P4503A43 in brain and metabolism of anti-anxiety drug alprazolam to its active metabolite," *PLoS One*, vol. 3, no. 6, 2008.

[289] A. Claesson and O. Spjuth, “On mechanisms of reactive metabolite formation from drugs,” *Mini Rev Med Chem*, vol. 13, no. 5, pp. 720–729, 2013.

[290] Z. Wang *et al.*, “HepaRG culture in tethered spheroids as an in vitro three-dimensional model for drug safety screening,” *J. Appl. Toxicol.*, vol. 35, no. 8, pp. 909–917, 2015.

[291] J. E. Laine, S. Auriola, M. Pasanen, and R. O. Juvonen, “Acetaminophen bioactivation by human cytochrome P450 enzymes and animal microsomes,” *Xenobiotica*, vol. 39, no. 1, pp. 11–21, 2009.

[292] K. E. Thummel, C. A. Lee, K. L. Kunze, S. D. Nelson, and J. T. Slattery, “OXIDATION OF ACETAMINOPHEN TO N-ACETYL-p-AMINOBENZOQUINONE IMME BY HUMAN CYP3A4,” *Biochem. Pharmacol.*, vol. 45, no. 8, pp. 1563–1569, 1993.

[293] K. M. Crofton, D. B. Peele, and M. E. Stanton, “Developmental neurotoxicity following neonatal exposure to 3,3′-iminodipropionitrile in the rat,” *Neurotoxicol. Teratol.*, vol. 15, no. 2, pp. 117–129, 1993.

[294] N. Takahashi, W. Tarumi, and B. Ishizuka, “Acute reproductive toxicity of 3,3’-iminodipropionitrile in female rats,” *Reprod. Toxicol.*, vol. 33, no. 1, pp. 27–34, 2012.

[295] P. Boadas-Vaello, L. Sedó-Cabezón, E. Verdú, and J. Llorens, “Strain and sex differences in the vestibular and systemic toxicity of 3,3’-iminodipropionitrile in mice,” *Toxicol. Sci.*, vol. 156, no. 1, pp. 109–122, 2017.

[296] A. Morandi, P. Gambetti, P. K. Arora, and L. M. Sayre, “Mechanism of neurotoxic action of β,β′-iminodipropionitrile (IDPN): N-hydroxylation enhances neurotoxic potency,” *Brain Res.*, vol. 437, no. 1, pp. 69–76, 1987.

[297] C. G. Nace, M. B. Genter, L. M. Sayre, and K. M. Crofton, “Effect of methimazole, an FMO substrate and competitive inhibitor, on the neurotoxicity of 3,3′-iminodipropionitrile in male rats,” *Fundam. Appl. Toxicol.*, vol. 37, no. 2, pp. 131–140, 1997.

[298] C. S. Ferguson and R. F. Tyndale, “Cytochromes P450 in the brain: Emerging evidence for biological significance,” *Trends Pharmacol Sci*, vol. 32, no. 12, pp. 708–714, 2011.

[299] E. Bromek, A. Haduch, K. Gołembiowska, and W. A. Daniel, “Cytochrome P450 mediates dopamine formation in the brain in vivo,” *J. Neurochem.*, vol. 118, no. 5, pp. 806–815, 2011.

[300] M. Mannerström, T. Toimela, T. Ylikomi, and H. Tähti, “The combined use of human neural and liver cell lines and mouse hepatocytes improves the predictability of the neurotoxicity of selected drugs,” *Toxicol. Lett.*, vol. 165, no. 2, pp. 195–202, 2006.

[301] B. T. Hawkins and T. P. Davis, “The Blood-Brain Barrier/Neurovascular Unit in Health and Disease,” *Pharmacol. Rev.*, vol. 57, no. 2, p. 173 LP-185, Jun. 2005.

[302] Y. Sharif, F. Jumah, L. Coplan, A. Krosser, K. Sharif, and R. S. Tubbs, “Blood brain barrier: A review of its anatomy and physiology in health and disease,” *Clin. Anat.*, vol. 31, no. 6, pp. 812–823, 2018.

APPENDIX

Apart from voltage-gated potassium channels and store-operated calcium channels, chloride ion channel assays were also investigated on monolayers of ReNcell VM in the 96-well plate using Premo™ halide sensor kit (Thermo Fisher). This assay consists of baculovirus-mediated gene delivery (BacMam technology) to introduce genes for the Premo™ halide sensor into the cells and express the corresponding protein. The Premo™ halide sensor is based on a green fluorescent protein (GFP) that is sensitive to iodide ions, an analog of halide ions. When iodide ions permeate through chloride ion channels, they react with the Premo™ halide sensor, resulting in a loss of fluorescence emission intensity. Thus, bright intracellular fluorescence can be observed at an excitation/emission wavelength of 515/530 nm when chloride ion channels are closed in the presence of blockers. Similarly, the opening of chloride ion channels with activators can be detected by measuring decrease in GFP fluorescence.

The expression level of Premo™ halide sensor was optimized on 2D-cultured ReNcell VM. Briefly, ReNcell VM was seeded in the laminin-coated 96-well plate at 10,000 cell/well and incubated for 24 h prior to infection with varying concentrations of the baculovirus carrying genes for Premo™ halide sensor. Five different concentrations of the baculovirus solutions were prepared by mixing the baculovirus stock solution with growth media at different ratios (10:90, 20:80, 30:70, 40:60, and 50:50), and then 50 μL of the mixtures were added in the 96-well plate with ReNcell VM monolayers for over 16 h to allow the expression of Premo™ halide sensor. The optimum ratio of baculovirus to growth media was determined by analyzing green fluorescent cell images obtained from S+

Scanner **(Figure 1)**. As a result, the optimum level of Premo™ halide sensor expression was achieved at the 40:60 ratio of baculovirus to growth media. The opening of chloride ion channels and subsequent quenching of Premo™ halide sensor was achieved by adding a stimulus buffer containing sodium iodide (NaI) at a final concentration of 75 mM **(Figure 1)**. The decrease in green fluorescence signals in the cell images indicates the entry of iodide ions into the cells through chloride ion channels and subsequent reaction with Premo™ halide sensor.

After determining the optimum transduction condition with the baculovirus, the Premo™ halide ion channel assay was tested with a chloride ion channel activator, lubiprostone, on monolayers of ReNcell VM. Briefly, ReNcell VM was seeded in the laminin-coated 96-well plate at 10,000 cell/well and incubated for 24 h prior to the baculovirus infection with the 40:60 ratio of baculovirus to growth media. After the baculovirus infection for over 16 h for expressing the Premo™ halide sensor, the monolayers of ReNcell VM in the 96-well plate were exposed to 6 different concentrations of lubiprostone for 30 min. This was followed by adding a stimulus buffer containing 75 mM of sodium iodide and imaging the cells with S+ Scanner. To obtain baseline fluorescence and investigate the effect of lubiprostone on 2D-cultured ReNcell VM expressing the Premo™ halide sensor, the pictures were taken before and after stimulation and the dose response curve was obtained (**Figure 2**). As expected, dose-dependent decrease in fluorescence was observed, which indicate that chloride ion channels were activated with lubiprostone and iodide ions entered through chloride ion channels reacted with the Premo™ halide sensor, resulting in the quenching of fluorescence.

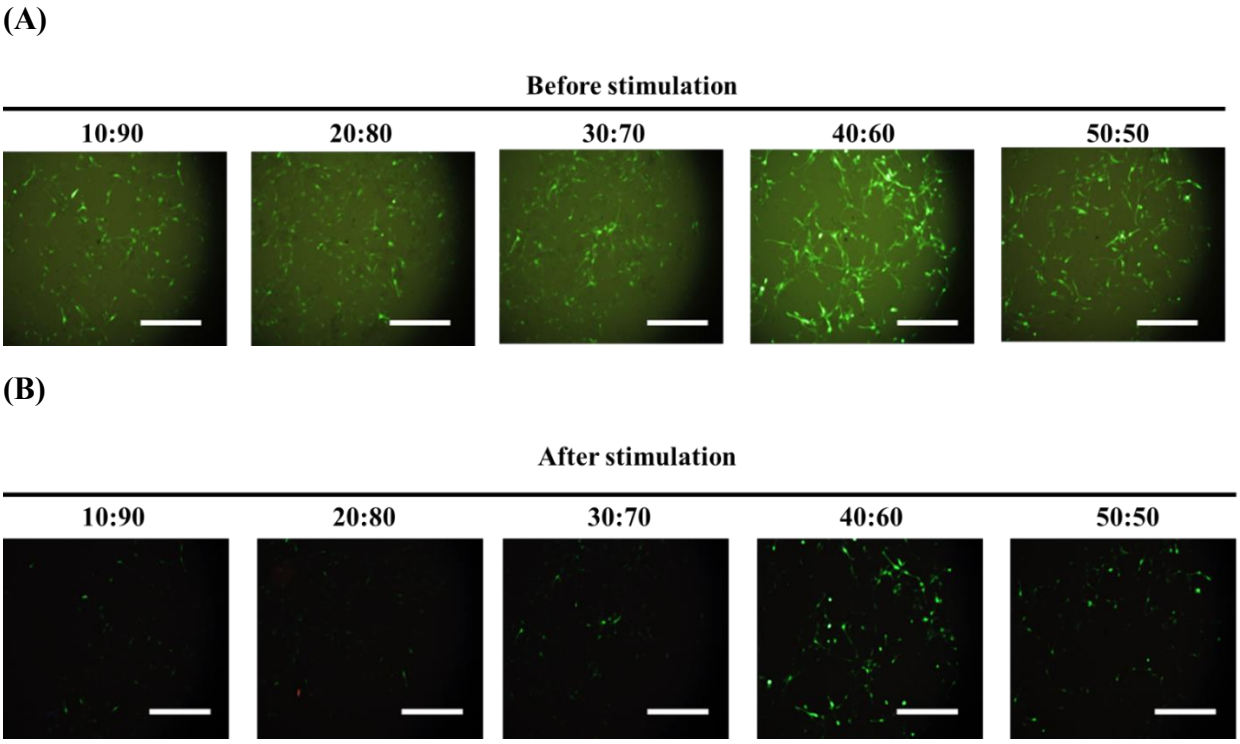

Figure 1. Optimization of Premo™ halide sensor performed on monolayers of ReNcell VM in a 96-well plate. ReNcell VM was seeded in the 96-well plate at 10,000 cells/well and cultured for 24 h prior to infection with recombinant baculovirus carrying genes for Premo™ halide sensor. Baculovirus solutions were prepared by mixing the baculovirus stock solution with growth media at different ratios (10:90, 20:80, 30:70, 40:60, and 50:50). In addition, 50 µL of the mixtures were added in the 96-well plate with ReNcell VM monolayers and incubated for over 16 h as recommended by the vendor to infect ReNcell VM and allow the expression of Premo™ halide sensor. (A) Images of baculovirus-infected ReNcell VM obtained at exposure time of 500 milliseconds. The optimum expression of Premo™ halide sensor in ReNcell VM was observed at a ratio of 40:60 for baculovirus to growth media. Scale bar: 100 µm. (B) Images of baculovirus-infected ReNcell VM obtained after stimulation with a buffer containing sodium iodide (NaI) at 75 mM. The decrease in fluorescence intensity after stimulation is indicative of the subsequent entry of iodide ions into the cells. Scale bar: 100 µm.

(A)

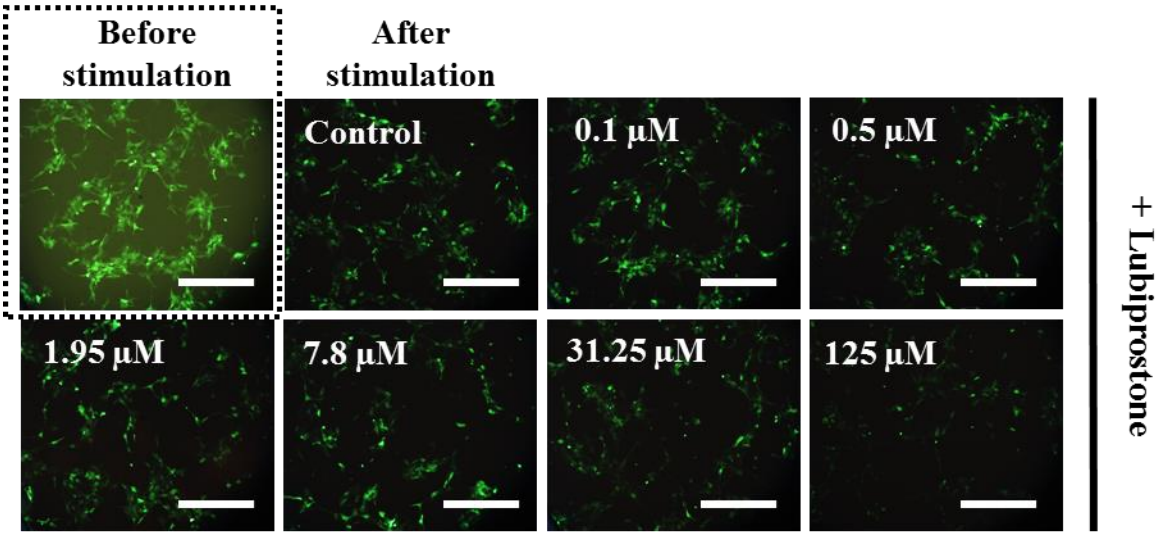

(B)

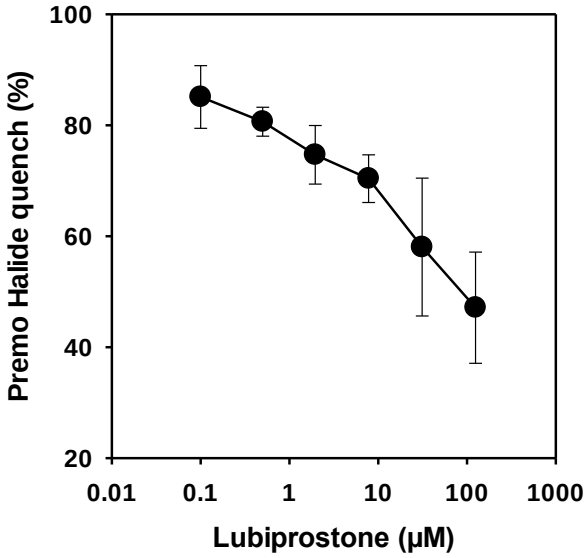

Figure 2. Premo™ halide sensor-based chloride channel assay performed on monolayers of ReNcell VM in a 96-well plate with an activator. ReNcell VM was seeded in the 96-well plate at 10,000 cells/well and cultured for 24 h prior to infection with recombinant baculovirus carrying genes for Premo™ halide sensor. A baculovirus solution was prepared by mixing the baculovirus stock solution with growth media at 40:60 ratio. In addition, 50 µL of the mixture was added in the 96-well plate with ReNcell VM monolayers and incubated for over 16 h to infect ReNcell VM and allow the expression of Premo™ halide sensor. (A) Images of baculovirus-infected ReNcell VM after stimulation

with a buffer containing sodium iodide (NaI) at 75 mM and exposure to lubiprostone, a potent chloride channel activator. The decrease in fluorescence intensity after stimulation and exposure to lubiprostone is indicative of the subsequent entry of iodide ions into the cells. The black dotted image represents baculovirus-infected ReNcell VM before stimulation and lubiprostone exposure (control). All images were obtained at exposure time of 700 milliseconds with S+ Scanner. Scale bar: 100 μm. (B) Decrease in green fluorescence intensity due to lubiprostone-induced chloride ion channel opening, obtained from baculovirus-infected ReNcell VM in the 96-well plate. Scale bar: 100 μm.